

**FABRICATION OF 3D CALCIUM-ALGINATE
SCAFFOLD CELL CULTURE SYSTEM AS
A NERVE-TISSUE CANCER MODEL FOR
ANTICANCER DRUG STUDIES**



**A Thesis Submitted in Partial Fulfillment of the Requirements for the
Degree of Doctor of Philosophy in Biotechnology
Suranaree University of Technology
Academic Year 2018**

การพัฒนากระบวนการสร้างระบบการเลี้ยงเซลล์แบบสามมิติด้วย
แคลเซียม-อัลจิเนต เพื่อเป็นแบบจำลองในการศึกษามะเร็งเนื้อเยื่อ
ระบบประสาทและประเมินประสิทธิภาพยาต้านมะเร็ง

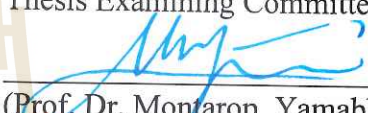


วิทยานิพนธ์นี้เป็นส่วนหนึ่งของการศึกษาตามหลักสูตรปริญญาวิทยาศาสตรดุษฎีบัณฑิต
สาขาวิชาเทคโนโลยีชีวภาพ
มหาวิทยาลัยเทคโนโลยีสุรนารี
ปีการศึกษา 2561

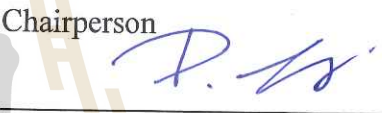
**FABRICATION OF 3D CALCIUM-ALGINATE SCAFFOLD
CELL CULTURE SYSTEM AS A NERVE-TISSUE CANCER
MODEL FOR ANTICANCER DRUG STUDIES**

Suranaree University of Technology has approved this thesis submitted in partial fulfillment of the requirements for the Degree of Doctor of Philosophy.

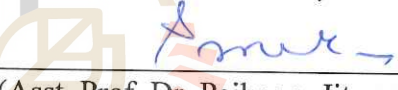
Thesis Examining Committee


(Prof. Dr. Montarop Yamabhai)

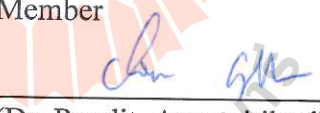
Chairperson


(Asst. Prof. Dr. Parinya Noisa)

Member (Thesis Advisor)


(Asst. Prof. Dr. Paiboon Jitprasertwong)

Member


(Dr. Pundit Asavaritikrai)

Member


(Asst. Prof. Dr. Areechun Sotthibundhu)

Member


(Prof. Dr. Neung Teaumroong)


(Prof. Dr. Sunti Maensiri)

Vice Rector for Academic Affairs
and Internationalization

Dean of Institute of Agricultural Technology

นิภา ชัยเจริญอุดมรุ่ง : การพัฒนากระบวนการสร้างระบบการเลี้ยงเซลล์แบบสามมิติด้วยแคลเซียม-อัลจิเนต เพื่อเป็นแบบจำลองในการศึกษามะเร็งเนื้อเยื่อระบบประสาทและประเมนประสิทธิภาพยาต้านมะเร็ง (FABRICATION OF 3D CALCIUM-ALGINATE SCAFFOLD CELL CULTURE SYSTEM AS A NERVE-TISSUE CANCER MODEL FOR ANTICANCER DRUG STUDIES) อาจารย์ที่ปรึกษา : ผู้ช่วยศาสตราจารย์ ดร.ปริญญา น้อยสา, 167 หน้า.

มะเร็งเนื้อเยื่อระบบประสาทโดยเฉพาะอย่างยิ่ง มะเร็งกลัยโอบลาสโตมา และมะเร็งนิวโรบลาสโตมา เป็นความท้าทายระดับโลกต่อสุขภาพของมนุษย์ ยิ่งไปกว่านั้นกลัยโอบลาสโตมาเป็นมะเร็งของเนื้อเยื่อระบบประสาทที่มีความรุนแรงมากที่สุดและดื้อต่อยาเคมีบำบัด โดยมีอัตราการรอดชีวิตของผู้ป่วยเฉลี่ย 12-15 เดือน สำหรับผู้ป่วยมะเร็งกลัยโอบลาสโตมาที่ได้รับการวินิจฉัยใหม่ และ 5-7 เดือน สำหรับผู้ที่เกิดมะเร็งซ้ำ คอร์โดเซป็นเป็นสารสกัดจากถั่งเช่า จากรายงานการศึกษาภายใต้การทดสอบกับเซลล์ที่เพาะเลี้ยงในห้องทดลองด้วยระบบสองมิติ พบว่าคอร์โดเซป็นเป็นสารต้านมะเร็งที่มีกระบวนการทำงานผ่านหลากหลายกลไก อย่างไรก็ตามกลไกการต้านมะเร็งระบบประสาทของคอร์โดเซป็นยังไม่เป็นที่เข้าใจแน่ชัด ในการศึกษานี้ได้ทำการตรวจสอบกลไกการทำงานของคอร์โดเซป็นต่อเซลล์มะเร็งเนื้อเยื่อระบบประสาทของมนุษย์ พบว่าคอร์โดเซป็นสามารถยับยั้งการเจริญเติบโตของเซลล์ และเหนี่ยวนำให้เกิดการตายแบบอะพอพโทซิสของเซลล์มะเร็งกลัยโอบลาสโตมา (U-251) และมะเร็งนิวโรบลาสโตมา (SH-SY5Y) ผ่านวิถีจากภายในที่มีไมโทคอนเดรียเป็นตัวกลาง และการปรับเปลี่ยนของกระบวนการออกได้ไฟฟ้า อย่างไรก็ตามมีมุมมองที่กระตุ้นใหม่ พบว่าการเพาะเลี้ยงเซลล์แบบดั้งเดิมในระบบสองมิติอาจไม่สามารถเลียนแบบสภาพแวดล้อมแบบสามมิติซึ่งเซลล์มะเร็งอาศัยอยู่จริงได้ รูปแบบการเพาะเลี้ยงเซลล์สามมิติจึงมีการใช้กันอย่างแพร่หลายมากขึ้นเพื่อการศึกษาชีววิทยาของมะเร็ง และเพื่อคัดกรองสารต้านมะเร็ง เนื่องจากการเพาะเลี้ยงเซลล์แบบสามมิติมีการจำลองสถานะแวดล้อมที่เซลล์มะเร็งอาศัยอยู่ได้ใกล้เคียงกับชั้นเนื้อเยื่อที่พบในร่างกายมนุษย์ ดังนั้นโครงสร้างสามมิติแคลเซียม-อัลจิเนต จึงถูกพัฒนาขึ้นสำหรับการเพาะเลี้ยงเซลล์มะเร็งกลัยโอบลาสโตมา และตรวจสอบการตอบสนองต่อสารต้านมะเร็งเทโมโซโลไมด์ ค็อกโซรูบิซิน และคอร์โดเซป็น ผลการทดลอง พบว่าเซลล์มะเร็งกลัยโอบลาสโตมาที่เลี้ยงในโครงสร้างสามมิติแคลเซียม-อัลจิเนตมีการเพิ่มจำนวนเซลล์ที่ลดลง ขณะเดียวกันมีการก่อตัวเป็นก้อนเนื้อออกเพิ่มมากขึ้น และเพิ่มการแสดงออกของยีนในกลุ่มเซลล์ต้นกำเนิดมะเร็ง และยีนที่เกี่ยวข้องกับการเปลี่ยนแปลงของเซลล์ไปเป็นเซลล์ชนิดอื่นที่มีความจำเพาะ นอกจากนี้ศึกษาพบว่าการเกิดหลอดเลือดใหม่ของเซลล์มะเร็งกลัยโอบลาสโตมาแบบสามมิติมีเพิ่มมากขึ้นเนื่องจากการแสดงออกของตัวบ่งชี้ทางชีวภาพในกระบวนการสร้างหลอดเลือดใหม่สูงกว่าในเซลล์ที่เพาะเลี้ยงในระบบสองมิติ นอกจากนี้เซลล์มะเร็งกลัยโอบลาสโตมาแบบสามมิติได้รับการทดสอบด้วย

สารต้านมะเร็ง เทโมโซโลไมด์ คีอ็อกโซรูบิซิน และคอร์โคเซป็น ผลการทดลองแสดงให้เห็นว่า เซลล์มะเร็งกลัยโอบลาสโตมาแบบสามมิตีมีความสามารถในการต้านทานต่อสารต้านมะเร็งมากกว่า เซลล์ที่เพาะเลี้ยงในระบบสองมิติ

เพื่อทำความเข้าใจชีววิทยาของมะเร็งกลัยโอบลาสโตมา และเปิดเผยกลไกการดื้อต่อยาต้านมะเร็ง ดังนั้นในการศึกษานี้ได้ทำการตรวจสอบการแสดงออกของยีนแบบองค์รวมด้วยแบบแผนทางทรานสคริปโตมิกส์ และวิธีระดับโมเลกุลที่เกี่ยวข้องกับการดื้อยาของมะเร็งกลัยโอบลาสโตมาแบบสามมิตีที่สูงกว่าเซลล์ที่เพาะเลี้ยงในระบบสองมิติ โดยใช้เทคโนโลยีการวิเคราะห์ลำดับเบสยุคใหม่ด้วยเครื่อง Illumina HiSeq ผลการวิจัยพบว่า ยีนเซลล์มะเร็งกลัยโอบลาสโตมาแบบสามมิตีจำนวน 7,411 และ 3,915 ยีน มีการแสดงออกเพิ่มขึ้น และลดลงตามลำดับ เมื่อเทียบกับเซลล์มะเร็งกลัยโอบลาสโตมาที่เพาะเลี้ยงในระบบสองมิติ นอกจากนี้การวิเคราะห์จากฐานข้อมูลวิถี KEGG แสดงให้เห็นว่ายีนในวิถีวัฏจักรของเซลล์ และการจำลองตัวเองของดีเอ็นเอมีการแสดงออกลดลง ขณะที่ยีนในวิถี วิถีไมโทเจน-แอกทิเวเตดโปรตีนไคเนส, ออโตฟาจี, การเมแทบอลิซึมยา-ไซโตโครมพี 450 และ ABC ทรานสปอร์เตอร์ มีการแสดงออกเพิ่มมากขึ้น การเปลี่ยนแปลงการแสดงออกของยีนดังกล่าวนี้ทำให้เราเข้าใจกลไกที่เกี่ยวข้องกับการดื้อยาของมะเร็งกลัยโอบลาสโตมาได้ดียิ่งขึ้น จากผลการทดลองข้างต้นอาจสรุปได้ว่า โครงสร้างสามมิติแคลเซียม-อัลจินตสามารถเป็นแบบจำลองที่มีความเป็นไปได้สำหรับการศึกษามะเร็งเนื้อเยื่อระบบประสาทของมนุษย์ การคัดกรองยาต้านมะเร็ง และการระบุเป้าหมายใหม่ระดับโมเลกุล พร้อมทั้งต้นทุนต่ำ และง่ายต่อการใช้งาน

สาขาวิชาเทคโนโลยีชีวภาพ
ปีการศึกษา 2561

ลายมือชื่อนักศึกษา Nipha
ลายมือชื่ออาจารย์ที่ปรึกษา P. W.

NIPHA CHAICHAROENAUDOMRUNG : FABRICATION OF 3D CALCIUM-
ALGINATE SCAFFOLD CELL CULTURE SYSTEM AS A NERVE-TISSUE
CANCER MODEL FOR ANTICANCER DRUG STUDIES.

THESIS ADVISOR : ASST. PROF. PARINYA NOISA, Ph.D. 167 PP.

3D CALCIUM-ALGINATE SCAFFOLDS/ANTICANCER DRUGSCREENING/NERVE-
TISSUE CANCER MODEL/CORDYCEPIN/TRANSCRIPTOMIC

Nerve-tissue cancer, in particular glioblastoma and neuroblastoma, is a global challenge to human health. Besides, glioblastoma is the most aggressive type of brain malignancy and highly resistant to chemotherapy, with a median survival rate of 12-15 months for a newly diagnosed glioblastoma, and 5-7 months for recurrent glioblastoma. Cordycepin, a bioactive compound of *Cordyceps* ssp., has been revealed as a strong anti-cancer agent through several pathways under the traditional two-dimension (2D) *in vitro* cell culture condition. However, the mechanisms, by which cordycepin counteracts nerve-tissue cancer, is still poorly understood. In this study, the underlying mechanisms of cordycepin against human nerve-tissue cancer cell line were explored. Here, it was found that cordycepin inhibited cell growth and induced apoptosis in both U-251 glioblastoma and SH-SY5Y neuroblastoma cell lines through the mitochondrial-mediated intrinsic pathway and the modulation of autophagy. However, an emerging view finds that the traditional 2D cell culture may not accurately mimic the three-dimensional environment, in which cancer cells reside. The three-dimensional (3D) cell culture model has been increasingly used to study cancer biology and screen for anticancer agents due to its close mimicry to the *in vivo* tumor biopsies. Therefore, the 3D calcium (Ca)-alginate scaffolds were developed for glioblastoma cell culture and an examination of the responses to the anticancer agents, including temozolomide, doxorubicin and cordycepin. Compared to the 2D culture, glioblastoma cells cultured on the 3D Ca-alginate scaffolds showed reduced cell

proliferation, increased tumor spheroid formation, enhanced expression of cancer stem cell genes, and improved the expression of differentiation potential-associated genes. Additionally, the vascularization potential of the 3D glioblastoma cells was increased, as indicated by a higher expression of tumor angiogenesis biomarker than that of the cells in the 2D culture. Then, the 3D glioblastoma cells were treated with the anticancer agents, including temozolomide, doxorubicin, and cordycepin. The results demonstrated that the 3D glioblastomas presented a greater resistance to the tested anticancer agents than that of the cells in the 2D culture. Additionally, to understand this glioblastoma biology and reveal the mechanism of anticancer drugs resistance, the transcriptomic profiles and molecular pathways were analyzed using Next Generation Sequencing Illumina HiSeq technology. The data demonstrated that glioblastoma cells in the 3D Ca-alginate scaffolds exhibited higher resistance to anti-cancer drugs than the 2D condition. The results revealed that 7,411 and 3,915 genes of 3D glioblastoma were upregulated and downregulated, respectively as compared with the 2D monolayer glioblastoma culture. Further, the KEGG pathway analysis showed that the downregulated genes were mainly enriched in cell cycle and DNA replication pathways, while the upregulated genes were mainly enriched with MAPK signaling, autophagy, drug metabolism-cytochrome P450, and ABC transporter pathways. Such alterations of gene expression gave us a clue to better understand the related-mechanisms to anticancer drug resistance of human glioblastoma. Taken together, the 3D calcium-alginate scaffolds developed in this research could be a feasible platform for human nerve-tissue cancer study, anti-cancer drug screening, and novel molecular target identification with a low-cost and easy-to-use approach.

School of Biotechnology

Academic Year 2018

Student's Signature Nipha

Advisor's Signature P. S.

ACKNOWLEDGEMENT

I would like to thank my thesis advisor, Asst. Prof. Dr. Parinya Noisa for his invaluable help and constant encouragement throughout the course of this research. I am most grateful for his teaching and advice, not only the research methodologies but also many other methodologies in life. I would not have achieved this far and this thesis would not have been completed without all the support that I have always received from him.

In addition, I am grateful for the lecture at School of Biotechnology: Prof. Dr. Neung Teaumroong, Prof. Dr. Montarop Yamabhai, Associate prof. Dr. Mariena Ketudatcairns, Assoc. Prof. Dr. Chokchai Wanapu, Associate prof. Dr. Apichat Boontawan, Assoc. Prof. Dr. Kaemwich Jantama, Associate prof. Dr. Panlada Tittabutr for teaching and suggestions and all their help.

I would like to express my gratitude to the dissertation committee, Prof. Dr. Montarop Yamabhai, Asst. Prof. Dr. Paiboon Jitprasertwong, Dr. Pundit Asavaritikrai, and Asst. Prof. Dr. Areechun Sotthibundhu for their time, knowledge, comments and advices on my work.

I wish to thank my best friends in CBAI-Lab: Toon, Wi, Bom, Koy, Aoei and Ben for all their friendship, understanding and sharing the stressful moments, assistance and warm soiree. Also I am very grateful to the Suranaree University of Technology for granting me a scholarship during the course of my Doctoral studies and laboratory facilities support during my study me on their doctoral program. Finally, I would like to express my deepest gratitude to my parents, my uncle, and my brother for all their support throughout the period of this study.

CONTENTS

	Page
ABSTRACT IN THAI	I
ABSTRACT IN ENGLISH	III
ACKNOWLEDGEMENTS	V
CONTENTS	VI
LIST OF TABLES	XIII
LIST OF FIGURES	XIV
LIST OF ABBREVIATIONS	XVII
CHAPTER	
I INTRODUCTION	1
1.1 Rational and background	1
1.2 Research objectives	3
1.3 Research hypotheses	4
1.4 Scope of the study	4
1.5 Expected results	5
1.6 References	6
II LITERATURE REVIEW	9
2.1 Glioblastomas	9
2.2 Human glioblastoma cell line U-251	11
2.3 Neuroblastoma	11
2.4 Human neuroblastoma cell line SH-SY5Y	12
2.5 Cordycepin	12

CONTENTS (Continued)

	Page
2.6 Cell cultures as a research model.....	14
2.7 Two- versus three-dimensional cell culture models.....	16
2.8 Three-dimensional cell culture technologies.....	21
2.8.1 Multicellular spheroid formation.....	24
2.8.2 Hydrogels.....	25
2.8.3 Scaffolds.....	28
2.8.4 Three-dimensional bioprinting.....	30
2.9 Application of 3D cell culture.....	33
2.9.1 Cancer modelling.....	40
2.9.2 Stem cell modelling.....	45
2.5 References.....	50
III CORDYCEPIN INDUCES APOPTORIC CELL DEATH OF HUMAN BRAIN CANCER THROUGH THE MODULATION OF AUTOPHAGY.....	65
3.1 Abstract.....	65
3.2 Introduction.....	66
3.3 Materials and methods.....	67
3.3.1 Chemicals and reagents.....	67
3.3.2 Cell culture.....	67
3.3.3 MTT assay.....	68
3.3.4 Annexin V and 7-AAD staining.....	68
3.3.5 DAPI staining.....	68

CONTENTS (Continued)

	Page
3.3.6 RNA isolation and reverse transcription (RT)-PCR.....	69
3.3.7 Measurement of intracellular ROS generation.....	69
3.3.8 Immunofluorescence staining.....	70
3.3.9 Statistical analysis.....	71
3.4 Results.....	71
3.4.1 Cordycepin inhibited the growth of human neuroblastoma and glioblastoma cell lines.....	71
3.4.2 Cordycepin induced apoptotic cell death in human nerve-tissue cancer cells via caspase-dependent pathways.....	73
3.4.3 Cordycepin-induced apoptosis was involved the generation of ROS in human nerve-tissue cancer cells.....	75
3.4.4 Cordycepin induced autophagy in human nerve-tissue cancer cells.....	77
3.4.5 Autophagy involved in cordycepin-induced apoptosis of human nerve-tissue cancer cells.....	77
3.5 Discussion.....	81
3.6 Conclusion.....	86
3.7 References.....	87

CONTENTS (Continued)

	Page
IV FABRICATION OF 3D CALCIUM-ALGINATE SCAFFOLDS FOR HUMAN GLIOBLASTOMA MODELLING AND ANTICANCER DRUG RESPONSE EVALUATION	95
4.1 Abstract	95
4.2 Introduction	96
4.3 Materials and methods	99
4.3.1 Chemicals and reagents	99
4.3.2 Calcium-alginate scaffold fabrication and preparation	100
4.3.3 Ca-alginate scaffold characterization	100
4.3.4 Cell seeding on Ca-alginate scaffolds	101
4.3.5 Live/dead staining	101
4.3.6 Scanning electron microscopy	102
4.3.7 Cell proliferation analysis	102
4.3.8 Cell size distribution	102
4.3.9 Quantitative polymerase chain reaction quantification	103
4.3.10 Immunofluorescence staining	104
4.3.11 Combination of 3D U-251 and 2D hCMEC/D3	104
4.3.12 Cytotoxicity of anticancer agents	105
4.3.13 Statistical analysis	106
4.4 Results	106
4.4.1 Ca-alginate scaffold properties	108

CONTENTS (Continued)

	Page
4.4.2 Live/dead glioblastoma cells inside the Ca-alginate scaffolds.....	110
4.4.3 Characterization of U-251 glioblastoma cells inside the Ca-alginate scaffolds.....	112
4.4.4 Stemness, differentiation, proliferation, and angiogenesis properties of glioblastoma cells in both culture conditions.....	113
4.4.5 Characterization of combination 3D U-251 and 2D hCMEC/D3.....	115
4.4.6 Effect of anticancer agents on glioblastoma cells in both culture conditions.....	117
4.5 Discussion.....	120
4.6 Conclusion.....	127
4.7 References.....	127
V THE TRANSCRIPTOMIC PROFILES FOR IDENTIFICATION OF DRUG RESISTANCE-RELATED MECHANISMS OF HUMAN GLIOBLASTOMA CELL ON THE 3D CULTURE CONDITION EVALUATION.....	134
5.1 Abstract.....	134
5.2 Introduction.....	135
5.3 Materials and methods.....	136
5.3.1 Chemicals and reagents.....	136

CONTENTS (Continued)

	Page
5.3.2 Fabrication of porous scaffolds.....	137
5.3.3 Cell cultures.....	138
5.3.4 RNA extraction.....	138
5.3.5 RNA sequencing library construction.....	139
5.3.6 Quantification of gene expression level and differential expression analysis.....	140
5.3.7 Bioinformatics evaluation.....	140
5.3.8 Quantitative real time PCR (qRT-PCR) validation.....	141
5.3.9 Statistical analysis.....	141
5.4 Results.....	142
5.4.1 U-251 glioblastoma cell cultures.....	142
5.4.2 Transcriptome sequencing and mapping to the reference genome.....	143
5.4.3 Differential gene expression between 2D and 3D culture conditions.....	144
5.4.4 Differential gene GO enrichment analysis.....	146
5.4.5 KEGG pathway analysis of U-251 cells cultured under 2D and 3D conditions.....	149
5.5 Discussion.....	153
5.6 Conclusion.....	159
5.7 References.....	159
VI SUMMARY.....	165

CONTENTS (Continued)

	Page
BIOGRAPHY.....	167



LIST OF TABLES

Table	Page
2.1	Differences between 2D and 3D cell culture models.....19
2.2	Proposed advantages, disadvantages and research stage of different 3D cell culture methods.....22
2.3	Examples of three-dimensional research systems used for cancer and stem cell cancer studies.....34
3.1	The primer sequences used for RT-PCR.....69
4.1	The primer sequences used for real-time RT-PCR.....104
5.1	The primer sequences used for real-time RT-PCR.....142
5.2	Data quality, filtration and alignment summary for transcriptome of U-251 cells on 2D and 3D cultures condition.....145

LIST OF FIGURES

Figure	Page
2.1	Chemical structure of cordycepin.....13
2.2	Schematic diagrams of (a) the traditional 2D monolayer cell culture and (b) 3D cell culture systems. (c) The structure of a 3D spheroid with different cell zones.....21
2.3	Different techniques used for 3D cell culture tubules of the testes.....32
2.4	(a) Gene expression profiles of monolayer, P-MCTS (proliferative spheroids) and Q- MCTS (quiescent spheroids) models. (b) Gene Set Enrichment Analysis (GSEA) plots of hypoxia and cell-cycle progression gene sets.....42
2.5	Effect of Paclitaxel (PTX), doxorubicin (ADR), and 5-fluorouracil (5FU) on the cell growth of 2D- and 3D-cultured breast cancer cell lines44
2.6	Demonstration of morphology and localization of typical proteins in cardiac microtissues using different techniques.....48
2.7	Potential applications of 3 D cell culture systems.....49
3.1	Cordycepin inhibited cell viability of human nerve-tissue cancer cells.....72
3.2	Cordycepin induced apoptotic cell death of human nerve-tissue cancer cells.....74
3.3	Cordycepin-induced apoptosis associated with ROS generation in human nerve-tissue cancer cells.....76
3.4	Cordycepin induced autophagy in human nerve-tissue cancer cells by the upregulation of LC3I/II.....79

LIST OF FIGURES (Continued)

Figure	Page
3.5 Inhibition of autophagy promoted cordycepin-induced apoptosis in human nerve-tissue cancer cells.....	80
3.6 Diagram of catalytic reactions of the cooperative action of Superoxide dismutases (SOD), Catalase (CAT), glutathione peroxidases (GPX).....	85
4.1 Schematic illustration of the platform for drug screening of nerve-tissue cancer in the 3D human glioblastoma cell culture system.....	107
4.2 Ca-alginate scaffold morphology and properties.....	109
4.3 The influence of Ca-alginate scaffolds on glioblastoma stem cells U-251 viability before and after differentiation.....	111
4.4 Cell proliferation, spheroids size distribution, and morphology of glioblastoma spheroids.....	112
4.5 Gene expression levels and protein expression of glioblastoma U-251 cells growing on the 2D and inside the 3D Ca-alginate scaffolds.....	114
4.6 (a-c) Optical microscopy and (d-i) scanning electron microscopy of combined cultures of U-251 cultivated for 14 days in Ca-alginate scaffold and U-251 spheroid deposited on hCMEC/D3 endothelial cells on glass coverslips for 7 and 14 days.....	116
4.7 Immunofluorescence for VEGF and Collagen IV of combined 3D U-251 and 2D hCMEC/D3 culture after 14 days compared to each type of cells cultured in 2D monolayer and 3D U-251 alone.....	117
4.8 Glioblastoma cells responded to anticancer agents.....	119

LIST OF FIGURES (Continued)

Figure	Page
5.1 (a) Morphology of Ca-alginate scaffolds. (b) Disk-shaped of Ca-alginate scaffolds (c) SEM images of the Ca-alginate scaffold.....	137
5.2 Glioblastoma cells in 2D and 3D conditions for 14 days.....	143
5.3 Principal Component Analysis (PCA) chart.....	146
5.4 (a) Differential expression volcano plot (b) Bar graph of genes significantly up- or down-regulation between 2D and 3D conditions.....	147
5.5 Heatmap of gene expression in 2D and 3D culture condition for 14 days.....	148
5.6 GO enrichment histogram.....	150
5.7 Different expressed genes within pathways under 2D and 3D cell culture condition for 14 days.....	151
5.8 Gene expression of glioblastoma cells under 2D and 3D cell culture condition for 14 days.....	152

LIST OF ABBREVIATIONS

%	=	Percentage
(m, μ) g	=	(milli, micro) Gram
(m, μ) l	=	(milli, micro) Liter
(m, μ) mol	=	(milli, micro) Mole
$^{\circ}$ C	=	Degree Celsius
2D	=	Two-dimensional
3D	=	Three-dimensional
ABC	=	ATP-binding cassette
ABCA	=	ATP binding cassette subfamily A
ADH6	=	alcohol dehydrogenase 6 (class V)
ALDH	=	Aldehyde dehydrogenases
ANGPT2	=	angiopoietin 2
AOX1	=	aldehyde oxidase 1
ATG14	=	autophagy related 14
ATG9B	=	autophagy related 9B
BNIP3	=	BCL2/adenovirus E1B 19kDa interacting protein 3
BNIP3P1	=	BCL2/adenovirus E1B 19kDa interacting protein 3 pseudogene 1
BSA	=	Bovine serum albumin
BUB1	=	BUB1 mitotic checkpoint serine/threonine kinase
BUB3	=	BUB3 mitotic checkpoint protein
CACNA1A	=	calcium channel, voltage-dependent, P/Q type, alpha 1A subunit
CACNA1C	=	calcium channel, voltage-dependent, L type, alpha 1C subunit

LIST OF ABBREVIATIONS (Continued)

<i>CACNA1D</i>	=	calcium channel, voltage-dependent, L type, alpha 1D subunit
<i>CACNA2D2</i>	=	calcium channel, voltage-dependent, alpha 2/delta subunit 2
<i>CACNB1</i>	=	calcium channel, voltage-dependent, beta 1 subunit
<i>CACNB2</i>	=	calcium channel, voltage-dependent, beta 2 subunit
<i>CACNB3</i>	=	calcium channel, voltage-dependent, beta 3 subunit
<i>CACNB4</i>	=	calcium channel, voltage-dependent, beta 4 subunit
<i>CAMKK1</i>	=	calcium/calmodulin-dependent protein kinase kinase 1, alpha
<i>CCNA1</i>	=	cyclin A2
<i>CCNB2</i>	=	cyclin B2
<i>CCNB3</i>	=	cyclin B3
<i>CCND1</i>	=	cyclin D1
<i>CCNE1</i>	=	cyclin E1
<i>CCNH</i>	=	cyclin H
<i>CD14</i>	=	CD14 molecule
<i>CDC14</i>	=	cell division cycle 14B
<i>CDC20</i>	=	cell division cycle 20
<i>CDC25A</i>	=	cell division cycle 25A
<i>CDC25B</i>	=	cell division cycle 25B
<i>CDC25C</i>	=	cell division cycle 25C
<i>CDC45</i>	=	cell division cycle 45
<i>CDC6</i>	=	cell division cycle 6
<i>CDC7</i>	=	cell division cycle 7
<i>CDK1</i>	=	cyclin dependent kinase 1
<i>CDK2</i>	=	cyclin dependent kinase 2

LIST OF ABBREVIATIONS (Continued)

<i>CDK4</i>	=	cyclin dependent kinase 4
<i>CHEK1</i>	=	checkpoint kinase 1
CPD	=	Critical-point drying
<i>CTSD</i>	=	cathepsin D
<i>CTSD</i>	=	cathepsin D
CYP	=	Cytochrome
<i>CYP11A1</i>	=	cytochrome P450, family 11, subfamily A, polypeptide 1
<i>CYP1A1</i>	=	cytochrome P450, family 1, subfamily A, polypeptide 1
<i>CYP1B1</i>	=	cytochrome P450, family 1, subfamily B, polypeptide 1
<i>CYP26A1</i>	=	cytochrome P450, family 26, subfamily A, polypeptide 1
<i>CYP2A6</i>	=	cytochrome P450, family 2, subfamily A, polypeptide 6
<i>CYP2D6</i>	=	cytochrome P450, family 2, subfamily D, polypeptide 6
<i>CYP2D8P</i>	=	cytochrome P450, family 2, subfamily D, polypeptide 8, pseudogene
<i>CYP2E1</i>	=	cytochrome P450, family 2, subfamily E, polypeptide 1
<i>CYP2G1P</i>	=	cytochrome P450, family 2, subfamily G, polypeptide 1 pseudogene
<i>CYP2W1</i>	=	cytochrome P450, family 2, subfamily W, polypeptide 1
<i>CYP3A5</i>	=	cytochrome P450, family 3, subfamily A, polypeptide 5
<i>CYP4V2</i>	=	cytochrome P450, family 4, subfamily V, polypeptide 2
DAPI	=	4,6-diamidino-2-phenylindole
DCFH-DA	=	2'7'-dichlorodihydrofluorescein diacetate
<i>DDIT3</i>	=	DNA-damage-inducible transcript 3
<i>DDIT4</i>	=	DNA-damage-inducible transcript 4
DEGs	=	Differentially expressed genes
DMSO	=	Dimethyl sulfoxide

LIST OF ABBREVIATIONS (Continued)

<i>DNA2</i>	=	DNA replication ATP-dependent helicase Dna2
<i>DUSP3</i>	=	dual specificity phosphatase 3
<i>E2F1</i>	=	E2F transcription factor 1
<i>E2F2</i>	=	E2F transcription factor 2
<i>E2F3</i>	=	E2F transcription factor 3
<i>E2F4</i>	=	E2F transcription factor 4, p107/p130-binding
<i>E2F4</i>	=	E2F transcription factor 4
EDTA	=	Ethylenediaminetetraacetic acid
<i>EFNA1</i>	=	ephrin-A1
<i>EFNA3</i>	=	ephrin-A3
<i>ESPL1</i>	=	extra spindle pole bodies like 1
FBS	=	Fetal bovine serum
FDR	=	False discovery rate
<i>FEN1</i>	=	flap endonuclease-1
<i>FGF19</i>	=	fibroblast growth factor 19
<i>FLNB</i>	=	filamin B, beta
<i>FLT3LG</i>	=	fms-related tyrosine kinase 3 ligand
<i>FOS</i>	=	FBJ murine osteosarcoma viral oncogene homolog
FPKM	=	Frackments per kilobase of target transcript length per million reads mapped
<i>GAPDH</i>	=	Glyceraldehyde-3-phosphate dehydrogenase
<i>GFAP</i>	=	Glial fibrillary acidic protein
GO	=	Gene ontology
GST	=	Glutathione S-transferase

LIST OF ABBREVIATIONS (Continued)

<i>GSTM2</i>	=	glutathione S-transferase mu 2 (muscle)
<i>GSTM5</i>	=	glutathione S-transferase mu 5
<i>GSTO2</i>	=	glutathione S-transferase omega 2
<i>GSTP1</i>	=	glutathione S-transferase pi 1
<i>GSTT2</i>	=	glutathione S-transferase theta 2 (gene/pseudogene)
<i>GSTTP2</i>	=	glutathione S-transferase theta pseudogene 2
h	=	Hour
<i>HGF</i>	=	hepatocyte growth factor (hepapoietin A; scatter factor)
IC ₅₀	=	Half maximal "Inhibitory Concentration"
<i>IL1A</i>	=	interleukin 1, alpha
<i>INSRR</i>	=	insulin receptor-related receptor
<i>IRS2</i>	=	Insulin Receptor Substrate 2
<i>ITPR1</i>	=	inositol 1,4,5-trisphosphate receptor, type 1
<i>ITPR1-AS1</i>	=	ITPR1 antisense RNA 1 (head to head)
<i>JUN</i>	=	jun proto-oncogene
<i>JUND</i>	=	jun D proto-oncogene
KEGG	=	Kyoto Encyclopedia of Genes and Genomes
M	=	Molar
<i>MAP3K12</i>	=	mitogen-activated protein kinase kinase kinase 12
MAPK	=	A mitogen-activated protein kinase
<i>MAPK10</i>	=	mitogen-activated protein kinase 10
<i>MAPK10</i>	=	mitogen-activated protein kinase 10
<i>MAPK7</i>	=	mitogen-activated protein kinase 7
<i>MAPK8IP2</i>	=	mitogen-activated protein kinase 8 interacting protein 2

LIST OF ABBREVIATIONS (Continued)

<i>MAPK8IP3</i>	=	mitogen-activated protein kinase 8 interacting protein 3
<i>MAPT</i>	=	microtubule-associated protein tau
<i>MCM2</i>	=	minichromosome maintenance complex component 2
<i>MCM2</i>	=	minichromosome maintenance complex component 2
<i>MCM3</i>	=	minichromosome maintenance complex component 3
<i>MCM4</i>	=	minichromosome maintenance complex component 4
<i>MCM4</i>	=	minichromosome maintenance complex component 4
<i>MCM6</i>	=	minichromosome maintenance complex component 6
<i>MCM7</i>	=	minichromosome maintenance complex component 7
<i>MCM7</i>	=	minichromosome maintenance complex component 7
min	=	Minute
MTT	=	3-(4,5-dimethylthiazol-2-yl)-2,5-diphenyl tetrazolium bromide
<i>MYC</i>	=	v-myc avian myelocytomatosis viral oncogene homolog
NAC	=	N-acetyl-L-cysteine
<i>NF1</i>	=	neurofibromin 1
<i>NFKB2</i>	=	nuclear factor of kappa light polypeptide gene enhancer in B-cells 2 (p49/p100)
<i>NGFR</i>	=	nerve growth factor receptor
<i>NR4A1</i>	=	nuclear receptor subfamily 4, group A, member 1
<i>NTF4</i>	=	neurotrophin 4
<i>ORC1</i>	=	origin recognition complex, subunit 1
<i>ORC3</i>	=	origin recognition complex, subunit 3
<i>ORC5</i>	=	origin recognition complex, subunit 5
<i>ORC6</i>	=	origin recognition complex, subunit 6

LIST OF ABBREVIATIONS (Continued)

<i>PBS</i>	=	Phosphate buffered saline
<i>PCA</i>	=	Principal Component Analysis
<i>PCNA</i>	=	proliferating cell nuclear antigen
<i>PCNA</i>	=	proliferating cell nuclear antigen
<i>PCR</i>	=	Polymerase chain reaction
<i>PI</i>	=	Propidium iodide
<i>PKMYT1</i>	=	protein kinase, membrane associated tyrosine/threonine 1
<i>PKMYT1</i>	=	protein kinase, membrane associated tyrosine/threonine 1
<i>PLA2G4D</i>	=	phospholipase A2, group IVD (cytosolic)
<i>PLK1</i>	=	polo like kinase 1
<i>POLA1</i>	=	DNA polymerase alpha subunit A
<i>POLA1</i>	=	DNA polymerase alpha subunit B
<i>POLD1</i>	=	polymerase (DNA directed), delta 1, catalytic subunit
<i>POLD2</i>	=	polymerase (DNA directed), delta 2, accessory subunit
<i>POLD3</i>	=	polymerase (DNA-directed), delta 3, accessory subunit
<i>POLE</i>	=	polymerase (DNA directed), epsilon, catalytic subunit
<i>POLE2</i>	=	polymerase (DNA directed), epsilon 2, accessory subunit
<i>POLE3</i>	=	polymerase (DNA directed), epsilon 3, accessory subunit
<i>PRIM1</i>	=	primase, DNA, polypeptide 1
<i>PRIM2</i>	=	primase, DNA, polypeptide 2
<i>PRKCG</i>	=	protein kinase C, gamma
<i>PRKDC</i>	=	protein kinase, DNA-activated, catalytic polypeptide
<i>PTPRR</i>	=	protein tyrosine phosphatase, receptor type, R
<i>PTPRR</i>	=	protein tyrosine phosphatase, receptor type, R

LIST OF ABBREVIATIONS (Continued)

<i>RAD21</i>	=	RAD21 cohesin complex component
<i>RASGRP1</i>	=	RAS guanyl releasing protein 1 (calcium and DAG- regulated)
<i>RASGRP2</i>	=	RAS guanyl releasing protein 2 (calcium and DAG- regulated)
<i>RASGRP3</i>	=	RAS guanyl releasing protein 3 (calcium and DAG- regulated)
<i>RB1</i>	=	RB transcriptional corepressor 1
<i>RB1</i>	=	retinoblastoma 1
<i>RBL1</i>	=	RB transcriptional corepressor like 1
<i>RELB</i>	=	v-rel avian reticuloendotheliosis viral oncogene homolog B
<i>RFC1</i>	=	replication factor C (activator 1) 1
<i>RFC2</i>	=	replication factor C (activator 1) 2
<i>RFC3</i>	=	replication factor C (activator 1) 3
<i>RNASEH1</i>	=	ribonuclease H1
<i>RNASEH2A</i>	=	ribonuclease H2, subunit A
<i>RNASEH2B</i>	=	ribonuclease H2, subunit B
<i>RPA1</i>	=	replication protein A1
<i>RPA2</i>	=	replication protein A2
<i>RPA3</i>	=	replication protein A3
rpm	=	Revolution per minute
<i>RPTOR</i>	=	regulatory associated protein of MTOR, complex 1
<i>RRAGB</i>	=	Ras-related GTP binding B
<i>RRAGD</i>	=	Ras-related GTP binding D
<i>RRAGD</i>	=	Ras Related GTP Binding D
<i>RRAS</i>	=	related RAS viral (r-ras) oncogene homolog
<i>RRAS</i>	=	related RAS viral (r-ras) oncogene homolog

LIST OF ABBREVIATIONS (Continued)

<i>SEM</i>	=	Scanning Electron Microscope
<i>SFN</i>	=	stratifin
<i>SHCBP1 G</i>	=	SHC SH2-domain binding protein 1
<i>SKP2</i>	=	S-phase kinase-associated protein 2, E3 ubiquitin protein ligase
<i>SKP2</i>	=	S-phase kinase associated protein 2
<i>SMC1A</i>	=	structural maintenance of chromosomes 1A
<i>SMC3</i>	=	structural maintenance of chromosomes 3
<i>SYNGR1</i>	=	synaptogyrin 1
<i>TEK</i>	=	TEK tyrosine kinase, endothelial
<i>TFDP1</i>	=	transcription factor Dp-1
<i>TFDP1</i>	=	transcription factor Dp-1
<i>TFDP2</i>	=	transcription factor Dp-2
<i>TFDP2</i>	=	transcription factor Dp-2
<i>TGFA</i>	=	transforming growth factor, alpha
<i>TGFB2</i>	=	transforming growth factor, beta 2
<i>TGFB3</i>	=	transforming growth factor, beta 3
<i>TP53</i>	=	tumor protein p53
<i>TSC1</i>	=	tuberous sclerosis 1
<i>VEGFA</i>	=	vascular endothelial growth factor A
<i>VEGFB</i>	=	vascular endothelial growth factor B
<i>WIP11</i>	=	WD repeat domain, phosphoinositide interacting 1

CHAPTER I

INTRODUCTION

1.1 Rational and background

Glioblastoma is the most aggressive malignant primary human nerve-tissue cancer, originating from either glial cells or their precursors (Behin et al., 2003). Patients suffering from glioblastoma have a poor prognosis with a median survival rate of only 12-15 months for a newly diagnosed glioblastoma and 5-7 months for recurrent glioblastoma (Johnson and O'Neill, 2012). Another nerve-tissue cancer is neuroblastoma that is the most predominant extracranial solid cancer in infancy and childhood (Brodeur, 2003). Despite the remarkable advances in glioblastoma and neuroblastoma therapy, such as neurosurgery, radiotherapy, and chemotherapy, the low median survival period is still a burden to society (Maris, 2010; Ohgaki and Kleihues, 2005). To date, anticancer agents extracted from natural sources have been widely applied to prevent and cure cancers (Mehta et al., 2010). Cordycepin, a major bioactive component found in insect fungus, *Cordyceps* spp., exhibits significant anticancer potential (Tuli et al., 2013). Cordycepin is a derivative of the nucleoside adenosine and the biological function of it has been elucidated for its anti-tumor, anti-inflammatory, anti-proliferation, anti-migration, apoptosis induction, and autophagy promotion in several disease models (Choi et al., 2014; Kondrashov et al., 2012; Li et al., 2015; Liao et al., 2015; Nakamura et al., 2006; Wang et al., 2015). Although the anticancer activity of cordycepin has been tested in human glioblastoma and neuroblastoma cell lines (Baik et al., 2015; Li et al., 2015), the underlying mechanisms of cordycepin to encounter human glioblastomas and neuroblastomas have not yet been clearly explicated. In this study, the therapeutic effects of cordycepin on human nerve-tissue cancer cell lines were

investigated, where its mechanisms of action were explored under traditional 2D *in vitro* model.

However, the traditional 2D cell culture cannot accurately simulate the 3D environment in which cancer cells reside within the body. Since *in vivo* cells are encompassed by other cells and an extracellular matrix (ECM) in the 3D model, 2D cell culture does not sufficiently reflect the natural 3D environment of the cells. Hence, there is a growing demand for developing 3D *in vitro* tumor models, which can simulate the tumor microenvironment, mimic *in vivo* cell behaviors, and provide comparable results to *in vivo* assays. In addition, 3D *in vitro* models have the potential to bridge the gap between traditional 2D cultures and animal models (Pampaloni et al., 2007). Over the past few decades, sodium alginate has been used as a biomaterial in tissue engineering (Wang et al., 2003). Alginate is approved by the Food and Drug Administration (FDA) for broad tissue engineering applications because of its biocompatibility, biodegradability, and limited immunogenicity (Rinaudo, 2008). Alginate is a family of natural polysaccharides composed of different lengths of G (α -L-glucuronate), M (β -D-mannuronate), and GM alternating blocks. Alginate can form noncovalent crosslinks through interaction with bivalent metal ions, such as calcium ions (Shull, 2012). Hydrophilic alginate hydrogels have been used as an artificial ECM to provide temporary support for many kinds of cell types, including chondrocytes (Awad et al., 2004), osteoblasts (Kuo and Ma, 2001), fibroblasts (Hunt et al., 2010), and embryonic stem cells (Hwang et al., 2009). Alternatively, alginate scaffolds can be generated through a freeze-drying process (Shapiro and Cohen, 1997). The porosity and pore interconnectivity of alginate scaffolds benefits the exchange of oxygen and nutrients, and waste elimination from the cells. Nowadays, Life Technologies Corporation Company commercially provide AlgiMatrix™ alginate scaffolds, for 3D culture for various cell type, including human embryonic stem cells (Gerecht et al., 2004), human osteoblast (Chen et al., 2015), non-small cell lung cancer

(NSCLC) (Godugu et al., 2013) U87 glioblastoma and C6 glioma cell lines (Sams et al., 2009). Therefore, in this study, I modified 3D Ca-alginate scaffolds via a freeze-drying technique and applied this to human glioblastoma cell lines (U-251). The growth characteristics, stemness, and differentiation properties of cells in the Ca-alginate scaffold system were verified, in comparison with the 2D monolayer platform for screening new anti-glioblastoma agents, the sensitivity of anticancer agents (temozolomide, doxorubicin and cordycepin) on glioblastoma cell line in the 3D Ca-alginate scaffolds was evaluated and compared to the cells in 2D culture. Additionally, to understand this glioblastoma biology and reveal the mechanism of resistant to anti-cancer drugs, transcriptomic profiles and molecular pathways that related glioblastoma in 3D Ca-alginate scaffolds higher resistance to anti-cancer drugs than 2D condition were analyzed by using Next Generation Sequencing Illumina HiSeq technology. Taken together, 3D Ca-alginate scaffolds can be cost-effective, low-cost, easy-to-use method, availability, suitability, reproducibility and can also practical in anti-glioblastoma drug screening, and novel molecular target identification for the treatment of human glioblastoma.

1.2 Research objectives

The primary objectives of this study were:

1. To assess the potential of cordycepin on inducing apoptosis and/or autophagy in U-251 human glioblastoma and SH-SY5Y human neuroblastoma cell lines, and the mechanisms of its action under the traditional 2D *in vitro* model.
2. To develop the 3D calcium-alginate scaffold cell culture system for U-251 human glioblastoma cell lines and verify the growth characteristics, proliferation, cancer stemness, and differentiation potential of the cell in the 3D Ca-alginate scaffold system.

3. To investigate the sensitivity of anti-cancer agents (*i.e.* temozolomide doxorubicin, and cordycepin) of glioblastoma cell line in the 3D Ca-alginate scaffolds and 2D culture system.

4. To explore the transcriptomic profiles in order to the identification of drug resistance-related mechanisms of U-251 human glioblastoma cell lines on the 3D Ca-alginate scaffolds.

1.3 Research hypotheses

In this study, I hypothesized that cordycepin contains a chemotherapeutic potential against human nerve-tissue cancer, and its action is via the induction of apoptosis cell death and autophagy modulation. Moreover, the 3D scaffolds can be fabricated from Ca-alginate via freeze-dry techniques, and used to support U-251 human glioblastoma cell growth. U-251 cells in the 3D Ca-alginate scaffolds can proliferate, retain characteristics of cancer stem cells, and improve their differentiation potential. Moreover, the resistance of U-251 cells against anti-cancer agents in the 3D Ca-alginate scaffolds is postulated to be higher than that of the cells in 2D culture system due to the increase of cell-cell and cell-ECM interactions. Finally, the underlying mechanisms associated with drug resistance of 3D Ca-alginate human glioblastoma could be approached by using Next Generation Sequencing.

1.4 Scope of this study

The cell viability and apoptosis cell death of U-251 and SH-SY5Y cells after treated with cordycepin will be determined under the traditional 2D *in vitro* model. The effect of cordycepin on the expression of gene related to apoptosis pathways in U-251 and SH-SY5Y cell lines will be determined by using RT-PCR. Then, the effect of cordycepin on the autophagy in U-251 and SH-SY5Y cell lines and the relationship between cordycepin-induced apoptosis with autophagy will be investigated via the expression of gene and

protein related to autophagy pathways by using RT-PCR and immunofluorescent assay, respectively. Moreover, the 3D Ca-alginate scaffolds for U-251 cell culture will be fabricated by using freeze-drying technique and U-251 cell lines will be cultured in the 3D Ca-alginate scaffolds. The growth characteristics, cancer stemness, and differentiation potential of the cells in the 3D Ca-alginate scaffolds will be evaluated, compared with the 2D culture system. Consequently, the sensitivity of cells in the 3D Ca-alginate scaffolds against the anti-cancer agents (*i.e.* temozolomide and cordycepin) will be compared with the cells in 2D culture condition. Finally, the drug resistance-related mechanisms of the glioblastoma cell line between 3D Ca-alginate scaffolds and 2D culture system will be explored by Next Generation Sequencing.

1.5 Expected results

Cordycepin could induces apoptotic cell death and/or autophagic activation in U-251 human glioblastoma and SH-SY5Y human neuroblastoma cell lines, and understand the mechanism of cordycepin on glioblastoma and neuroblastoma cell lines. In addition, the 3D scaffolds can be fabricated from Ca-alginate and used to support U-251 cell growth. U-251 cell lines in the 3D Ca-alginate scaffolds can support cell proliferation, retain characteristics of cancer stem cells, as well as establish cell differentiation potential. The resistance of U-251 cell line in the 3D culture system to anticancer agents (*i.e.* temozolomide and cordycepin) is expected to be higher than that of the 2D culture system due to the increase of cell-to-cell and cell-to-ECM interactions. The mechanisms associated with anti-glioblastoma drug resistance can be approached by using this 3D cell culture system with Next Generation Sequencing. Taken together, the 3D Ca-alginate scaffolds contain the high potential to serve as a powerful platform for glioblastoma study, anti-glioblastoma drug screening, and novel molecular target identification for the treatment of human glioblastoma.

1.6 References

- Awad, H. A., Wickham, M. Q., Leddy, H. A., Gimble, J. M., and Guilak, F. (2004). Chondrogenic differentiation of adipose-derived adult stem cells in agarose, alginate, and gelatin scaffolds. **Biomaterials**. 25(16): 3211-3222.
- Baik, J., Mun, S., Kim, K., et al. (2015). Apoptotic Effects of Cordycepin through the Extrinsic Pathway and p38 MAPK Activation in Human Glioblastoma U87MG Cells. **Journal of microbiology and biotechnology**. 26(2): 309-314.
- Behin, A., Hoang-Xuan, K., Carpentier, A. F., and Delattre, J.-Y. (2003). Primary brain tumours in adults. **The Lancet**. 361(9354): 323-331.
- Brodeur, G. M. (2003). Neuroblastoma: biological insights into a clinical enigma. **Nature reviews cancer**. 3(3): 203.
- Chen, C.-Y., Ke, C.-J., Yen, K.-C., et al. (2015). 3D porous calcium-alginate scaffolds cell culture system improved human osteoblast cell clusters for cell therapy. **Theranostics**. 5(6): 643.
- Choi, Y. H., Kim, G.-Y., and Lee, H. H. (2014). Anti-inflammatory effects of cordycepin in lipopolysaccharide-stimulated RAW 264.7 macrophages through Toll-like receptor 4-mediated suppression of mitogen-activated protein kinases and NF- κ B signaling pathways. **Drug design, development and therapy**. 8: 1941.
- Gerecht, S., Cohen, S., Ziskind, A., and Itskovitz-Eldor, J. (2004). Three-dimensional porous alginate scaffolds provide a conducive environment for generation of well-vascularized embryoid bodies from human embryonic stem cells. **Biotechnology and bioengineering**. 88(3): 313-320.
- Godugu, C., Patel, A. R., Desai, U., et al. (2013). AlgiMatrix™ based 3D cell culture system as an in-vitro tumor model for anticancer studies. **Plos one**. 8(1): 53708.
- Hunt, N., Smith, A. M., Gbureck, U., Shelton, R., and Grover, L. (2010). Encapsulation of fibroblasts causes accelerated alginate hydrogel degradation. **Acta Biomaterialia**.

termination of chain elongation. This activity has been well described *in vitro* with purified RNA polymerases and poly(A) polymerases from a number of organisms, including yeast and mammals (Müller et al., 1977). Cordycepin has also demonstrated various properties, such as antitumor (Nakamura et al., 2006), anti-fungal (Sugar and McCaffrey, 1998), anti-bacterial (Ahn et al., 2000) and anti-inflammatory effects (Jeong et al., 2010).

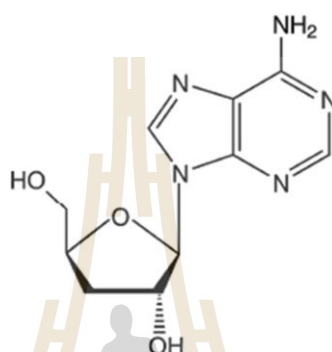


Figure 2.1 Chemical structure of cordycepin. Cordycepin, or 3'-deoxyadenosine, is a derivative of the nucleoside adenosine extracted from *Cordyceps* spp. **Source:** Lee et al. (2014)

Besides, several studies have shown that cordycepin has many anticancer activities, such as inhibition of cell proliferation, inhibition of cell migration, induction of apoptosis and autophagy (Choi et al., 2011; Li et al., 2015; Tao et al., 2016). Previous studies have reported that cordycepin inhibits cell growth in NB-4 and U937 leukemia cells by inducing DNA damage initiates cell cycle arrest and apoptosis through increasing the expression of p53 which promotes the release of cytochrome c from mitochondria to the cytosol and then cytochrome c can activate caspase-9 and trigger intrinsic apoptosis (Liao et al., 2015). Furthermore, Lee et al. (2013) reported that the apoptotic effects of cordycepin in human prostate PC-3 cells. It was demonstrated that cordycepin induced apoptosis through the generation of reactive oxygen species (ROS) in mitochondrial death pathway in human prostate PC-3 cells. On the other hand, Wang et al. (2015) reported that cordycepin reduced intracellular ROS levels- induced inhibition of osteogenesis in human bone marrow

6(9): 3649-3656.

Hwang, Y.-S., Cho, J., Tay, F., et al. (2009). The use of murine embryonic stem cells, alginate encapsulation, and rotary microgravity bioreactor in bone tissue engineering. **Biomaterials**. 30(4): 499-507.

Johnson, D. R., and O'Neill, B. P. (2012). Glioblastoma survival in the United States before and during the temozolomide era. **Journal of neuro-oncology**. 107(2): 359-364.

Kondrashov, A., Meijer, H. A., Barhet-Barateig, A., et al. (2012). Inhibition of polyadenylation reduces inflammatory gene induction. **Rna**. 18(12): 2236-2250.

Kuo, C. K., and Ma, P. X. (2001). Ionically crosslinked alginate hydrogels as scaffolds for tissue engineering: part 1. Structure, gelation rate and mechanical properties. **Biomaterials**. 22(6): 511-521.

Li, Y., Li, R., Zhu, S., et al. (2015). Cordycepin induces apoptosis and autophagy in human neuroblastoma SK-N-SH and BE (2)-M17 cells. **Oncology letters**. 9(6): 2541-2547.

Liao, Y., Ling, J., Zhang, G., et al. (2015). Cordycepin induces cell cycle arrest and apoptosis by inducing DNA damage and up-regulation of p53 in Leukemia cells. **Cell cycle**. 14(5): 761-771.

Maris, J. M. (2010). Recent advances in neuroblastoma. **New England Journal of Medicine**. 362(23): 2202-2211.

Mehta, R. G., Murillo, G., Naithani, R., and Peng, X. (2010). Cancer chemoprevention by natural products: how far have we come? **Pharmaceutical research**. 27(6): 950-961.

Nakamura, K., Yoshikawa, N., Yamaguchi, Y., et al. (2006). Antitumor effect of cordycepin (3'-deoxyadenosine) on mouse melanoma and lung carcinoma cells involves adenosine A3 receptor stimulation. **Anticancer research**. 26(1A): 43-47.

- Ohgaki, H., and Kleihues, P. (2005). Epidemiology and etiology of gliomas. **Acta neuropathologica**. 109(1): 93-108.
- Pampaloni, F., Reynaud, E. G., and Stelzer, E. H. (2007). The third dimension bridges the gap between cell culture and live tissue. **Nature reviews Molecular cell biology**. 8(10): 839.
- Rinaudo, M. (2008). Main properties and current applications of some polysaccharides as biomaterials. **Polymer International**. 57(3): 397-430.
- Sams, A., Zhensheng, L., Richard, F., Chao, Y. L., and Mark, P. (2009). The Application of Alginate Scaffolds for Three-Dimensional Cell Culture. **Invitrogen Corporation**. 1600 Faraday Avenue, Carlsbad, California 92008, USA.
- Shapiro, L., and Cohen, S. (1997). Novel alginate sponges for cell culture and transplantation. **Biomaterials**. 18(8): 583-590.
- Shull, K. R. (2012). Materials science: A hard concept in soft matter. **Nature**. 489(7414): 36-37.
- Tuli, H. S., Sharma, A. K., Sandhu, S. S., and Kashyap, D. (2013). Cordycepin: a bioactive metabolite with therapeutic potential. **Life sciences**. 93(23): 863-869.
- Wang, Shelton, R., Cooper, P., et al. (2003). Evaluation of sodium alginate for bone marrow cell tissue engineering. **Biomaterials**. 24(20): 3475-3481.
- Wang, Yin, P., Lu, Y., et al. (2015). Cordycepin prevents oxidative stress-induced inhibition of osteogenesis. **Oncotarget**. 6(34): 35496.

CHAPTER II

LITERATURE REVIEW

2.1 Glioblastomas

Glioma is a tumor that arises from supportive tissues of the brain glia and can originate in all types of glial cells. Astrocytoma, for example, is one type of glioma that originates in star-shaped brain cells called astrocytes. For the diagnosis and grading of glioma, the standard criteria used by pathologists and neuropathologists were defined in the 2007 version of the WHO classification based on degrees of malignancy and histologic diagnosis (Louis et al., 2007). Astrocytoma is therefore systemically graded according to such criteria, in order to describe their degree of abnormality and aggressiveness. WHO graded tumor ranging from grade I to grade IV, commonly based on a feature of the increase of malignancy along with the presence, the degree of a structural abnormality in a cell, and mitotic activity (Cahill et al., 2015). Regarding that grading system, grade I gliomas are considered to be benign and can possibly be removed by complete surgical excision. Grade II gliomas are often considered “low-grade” since the label “benign” fails to reflect the recurrence tumors (Louis et al., 2016; Siegel et al., 2017). Grade II glioma patients need to be continuously monitored by MRI or CT scan every 6-12 months for observation of tumor recurrence (Dolecek et al., 2012; Holland, 2000). The term “malignant” or “high-grade” is referred to both grade III and IV gliomas with high recurrence rates and the management of these tumors is similar (Omuro and DeAngelis, 2013). Anaplastic astrocytomas, classified as grade III gliomas, are diffuse infiltrating neoplasms that present the spreading of abnormal irregular shape of cells and the increase of proliferation and growth compared to grade I and II gliomas (Louis et al., 2016). Glioblastomas (GBM), the top grade astrocytoma ranking as grade IV gliomas, are the most

malignant form of astrocytoma. The unique histologic characteristics that can be used to separate glioblastoma from all others are the appearance of necrosis (dead cells) and the increase of abnormal and dysfunctional blood vessels around the tumor (Dolecek et al., 2012; Louis et al., 2007).

The updated 2016 version of the World Health Organization classification has incorporated molecular information into the diagnostic system (Louis et al., 2016). The diagnosis of central nervous system (CNS) tumors is made by characterizing the physical feature and growth rates as well as genetic properties. The use of integrated genotypic and phenotypic criteria for CNS tumor category offers a narrower degree of purpose and more defined diagnostic entities than the previous classifications, which in turn should lead to better diagnostic accuracy as well as improve patient administration. Currently, WHO grade III anaplastic astrocytomas are divided into isocitrate dehydrogenase (IDH)-mutant and IDH-wild type. IDH-wild type of Grade III gliomas could be considered as pre-glioblastomas, with a poorer prognosis than that of IDH mutant gliomas (Arevalo et al., 2017). Generally, the brain tumor patient with age between 20 and 40 years tended to own IDH mutations instead of the wild type. Plus, approximately 70% of IDH-mutated gliomas are related to tumors of the frontal lobe and are located there (Louis et al., 2016).

For glioblastoma, histologically diagnostic criteria such as mitotic activity, microvascular proliferation and necrotic areas were similar in both primary and secondary glioblastoma causing the difficulty of distinction (Louis et al., 2007). Glioblastomas usually occur in adult patients with age around 60 years and disproportionately occur in men (male: female ratio 3:2). A median survival rate was about 1 year, which had an incidence of 3.19 per 100,000 people, and represented 16% of all primary brain cancers (Dolecek et al., 2012; Holland, 2000). Maximal possible surgery was recommended to reduce the symptoms from

mass effect, improve survival rate, and increase the efficacy of adjuvant chemotherapeutic therapies (Stummer et al., 2011).

2.2 Human glioblastoma cell line U-251

The U-251 cell line as established at the Wallenberg laboratory, Uppsala, Sweden, almost more than 40 years ago along with several other cell lines derived from human gliomas, and was derived from a male patient with malignant astrocytoma (Ponten and Westermark, 1978; Westermark et al., 1973). U-251 glioblastoma cell line has been widely used as a glioblastoma model for drug screening and molecular target identification (Feng et al., 2012). Bryukhovetskiy et al. (2016) studied the ability of glioblastoma cells to attract various tissue-specific human stem cells, and to compare normal and cancer stem cells. U-251 cell line human has been used for the extraction of cancer stem cells from U-251 human glioblastoma cell line. Fang et al. (2016) studies the role of JARID1B (jumonji AT-rich interactive domain 1B) in the pathogenesis of glioma by used U-251 cells. Moreover, Verreault et al. (2015) studies the therapeutic efficacy of irinophore C combined with temozolomide in U-251 glioblastoma tumor model. Cancer stem cells from U-251 human glioblastoma cell line were extract to study the mechanism of Pax6 (paired box protein)-associated increase in expression of Dkk3 (Dickkopf 3) (Forsdahl et al., 2014). In addition, U-251 cell line has been used to study the novel approach for the treatment of glioblastoma by the inhibiting of vasculogenesis and prevention of recurrence of glioblastoma after irradiation (Kioi et al., 2010).

2.3 Neuroblastoma

Neuroblastoma is an embryonal tumor of the autonomic nervous system, meaning that the cell of origin is thought to be a developing and incompletely committed precursor cell derived from neural-crest tissues (Hoehner et al., 1996). As may be expected with a disease of developing tissues, neuroblastomas generally occur in very young children; the median age at diagnosis is 17 months (London et al., 2005). The tumors arise in tissues of the

sympathetic nervous system, typically in the adrenal medulla or paraspinal ganglia, and thus can present as mass lesions in the neck, chest, abdomen, or pelvis. The clinical presentation is highly variable, ranging from a mass that causes no symptoms to a primary tumor that causes critical illness as a result of local invasion, widely disseminated disease, or both. The incidence of neuroblastoma is 10.2 cases per million children under 15 years of age; it is the most common cancer diagnosed during the first year of life (Ries et al., 1999).

2.4 Human neuroblastoma cell line SH-SY5Y

SH-SY5Y is a human derived cell line used in scientific research and the original cell line, called SK-N-SH, from which it was subcloned was isolated from a bone marrow biopsy taken from a four-year-old female with neuroblastoma. It serves as a model for neurodegenerative disorders since the cells can be converted to various types of functional neurons by the addition of specific compounds. In addition, the SH-SY5Y cell line has been used widely in experimental neurological studies, including analysis of neuronal differentiation, metabolism, and function related to neurodegenerative processes, neurotoxicity, anticancer and neuroprotection (Ross et al., 1983; Seçme et al., 2016).

2.5 Cordycepin

Cordycepin, also known as 3'-deoxyadenosine (Figure 2.1), is a major bioactive component found from insect fungus, *Cordyceps sinensis* and *Cordyceps militaris*. *Cordyceps*, the name given to the fungi on insects, has been known and used as a medication in China for over 300 years. In China, this fungus is usually called 'Dong Chong Xia Cao', which means 'Worm in winter and grass in summer'. Cordycepin has an extremely high structural similarity to adenosine. In mammalian cells, an enzyme named adenosine deaminase (ADA) can catalyze the hydrolysis of adenosine to yield inosine, and this also happens to cordycepin. When present within cells, ADA can convert cordycepin into 3'-deoxyinosine (Cristalli et al., 2001). Due to the absence of oxygen in the 3'-position of its ribose moiety, the incorporation of cordycepin during RNA synthesis will result in

mesenchymal stem cells (BM-MSCs). Also, Choi et al. (2011) has been demonstrated that cordycepin induces estrogen receptor-independent autophagic as well as apoptotic cell death in human breast cancer cells. Which the researcher did not determine whether cordycepin-induced autophagy acts as a tumor suppressor to promote cancer cell death or as a cytoprotective mechanism to shield cancer cells against cordycepin treatment. Lee et al. (2014) has been reported that cordycepin induces apoptosis and autophagy in human prostate LNCaP cells. Additionally, apoptosis induced by cordycepin was improved using an autophagic inhibitor. Their suggested that cordycepin-triggered autophagy contributed to survival of LNCaP cells. Furthermore, cordycepin showed significantly increases apoptosis and autophagy in neuroblastoma SK-N-SH and BE (2)-M17 cells (Li et al., 2015)

2.6 Cell cultures as a research model

Cell culture is the procedure in which cells are isolated from their native tissue to be grown in a favorable artificial environment. The cell isolation process can be carried out by direct removal from tissue and disaggregation by enzymatic or mechanical action, finally to obtain individual cells. Cell culture provides simple yet informative model systems for studying primarily the physiological and biochemical properties of cells from several drug screening and development aspects, such as the effects of bioactive or toxic compounds and cell mutagenesis/carcinogenesis. Consistent and reproducible result can be obtained (Antoni et al., 2015). Therefore, it was introduced into cancer research as one of the major tools for the study the biology of tumor cells in a suitable environment with controlled variables. Cell culture has become an even more cost/time-effective platform for high-throughput drug screening because of the simple scaling up and maintaining processes, and also the development of multi-channel liquid handler (Ledur et al., 2017). Besides, studies into the mechanisms underlying the formation, function and pathology of tissues and organs and the responses of cancer cells to anticancer drugs are largely manageable due to the use of cell culture systems alongside animal models (Gurski et al., 2010; Yamada and Cukierman,

2007). Harrison et al., First incorporated the cell culture technique into their research into the origin and development of nerve fibers in 1907 (Harrison et al., 1907). Since then, the technique has been continuously improved and cell- based experiments can now be effortlessly conducted based on such cell culture technique, using primary cells isolated from tissues or using established cell lines from cell banks (Torsvik et al., 2014). Consequently, cell culture provides endless possibilities to the modern day cell biology researcher and is applied to a broad range of advanced studies, such as the observation of cell growth and differentiation, the mechanisms of diseases, drug action, metabolomics of cells, protein production, and the development of tissue engineering (Chen et al., 2015; Harrison, 1910; Heiland et al., 2017; Jaroonwichawan et al., 2017; Sanyal, 2014; Zhang et al., 2013). For medical approaches, cell culture is often applied in the preclinical research into therapeutics, in cancer/stem cell research, and in studies on gene function related to the cellular responses to therapy (Stupp et al., 2009).

The decision to select the most appropriate cell culture procedures to be used in cancer research is the key to help us better understand tumor biology, resulting in the optimal and/or effective conditions for radio/ chemotherapy or the discovery of new cancer treatment strategies (Aggarwal et al., 2009). At the very beginning of the cell culture era, cultures were mostly carried out under adherent conditions, in which cells were attached to the flat surface of glass or plastic containers: the 2D cell culture model. In such condition, cells are grown and contact only other cells in their peripheral surroundings. Since gradients of gases (oxygen and carbon dioxide), nutrients or waste are absent, cells are not compelled to pile on top of one another, but are committed to grow in a monolayer morphology, which is not native behavior for all cell types. The later establishment of co-culture systems could to some extent promote intercellular interaction, but the fact that cells were grown in a monolayer not a multi-dimensional structure, as they behaved naturally, was still a concern (Antoni et al., 2015). In addition, since almost all cells *in vivo* are surrounded not only by other cells but

also by an extracellular matrix (ECM) in a 3D model (Edmondson et al., 2014), monolayer cells do not accurately mimic the actual 3D environment of *in vivo* cells. There is good evidence that experiments using the immortalized tumor lines grown in 2D culture systems could actually improve knowledge about the mechanism of cancer, but they also resulted in a 95% drug failure rate. This was a sign that 2D cell culture may be a poor drug development model, since the *in vivo* drug efficacy and toxicity were predicted unreliably (Hutchinson and Kirk, 2011). Therefore, drug discovery and validation processes integrated both 2D cell culture tests and the subsequent animal model tests as the standard procedure prior to clinical trials. However, both those models possess several weaknesses. The data collected from 2D cell culture model are often misleading for *in vivo* responses, as previously mentioned, while animal models are expensive, time-consuming, present controversial ethical dilemmas and also provide inconsistent data due to the species differences (Birgersdotter et al., 2005). The development of new models is needed to bridge the gap between 2D cell culture models, animal models and clinical trials. Thus, *in vitro* 3D cell culture models could be the potential candidates as will be proposed below (Yamada and Cukierman, 2007).

2.7 Two - versus three-dimensional cell culture models

Cell culture is a basic but essential tool for preclinical drug discovery. Even though the flaws of monolayer cell cultures have been pointed out, 2D cell culture models are still the first option for scientists, due to their simplicity in obtaining preliminary results. Nevertheless, 2D cultures may not mimic sufficiently well the physiological conditions in a 3D network where *in vivo* cells reside. Therefore, deceptive data from 2D cell culture models often lead to incorrect predictions of drug efficacy and toxicity and finally cause failure in drug validation and approval processes (Friedrich et al., 2007). One obvious advantage of 3D cell culturing over 2D is that it contributes the influence of ECM components, as well as cell-to-cell contact, and cell-matrix interactions. Because in the body, nearly all cells in tissues reside in an ECM consisting of a complex three-dimensional architecture and interact

with neighboring cells through biochemical and mechanical cues (Lodish et al., 2000). The ECM is primarily composed of various laminins, collagens, and glycoproteins serving as substrates for a myriad of adhesion molecules including cadherins, integrins, and discoidin domain receptors (Griffith and Swartz, 2006). Cell-to-cell and cell-ECM interactions establish a 3D communication network that maintains the specificity and homeostasis of the tissue (Kleinman et al., 2003). The characteristics of 3D cell cultures and the traditional 2D cell culture model are shown in Figure 2.2. Traditional 2D cell cultures result in a monolayer of cells expanding on a flat surface of glass or commercial polystyrene tissue-culture flasks (Figure 2.2a). In contrast, 3D cell cultures promote cells to form 3D spheroids by utilising an ECM material (Figure 2.2b). The cell spheroid is the important characteristic that resembles *in vivo* cells for further replicating cell differentiation, proliferation and function *in vitro*. Thus, a 3D spheroid culture is considered an improved model for predictive *in vitro* cell-based assays and may deliver high physiological relevance for preclinical drug discovery, especially in cancer/stem cell research.

Generally, cells of multicellular organisms capable of forming tissues are in 3D arrangements with complex cell-to-cell and cell-to-matrix interactions and dynamics for transport of nutrients and chemicals between cells. In *in vivo* conditions, cells are haemostatically maintained with a relatively constant supply of nutrients with a minimized level of waste products due to the activity of the circulatory system. Therefore, the 3D arrangements of cells are the major feature of 3D cell cultures, with the optimal spatial organisation of cells in 3D cell culture or tissue culture environment to be considered (Abbott, 2003; Langer and Tirrell, 2004; Lee et al., 2008). When cells are grown in a 3D culture system, they are also induced to form aggregates or spheroids within a matrix, on a matrix or in a suspension medium. In such spheroid culture models, cell-to-cell interactions and cell-to-matrix interactions are not modelled perfectly, but closely mimic the natural *in vivo* environment, such that the cell morphology is not relatively flat but closely resembles

its natural shape in the body (Figure 2.2c). Furthermore, a spheroid structure is comprised of cells in various stages, including proliferating, quiescent, apoptotic, hypoxic, and necrotic cells (Florczyk et al., 2016; Kim, 2005). The proliferating cells are found mainly in the outer spheroid layer, since they are then exposed to a sufficient amount of nutrients from the culture medium (Khaitan et al., 2006; Senkowski et al., 2016). Cells at the core of the spheroid tend to be in quiescent or hypoxic state, since they face a lack of oxygen, growth factors, and nutrients (Mehta et al., 2012). The cellular heterogeneity within a cell population is quite relevant to *in vivo* tissues, organs and even tumor. At this point, since cell morphology, interactions and heterogeneity of cells grown in a 3D culture could imitate that occurring *in vivo*, it is reasonable to hypothesize that the cellular processes of these cells are also applicable (Gurski et al., 2010).

Comparisons of 3D spheroid culture models and 2D monolayer cell culture models are shown in Table 2. 1. Numerous studies have proved the differences in cell viability, morphology, proliferation, differentiation, response to stimuli, cell-cell communication, stiffness, migration and invasion of tumor cells into surrounding tissues, angiogenesis stimulation and immune system evasion, drug responses, gene expression and protein synthesis, general cell function and *in vivo* relevance between cells cultured in 2D and 3D models. For example, cell polarization could be more accurately depicted in 3D cell cultures models than in 2D models, where the cells can be only partially polarized. Moreover, greater stability and longer lifespans were found in 3D culture models; 3D spheroids can be for cultured up to three weeks, whereas 2D monolayer cultures can last for less than a week due to the limitation of cell confluence (Dai et al., 2016). Therefore, the 3D cell culture model may be more appropriate for handling long-term experiments and for determining long-term effects of a drug on cellular responses.

Table 2.1 Differences between 2D and 3D cell culture models.

Type of culture	2D	3D	References
<i>In vivo</i> -like	Does not mimic the natural structure of the tissue or tumor mass	<i>In vivo</i> tissues and organs are in 3D form.	Takai et al. (2016)
Proliferation	Tumor cells grow faster in monolayer than in 3D spheroids	Similar to the situation <i>in vivo</i> .	Lv et al. (2016)
Polarity	Partial polarization	More accurate depiction of cell polarization.	Antoni et al. (2015)
Cell morphology	Sheet-like, flat and stretched cells in monolayer	Form aggregate/spheroid structures	Breslin and O'Driscoll (2016)
Stiffness	High stiffness ($\sim 3 \times 10^9$ Pa)	Low stiffness (>4000 Pa)	Krausz et al. (2013)
Cell-cell interaction	Limited cell-cell and cell-ECM interactions and no 'niches'.	<i>In vivo</i> -like, proper interactions of cell-cell and cell-ECM, environmental 'niches' are created.	Lv et al. (2016); Kang et al. (2016)
Gene/protein expression	Changes in gene expression, mRNA splicing, topology and biochemistry of cells, often display differential gene/protein levels compared to <i>in vivo</i> models.	Relevant expression of genes and proteins <i>in vivo</i> is present in 3D models.	Bingel et al. (2017); Ravi et al. (2015)
Drug responses	Lack of correlation between 2D monolayer cell cultures and human tumors in drug testing.	Tumor cells in 3D culture show drug resistance patterns similar to those observed in patients.	Lv et al. (2016); Bingel et al. (2017)

Table 2.1 (Continued).

Type of culture	2D	3D	References
Culture formation	Minutes to a few hours.	A few hours to a few days.	Dai et al. (2016)
Quality of culture	High performance, reproducibility, long-term culture, easy to interpret, simplicity of culture.	Worse performance and reproducibility, difficult to interpret, cultures are more difficult to carry out.	Hickman et al. (2014)
Access to essential compounds	Unlimited access to oxygen, nutrients, metabolites and signaling molecules (in contrast to <i>in vivo</i>).	Variable access to oxygen, nutrients, metabolites and signaling molecules (similar to <i>in vivo</i>).	Pampaloni et al. (2007) Senkowski et al. (2016)
Cost during maintenance of culture	Cheap, commercially available tests and media.	More expensive, more time-consuming, fewer commercially available tests.	Friedrich et al. (2009)

2.8 Three - dimensional cell culture technologies

Due to the advantages of 3D culture systems, there have been many studies focused intensively on the development and optimization of 3D cell culture technologies. With the integration of recent advances in cell biology, microfabrication techniques and tissue engineering, a wide range of 3D cell culture platforms have been constructed, including multicellular spheroid formation (liquid overlay culture and hanging drop method), hydrogel-based cultures, bioreactor-based culture, bioprinting and scaffold-based culture. A summary of the advantages, disadvantages and research stage of each model is shown in Table 2.2. Although several 3D culture techniques/platforms are different in both principle and protocol, they all share the same objectives which is to provide features similar to *in vivo* cells in terms of morphology, function and microenvironment. This section aims to describe briefly the key features of each technique.

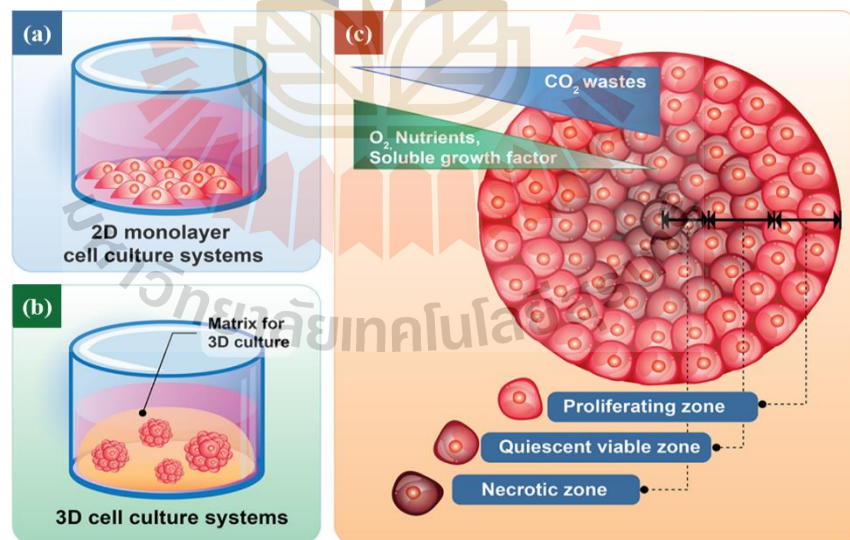


Figure 2.2 Schematic diagrams of (a) the traditional 2D monolayer cell culture and (b) 3D cell culture systems. (c) The structure of a 3D spheroid with different cell zones, with the models of oxygenation, nutrition and CO₂ removal. From inside to outside of the 3D spheroid, the regions are; necrotic zone (innermost), quiescent viable cell zone (middle), and proliferating zone (outermost). **Graphic by:** Phongsakorn Kunhorn

Table 2.2 Proposed advantages, disadvantages and research stage of different 3D cell culture methods.

Technique	Advantages	Disadvantages	Research Stage
Liquid overlay cultures	<ul style="list-style-type: none"> • Easy-to-use protocol • No added materials • Consistent spheroid formation; control over size 	<ul style="list-style-type: none"> • No support or porosity • Limited flexibility • Limited spheroid size. 	<ul style="list-style-type: none"> • Basic research • Drug discovery • Personalized medicine
Hanging drops	<ul style="list-style-type: none"> • Co-culture ability • High reproducibility • Inexpensive • Easy to image/harvest samples 	<ul style="list-style-type: none"> • Heterogeneity of cell lineage. • Lack of matrix interaction 	
Hydrogel	<ul style="list-style-type: none"> • Large variety of natural or synthetic materials • Customizable • Co-cultures possible • Inexpensive • High reproducibility 	<ul style="list-style-type: none"> • Gelling mechanism • Gel-to-gel variation and structural changes over time • Undefined constituents in natural gels • May not be transparent 	<ul style="list-style-type: none"> • Basic research • Drug discovery

Table 2.2 (Continued).

Technique	Advantages	Disadvantages	Research Stage
Scaffolds	<ul style="list-style-type: none"> • Large variety of materials possible for desired properties • Customizable • Co-cultures possible • Medium cost 	<ul style="list-style-type: none"> • Possible scaffold-to-scaffold variation • May not be transparent • Cell removal may be difficult 	<ul style="list-style-type: none"> • Basic research • Drug screening • Drug discovery • Cell expansion
3D bioprinting	<ul style="list-style-type: none"> • Custom-made architecture • High-throughput production • Co-culture ability 	<ul style="list-style-type: none"> • Requires expensive 3D bioprinting machine • Challenges with cells/materials 	<ul style="list-style-type: none"> • Cancer pathology • Anticancer drug screening, • Tissue engineering

Source; Breslin and O'Driscoll (2013); Fang and Eglén (2017); Leong and Ng (2014).

2.8.1 Multicellular spheroid formation

2.8.1.1 Liquid overlay culture

Liquid overlay culture could be the simplest of all 3D cell culture techniques (Figure 2.3a). To create 3D culture models, the surfaces for cell culture are covered with a thin film of inert substrates, such as agar (Vinci et al., 2012), agarose (Friedrich et al., 2009) or matrigel (Shin et al., 2014). By preventing cell adhesion to the surface and providing an artificial matrix, liquid overlay culture easily promotes the aggregation of cells to become spheroids (Carlsson and Yuhas, 1984). This technique is cost-effective and highly reproducible with no requirement for any specific equipment (Costa et al., 2014). Different cell types can be co-cultured with this technique (Metzger et al., 2011). However, it is difficult to monitor the number and size of spheroids formed (Lin and Chang, 2008). Recently, ultra-low attachment plates have been developed and commercialized for the liquid overlay technique. Such plates contain individual wells with a layer of hydrophilic polymer on the surface to overcome the requirement for manual coating to prevent cell attachment. This technique, with its specifically designed plates, exhibits the capability to produce one spheroid per well, and is suitable for medium-throughput applications (Thoma et al., 2014).

2.8.1.2 Hanging drop technique

The hanging drop technique for 3D spheroid production was firstly introduced by Johannes Holtfreter in 1944 for cultivating embryonic stem cells. The technique later became the foundation of scaffold-free 3D culture models capable of multicellular spheroid generation. The resulting spheroids could be generated with consistent size and shape controlled by adjusting the density of cell seeding. From 50 up to 15,000 cell densities could be varied to obtain the desired spheroids size (Kelm et al., 2003). In the very beginning, the hanging drop technique was performed in the lid of a petri dish by dropping

a small volume of cell suspension with a certain cell density onto the lid. The lid was subsequently inverted and aliquots of cell suspension turned into hanging drops without dripping due to surface tension. Consequently, cells were forced to accumulate at the bottom of the drop, at the liquid–air interface, and to further aggregate and proliferate until spheroids were formed (Figure 2.3b). Lately, bioassay dishes have been used in place of petri dishes for more well-controlled experiments and to facilitate the maintenance of the moisture levels of the culture system, so that cells can be incubated as per standard cell culture procedures. The hanging drop technique is relatively simple and is applicable to numerous cell lines; in addition, its reproducibility could be almost 100% generating one 3D spheroid per drop (Kelm et al., 2003). The 3D spheroids obtained from this technique tend to be tightly packed rather than loosely aggregated, and low variability in size are observed. Kelm et al. (2003) reported that the 3D spheroids exhibited patho/physiological relevance, since their structures were highly organized with their own ECM, and were thus described as “tissue-like” structures. As this technique is based on the tendency of cells to aggregate spontaneously with each other rather than relying on matrixes or scaffolds, concerns regarding their effects on 3D structure formation are relieved. However, the undeniable drawback of the hanging drop technique is the limitation of the volume of the cell suspension. Only up to 50 μ l of suspension, including the testing medium, can be accommodated on the upside-down surface before dripping occurs, as the surface tension is not sufficient to keep liquids attached to the surface against gravity (Kurosawa, 2007). Another limitation is the difficulty in changing culture medium during cultivation without disturbing the spheroids (Mehta et al., 2012).

2.8.2 Hydrogels

Hydrogels are three-dimensional crosslinked networks composed of hydrophilic polymers with high water content (Figure 2.3c) (Drury and Mooney, 2003). There are swollen structures or microspheres integrated within the network for cell encapsulation and the circulation of nutrients and cellular waste in and out of the hydrogels

(Nicodemus and Bryant, 2008). Additionally, gels exhibit a soft-tissue-like stiffness that potentially resemble natural ECM, since they are made from mixtures of natural polymers such as collagen, and alginate, two of the most widely used substrates in 3D cell culture history (Frampton et al., 2011). The most common use of hydrogels is incorporation with reconstituted basement membrane preparation extracted from mouse sarcoma, which has been commercialized under the Matrigel trademark (Corning Life Sciences, Tewksbury, MA, USA). Even though such commercialized hydrogels are rich in ECM proteins, they also possess some drawbacks, including poor control of gelation kinetics, uncontrolled material composition and lack of mechanical integrity. Lot-to-lot variability due to manufacturing errors and poorly defined composition also cause difficulties in the exact determination of the responses of cells to some particular stimuli (Fang and Eglén, 2017). Generally, hydrogels are fabricated based on both synthetic and natural polymers, which are water-absorbing, hydrophilic and highly flexible materials. With well-controlled fabrication processes and well-defined material composition, hydrogels provide many advantages that make them popular for 3D scaffold development for cell-based assay tissue engineering applications, since their structural similarity to native ECM are favorable for drug or growth factor delivery in a non-invasive manner (Drury and Mooney, 2003). A number of different synthetic and natural materials can be used in the formation of hydrogels, such as hyaluronic acid (HA), polyethylene glycol (PEG) (Leach and Schmidt, 2005), collagen, gelatin, fibrin, alginate, and agarose (Shelke et al., 2016). However, natural hydrogels, such as Matrigel and alginate gel, are considered to be much appropriate cell-encapsulated materials due to their great biocompatibility and mild gelling conditions. The hydrogel technique for cell culture in calcium alginate hydrogel was first developed by Lim and Sun (1980) by mixing the cells with alginate solution, then cross-linking and forming the gel microspheres in an isotonic CaCl_2 solution (Figure 2.3c). Alginate hydrogels show very limited cell adhesion, which is an advantage for cell encapsulation applications (Andersen et al., 2015), and provide rapid,

non-toxic, and versatile immobilization of cells within polymeric networks. In addition, the creation of artificial organs was also consolidated with encapsulating cells or tissue for the treatment of disease. The most well-known example is an artificial pancreas for the treatment of diabetes (Nicodemus and Bryant, 2008).

Hydrogel 3D cell cultures can also be combined with other models, such as spheroid cultures, scaffolds, and microchips (Justice et al., 2009). The use of hydrogels is one potential technique for use in 3D *in vitro* technology due to their biocompatibility, sufficient water content and ECM-like mechanical properties (Hosseinkhani et al., 2010). Although hydrogels are not commonly applied to the field of drug screening, they have been widely used in the development of tissue engineering, mimicking cartilaginous, vascular, bone and other tissues by mixing particular cells with hydrogel precursors before the gelling process, so the cells are distributed evenly and homogeneously throughout the gels. One reported case is the creation of differentiated cardiac tissues that were engineered by combining neonatal rat cardiac myocytes into collagen hydrogels and used for cyclic mechanical stretch experiment (Zimmermann et al., 2000). Hydrogels also facilitate the delivery of soluble or signaling molecules to cells, providing supporting structures for cell growth and function. For example, transforming growth factor β (TGF- β) as infused to polyethylene glycol (PEG) hydrogels to regulate smooth-muscle cell function. In a similar manner, bone morphogenetic protein (BMP-2) was covalently attached to alginate hydrogels to govern osteoblast migration and calcification (Zustiak et al., 2012). Despite a variety of hydrogel type applications, Ca-alginate hydrogels are surely potent candidate systems for delivery of cells to the infarcted heart, since they are non-toxic, non-immunogenic, do not facilitate pathogen transfer and allow good exchange of waste products and nutrients (Leor et al., 2009; Li and Guan, 2011). Ca-alginate hydrogels were primarily implanted into the heart and shown not to induce harmful responses such as thrombosis (Leor et al., 2009) or fibrosis (Hao et al., 2007). The gradual degradation, resulting from the dispersal of calcium

crosslinks (Hunt et al., 2010), generated non-toxic alginate polysaccharide degradation products, which can be excreted via urinary systems (Al-Shamkhani and Duncan, 1995). However, besides the number of advantages of hydrogels, disadvantages are still present and should not be disregarded. The uncertainty and complexity in composition influenced by the gelling mechanism may cause undesirable and non-specific cellular responses. Additionally, pH-based gelling mechanisms can negatively affect sensitive cells (Justice et al., 2009).

2.8.3 Scaffolds

3D scaffolds are described as synthetic 3D structures constructed from a wide range of materials and possessing different porosities, permeabilities, surface chemistries and mechanical characteristics. From a 3D culture point of view, they are mainly designed to mimic the in vivo ECM of the specific tissues for each particular cell type. 3D scaffold-based cell culture models have been applied to drug screening (Lv et al., 2016), drug discovery (Fang and Eglen, 2017), and investigation of cell behaviors (Fang and Eglen, 2017). 3D scaffolds are intended to be porous, biocompatible and biodegradable and so provide appropriate microenvironments in which cells naturally reside, supporting the mechanical, physical and biochemical requirements for cell growth and function (Florczyk et al., 2016). Several biopolymers are used to generate porous scaffolds, including collagen (Lv et al., 2016), gelatin (Sisson et al., 2010), silk (Jin et al., 2004), chitosan (Florczyk et al., 2016) and alginate (Chen et al., 2015; Florczyk et al., 2016). As such, various techniques have been used for the fabrication of such scaffolds, such as gas foaming, freeze-drying, phase separation, solvent casting and particulate leaching. Each technique results in different porosities, pore sizes and shapes, scaffold materials and features. Among them, freeze-drying is considered as the easiest technique to fabricate porous scaffolds (Wu et al., 2010).

Sequentially, natural or synthetic materials are polymerized, frozen and then freeze-dried, where the frozen water embedded in the material is sublimated directly from the solid to the gas phase, resulting in the formation of a porous structure (Sachlos and Czernuszka, 2003). The freeze-drying technique for fabricating porous biodegradable polylactic and polyglycolic acid (PLGA) co-polymeric scaffolds was first developed by Whang et al. (1995). With such a technique, the porosity and pore sizes of the scaffolds vary depending on various parameters, such as the ratio of water to polymer in solution and the viscosity of the emulsion (Mikos and Temenoff, 2000). Porous alginate-based scaffolds can also easily be manufactured by a simple freeze-drying process (Figure 2.3d). However, it is difficult to generate pores of uniform diameter, but this can partially be controlled by varying the freezing temperature (O'Brien et al., 2004). Another advantage of this technique is that no rinsing step is required, since the dispersed water and polymer solution are removed directly via sublimation (Whang et al., 1995). Additionally, the biodegradation rates of scaffolds are strongly dependent on polymer components and molecular weight (Sun and Tan, 2013).

To date, Ca–alginate copolymer is one of the most prominent materials for freeze-dried scaffolds. Several studies have used a 3D Ca–alginate scaffold as a cell culture platform for screening and efficacy testing of anticancer drugs and tissue engineering. 3D Ca–alginate scaffolds are proposed to allow more realistic cell phenomena, similar to those occurring *in vivo* during cancer formation and progression. Chen et al. (2015) have developed a 3D porous Ca- alginate scaffold cell culture system combined with a functionally-closed process bioreactor to mimic the *in vivo* environment in order to form bone-like tissue. The Ca–alginate scaffolds were reported to support the growth and differentiation of human bone cell clusters, along with the upregulation of bone-related gene expression. Florczyk et al. (2016) developed chitosan–alginate scaffolds using freeze-drying to study the transient behavior of cancer stem cells *in vitro*. They found that 3D scaffold-

based cultures of prostate, liver, and breast cancers exhibit reduced proliferation and tumor spheroid formation, and increased expression of cancer stem-like cell associated marker genes (*CD133* and *NANOG*) unlike those obtainable in 2D cell cultures. Chitosan–alginate scaffolds were also reported to allow the efficient seeding of human umbilical cord mesenchymal stem cells (hUMSCs), promoting the inhabitability of cells throughout the whole volume of the scaffold, which reflected good adhesion and proliferation (Kumbhar and Pawar, 2016).

Nowadays, the commercial porous alginate scaffold has been available on the market such as AlgiMatrix™. The AlgiMatrix™ 3D alginate scaffold is product of Life Technologies Corporation Company, which is ready-to-use for the development cell culture models that are more predictive of disease states and drug responses. Its sponge was made from lyophilized alginate gel which nontoxic, biodegradable and is stable at room temperature. According to Godugu et al. (2013), AlgiMatrix™ 3D alginate scaffold was used for *in vitro* tumor model for anticancer drug screening. They found that cancer cells can grow and form multicellular spheroids in 6 and 96 well AlgiMatrix™ scaffolds. Different marketed anticancer drugs were screened cytotoxicity of cells on AlgiMatrix™ system compared to the 2D monolayer cultures. IC₅₀ values for anticancer drugs were significantly higher in AlgiMatrix™ systems compared to 2D culture models. The results from their studies are strongly support that the 3D alginate scaffold may be used as an *in vitro* tumor model. It is possible to predict the anticancer effect of various drugs and formulations in a better than 2D monolayer cultures. As a result, the ability to predict outcomes in preclinical animal models and clinical trials can be better understood because the positive anticancer effects observed in 2D cultures often fail during *in vivo* testing. However, the price of AlgiMatrix™ quite expensive (17,000 baht/24 well plate) and require other solution (AlgiMatrix™ Firming Buffer and AlgiMatrix™ Dissolving Buffer) to support sponges.

2.8.4 Three-dimensional bioprinting

3D printing is the recently developed technology that, in general, is referred to as the customised construction of 3D structures on demand under computational control, in which materials are printed out, solidified and connected together (Andersen et al., 2015). 3D printing is used in a wide range of applications, including prototypic and industrial manufacturing, architecture, 3D art and design and importantly, tissue engineering and regenerative medicine (Murphy and Atala, 2014). The 3D tissue printing of biological constructs composed of cells and biomaterials is carried on a small scale, ranging from several millimetres to a centimetre. Such a process is called 3D bioprinting, since biocompatible materials, cells and supporting components, rather than any synthetic materials, are used to form a variety of 3D formats. Therefore, cell function and viability can be sustained within the printed constructs (Figure 2.3e) (Murphy and Atala, 2014). Various 3D bioprinting platforms can already generate vascular-like tubes (Yu et al., 2013), kidney tissues (Murphy and Atala, 2014), cartilage (Cui et al., 2012) artificial skin (Lee et al., 2013), and a wide range of stem cells including tissue constructs (Tasoglu and Demirci, 2013). 3D bioprinting is needed to precisely deposit cells, biomaterials and biomolecules layer-by-layer by computer-aided equipment and software, which has been made possible by recent advances in engineering, material science, computer science and cell biology (Jessop et al., 2017). By using alginate as the main biomaterial in a bio-ink, Zhao et al. (2014) formed an *in vitro* cervical tumor model in order to study disease pathogenesis. In their report, alginate, together with gelatin and fibrinogen, was mixed with HeLa cells to initiate gelation prior to printing and to resemble the ECM components. The printed constructs were later strengthened by the addition of a CaCl₂ solution. Printed HeLa cells subsequently formed spheroids that exhibited more resistance to paclitaxel than did 2D monolayer HeLa cells. Correspondingly, Dai et al. (2016) generated 3D bioprinted constructs of glioma stem cells by using modified gelatin/alginate/fibrinogen biomaterials, glioma stem cells printed within

constructs could survive, proliferate, and maintain the inherent characteristics of cancer stem cells, and exhibit differentiation and vascularization potential. In addition, their resistance against temozolomide was higher than those in the 2D cell culture models.

Besides the ability to generate geometric constructs containing viable cells, 3D bioprinting techniques also facilitate high-throughput applications with precise reproducibility (Knowlton et al., 2015). However, the main concerns are the requirements for expensive 3D bioprinting machines and negative effects on sensitive cells during the printing process. Cells could possibly be damaged due to osmotic, thermal and mechanical stresses.

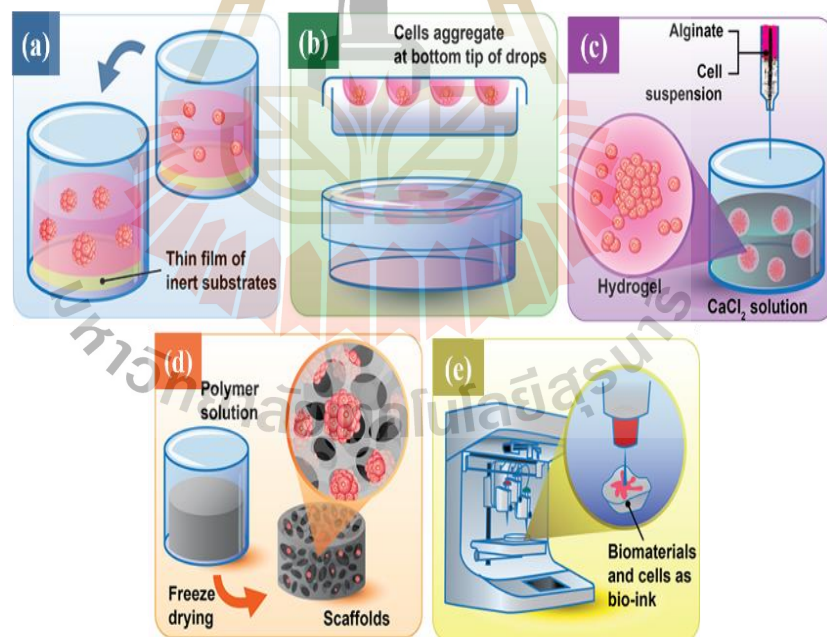


Figure 2.3 Different techniques used for 3D cell culture. These techniques include, (a) liquid overlay; (b) hanging drop; (c) hydrogel embedding; (d) scaffold; (e) 3D bioprinting. **Graphic by:** Phongsakorn Kunhorm

2.9 Application of 3D cell culture

Recently, 3D culture models have tended to be developed in a specific way to suit each particular cell type rather than to be versatile, because of the different physiological requirements. Despite the great number of reported 3D culture-based studies, some of them have not been optimized or validated for realistic applications. Advances have been made for cancer and stem cell modelling, and prominent studies applying 3D cell culture systems are summarized in Table 2.3.



Table 2.3 Examples of three-dimensional research systems used for cancer and stem cell cancer studies.

Application/ Platform	Cells type	3D model	Culture system/ matrix	Results	References
Drug screening	Breast cancer cells (BT-549, BT-474 and T-47D)	Comparison of 2D and 3D culture models as drug-testing platforms in breast cancer	Spheroid formation in 3D culture in 3D culture plates	Three breast cancer cell lines developed dense multicellular spheroids (MSCs) in 3D culture, and showed greater resistance to paclitaxel and doxorubicin compared to the 2D-cultured cells	Imamura et al. (2015)
Metastasis studies and assessing drug sensitivity	Breast cancer cells (MDA-MB-231 and MCF-7)	Breast cancer bone metastasis	3D bioprinting hydrogel	Breast cancer cells exhibited spheroid morphology and migratory characteristics, then co-culture of breast tumour cells with bone marrow mesenchymal stem cells increased the formation of spheroid clusters	Zhu et al. (2016)
Cancer cell behavior	Breast cancer cells (MCF-10)	Breast cancer progression	3D spheroid cultures used U-bottom ultra-low attachment plates	Genetic dependencies can be uncovered when cells are grown in 3D conditions similar to <i>in vivo</i>	Peela et al. (2016)

Table 2.3 (Continued).

Application/ Platform	Cells type	3D model	Culture system/ matrix	Results	References
Drug screening	Human colon cancer cells (HCT116)	Compared genes expression in 2D and 3D systems and identification of context-dependent drug responses	Three-dimensional spheroid cultures used low attachment plate	3D spheroids shown positively enriched for genes involved in response to hypoxia and negatively enriched with genes involved in cell-cycle progression when compared with monolayer profiles	Senkowski et al. (2016)
GBM biology, anti-GBM drug screening.	Human glioblastoma cells (U87)	Compared gene expression in 2D and 3D systems	3D polylactic acid (PLA) porous scaffolds	GBM cells in 3D PLA culture expressed 8117 and 3060 genes were upregulated and downregulated, respectively, compared to 2D cell culture conditions. Furthermore, KEGG pathway analysis showed the upregulated genes were mainly enriched in PPAR and PI3K-Akt signalling pathways while the downregulated genes were enriched mainly in metabolism, ECM-related and TGF-beta pathways	Ma et al. (2018)

Table 2.3 (Continued).

Application/ Platform	Cells type	3D model	Culture system/ matrix	Results	References
Cancer and tumour cell biology	Human glioblastoma cells (U-251)	Compared gene and protein expression in 2D and 3D systems	Electrospun polystyrene scaffolds coated with laminin	The results suggest the influence of 3D context on integrin expression upregulation of the laminin- binding integrins alpha 6 and beta 4	Ma et al. (2016)
Cancer and tumour cell biology	Human glioblastoma cells (U-251)	Compared drug sensitivity in 2D and 3D systems	3D bioprinting of gelatin/ alginate/ fibrinogen 3D collagen scaffold	3D bioprinted glioma stem cells were more resistant to temozolomide than 2D monolayer model at TMZ concentrations of 400–1600 $\mu\text{g ml}^{-1}$	Dai et al. (2016)
Cancer and tumour cell biology	Human glioblastoma cells (U-251)	Anticancer drug screening	3D collagen scaffold	Glioma cells in 3D collagen scaffold culture enhanced resistance to chemotherapeutic alkylating agents, with a much higher proportion of glioma stem cells and upregulation of MGMT	Lv et al. (2016)
Development of new therapies	iPSC-derived human cardiomyocytes	Cardiac microtissues	Hanging drops	A three-dimensional culture using iPSC-derived human CMs provides an organoid human-based cellular platform.	Beauchamp et al. (2015)

Table 2.3 (Continued).

Application/ Platform	Cells type	3D model	Culture system/ matrix	Results	References
Tissue engineering and toxicity assessment.	Human hepatoblastoma cells (HepG2/C3A)	A liver-on-a-chip platform for long term culture of 3D human HepG2/C3A spheroids	Bioprinting of hepatic constructs containing 3D hepatic spheroids	Hepatic construct by 3D bioprinting could function during the 30 days culture period and responded to acetaminophen, which induced a toxic response	Blaise et al. (2016)
Brain disease	Human embryonic stem cells (HUES66)	3D neural tissues for use as tractable models of brain disease	3D hydrogels	3D co-cultures of neuronal and astrocytic cells can express patterns that correlate with specific brain regions and developmental stages	Tekin et al. (2018)
Cancer and tumour cell biology, drug screening	Human neuroblastoma cells (IMR-32)	Compared gene expression profiles in 2D and 3D systems and tumour tissue	Polymeric scaffolds and bioreactor systems	The autophagy-controlling transcription factors, such as <i>TFEB</i> and <i>FOXO3</i> , are upregulated in tumours and 3D-grown cells have increased expression compared with cells grown in 2D conditions	Bingel et al. (2017)

Table 2.3 (Continued).

Application/ Platform	Cells type	3D model	Culture system/ matrix	Results	References
Neurodegenerative diseases	Dental pulp stem cells (DPSCs)	Differentiation to retinal ganglion-like cells	3D fibrin hydrogel	Three-dimensional network can mimic the natural environment of retinal cells	Roozafzoon et al. (2015)
Cardiovascular disease	Human induced pluripotent stem cells (hiPSCs)	Cardiomyocytes and endothelial cells	V-bottom 96-well microplates	Human cardiac microtissues were generated in complex 3D structures, and differentiation of human iPSCs into cardiomyocytes and endothelial cells	Giacomelli et al. (2017)
Bioartificial liver support devices, drug screening and transplantation	hiPSCs	Differentiation of hiPSCs into hepatocytes	Nanofiber hydrogel 3D scaffold	3D hydrogel culture conditions promote the differentiation of hiPSCs into hepatocytes	Luo et al. (2018)
Ovarian cancer biology,	Ovarian cancer cell lines (A2780 and OVCAR3)	Compared drug sensitivity in 2D and 3D systems	Hanging drop	3D tumour spheroids demonstrated greater resistance to cisplatin chemotherapy compared to 2D cultures	Raghavan et al. (2015)

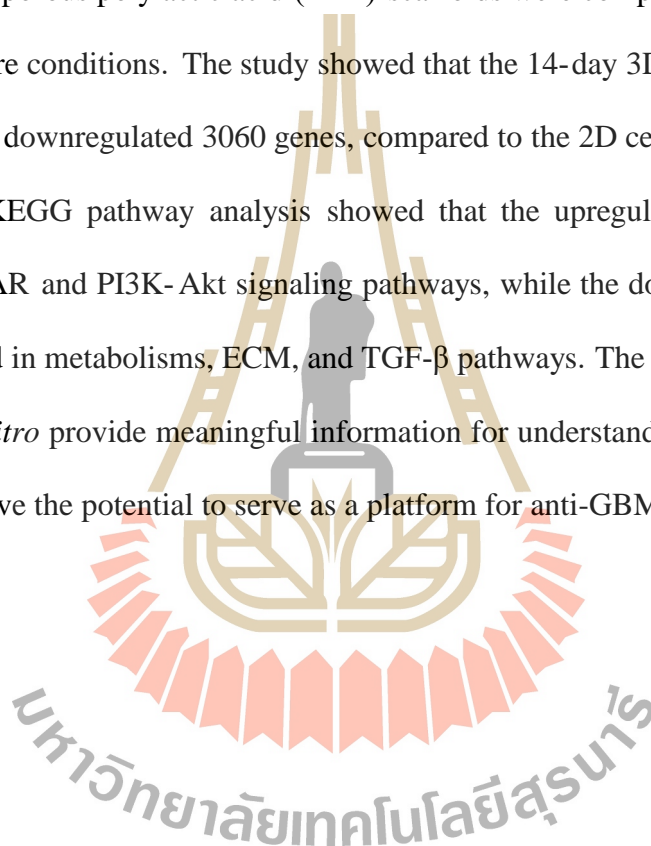
Table 2.3 (Continued).

Application/ Platform	Cells type	3D model	Culture system/ matrix	Results	References
Pathogenesis of prostate cancer, cancer therapy	Prostate cancer cell lines (PC3 and LNCaP)	Simulation of prostate cancer bone metastases	Collagen-based scaffolds	The two cell lines in 3D present increased resistance to docetaxel	Fitzgerald et al. (2015)
Radiosensitivity of cancer cells	Human lung adenocarcinoma cell line (A549)	The metabolic response of lung cancer cells to ionizing radiation.	Hydrogels	3D model can help regulate the exposure of oxygen to subpopulations of cells in a tissue-like construct either before or after irradiation	Simon et al. (2016)
Regenerative medicine, drug screening	Human umbilical vein endothelial cells (HUVECs)	Endothelialised myocardium construction	3D bioprinting	This technique could be translated to human cardiomyocytes derived from induced PSCs to construct endothelialised human myocardium	Zhang et al. (2016)
Developing therapies against cancer stem cells	Hepato-cellular carcinoma (TRAMP-C2 and MDA-MB-231)	Compared gene expression in 2D and 3D systems	Chitosan-alginate (CA) scaffolds	The cell lines in 3D porous CA scaffolds promote cancer stem-like cell enrichment and increased expression of cancer stem cells genes (<i>CD133</i> and <i>NANOG</i>)	Florczyk et al. (2016)

2.9.1 Cancer modelling

Cancer epithelial cells cultured in the 3D culture systems have been reported to change shape and lose polarity. Such a feature typically shows up in cancer progression in *in vivo* environments (Yamada and Cukierman, 2007). As with other key parameters, cell proliferation, gene/protein expression, and drug sensitivity of 3D cancer cell models are also more illustrative of *in vivo* cancer cells compared to those cultured as monolayers (Gurski et al., 2010). Therefore, to obtain the more relevant data, several studies have used 3D cell culture systems as a platform for cancer models. For example, Peela et al. (2016) revealed the 3D MCF10 human mammary gland cells to uncover novel genetic dependencies linked to breast cancer progression. The study showed that the genetic dependencies could be revealed when cells were grown in 3D conditions similar to *in vivo*. This MCF10 progression series therefore represented a suitable system to dissect the potential biomarkers as well as to evaluate therapeutic targets involved in human breast cancer progression. Zhu et al. (2016) employed novel stereolithography-based 3D printing with a unique 3D printed nano-ink. This system consisted of hydroxyapatite nanoparticles suspended in hydrogel to develop a biomimetic bone-specific environment for assessing breast cancer/bone invasion. The study showed that breast cancer cells cultured in the 3D bioprinted structures exhibited spheroid morphology and high migratory characteristics. In addition, co-culture of tumor cells with bone marrow mesenchymal stem cells increased the formation of spheroid clusters. The 3D matrix also allowed for a higher degree of anticancer drug resistance in breast cancer cells than that shown by 2D culture cells. The evidence suggested that the 3D bone matrix mimicked tumor/bone microenvironments, serving as a tool for exploring cancer metastasis and assessing anticancer drug sensitivity. In another report, Senkowski et al. (2016) demonstrated gene expression profiling of 3D multicellular tumor spheroids compared to 2D monolayer cells. The gene expression profile of 3D spheroids was positively enriched for genes involved in the response to hypoxia, and negatively enriched with genes involved in

cell-cycle progression (Figure 2.4). Further, the mevalonate pathway was upregulated in quiescent cells of the 3D spheroids during oxidative phosphorylation (OXPHOS) inhibition, and OXPHOS inhibitors and mevalonate pathway inhibitors were synergistically toxic to quiescent spheroids. This suggested the context-dependence of anticancer drug responses of the 3D tumour spheroids. Recently, the whole genome of 3D glioblastoma multiforme (GBM) cells in porous polylactic acid (PLA) scaffolds were compared against those grown in 2D cell culture conditions. The study showed that the 14-day 3D GBM cells upregulated 8117 genes and downregulated 3060 genes, compared to the 2D cell culture conditions (Ma et al., 2018). KEGG pathway analysis showed that the upregulated genes were mainly enriched in PPAR and PI3K-Akt signaling pathways, while the downregulated genes were mainly enriched in metabolisms, ECM, and TGF- β pathways. The results acquired from the 3D tumors *in vitro* provide meaningful information for understanding the intrinsic features of GBM and have the potential to serve as a platform for anti-GBM drug screening.



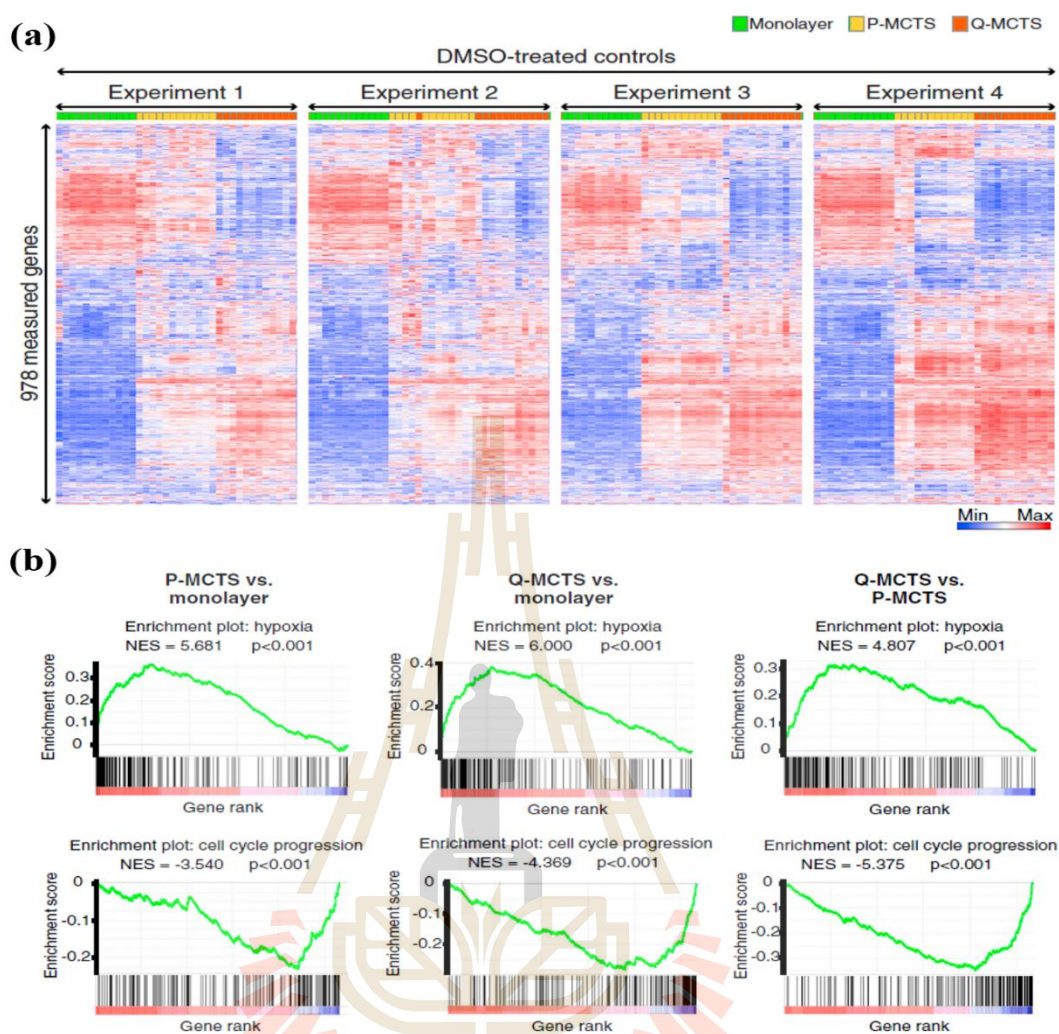


Figure 2.4 (a) Gene expression profiles of monolayer, P-MCTS (proliferative spheroids) and Q-MCTS (quiescent spheroids) models. (b) Gene Set Enrichment Analysis (GSEA) plots of hypoxia and cell-cycle progression gene sets. **Source:** Senkowski et al. (2016).

The discovery of an anticancer drug often begins with the lack of suitable medical products for a particular clinical condition (Hughes et al., 2011). To date, 3D cancer models have gained popularity in elucidating tumor biology, since the standard 2D cell models are inadequate to address certain questions, including indolent disease, metastatic colonisation, dormancy, relapse, and the rapid evolution of anticancer drug resistance (Tanner and Gottesman, 2015), and some of these issues were exhibited. For example, Imamura et al. (2015) compared the anticancer drug sensitivity of 2D and 3D cells, and found

that 3D cancer spheroids showed greater resistance to paclitaxel and doxorubicin than did the 2D cultured cells (Figure 2.5). 3D ovarian cancer spheroids forming by hanging drops also showed a greater resistance (70-80% viability) to cisplatin, compared to the 2D cultures (30-50 %viability) (Raghavan et al., 2015). The ovarian cancer spheroids were of uniform geometry and showed over 85% cell viability. Besides, the combination of the 3D context and ECM in the development of glioma stemness in a 3D model was also examined (Ma et al., 2016). They found that U-251 human glioblastoma cells increased expression of stemness markers (Integrin) when cultured on electrospun polystyrene (ESPS) scaffolds coated with laminin. In another study, 3D tumor cells stimulated autophagic flux and chemotherapy resistance. The cells were grown in 3D static and 3D bioreactor systems that could modulate the key hallmarks of cancer properties, including proliferation, cell death and macroautophagy. The autophagy-controlling transcription factors, in particular TFEB and FOXO3, were upregulated in the 3D tumor spheroids. The combination of cytotoxic treatment with compounds affecting autophagic flux, such as chloroquine, rendered the 3D-grown cells more susceptible to chemotherapy. Altogether, the 3D cancer cultures were a valuable system to study anticancer drug response, as these models closely mimic patho/physiology of tumour-involving pathways (Bingel et al., 2017).

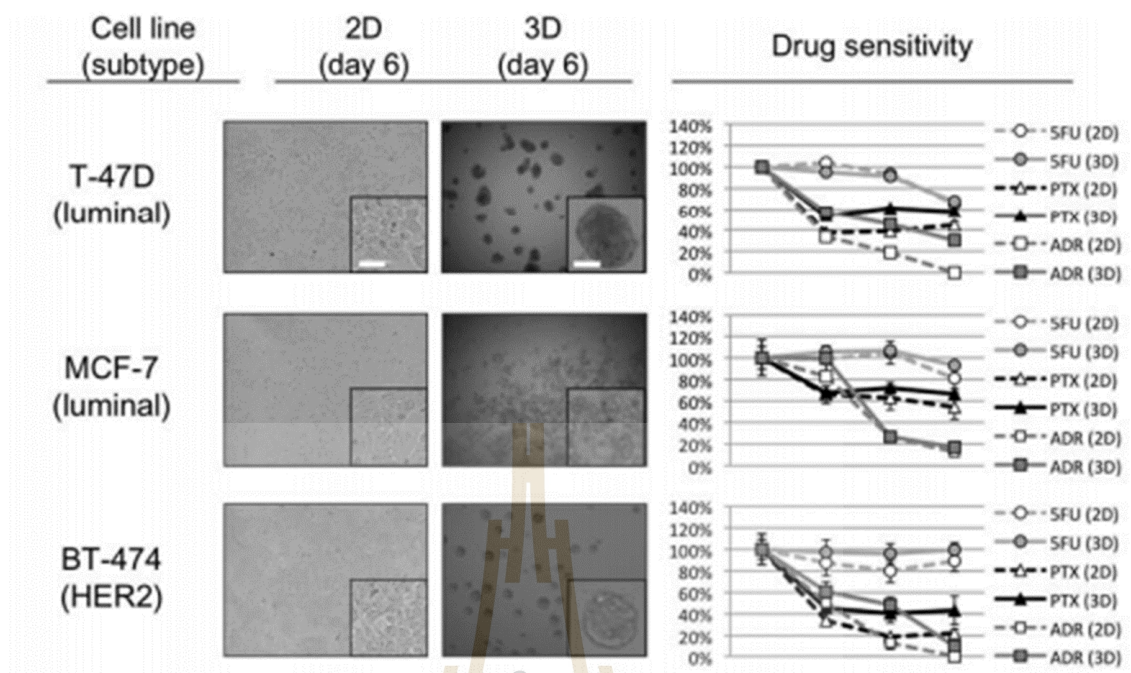


Figure 2.5 Effect of Paclitaxel (PTX), doxorubicin (ADR), and 5-fluorouracil (5FU) on the cell growth of 2D- and 3D-cultured breast cancer cell lines. Six breast cancer cell lines were cultured in 2D- or 3D-conditions through day 6. Each cell line was treated with or without PTX, ADR or 5FU from day 3 through day 6. The concentration of each drug was adjusted to achieve 0.1, 1 and 10x the areas under the curve (AUC). The number of viable cells present on day 6 is shown relative to that of the control cells without drug. Dashed lines represent 2D-culture and solid lines represent 3D-culture. Scale bars indicate 100 μm . **Source:** Imamura et al. (2015).

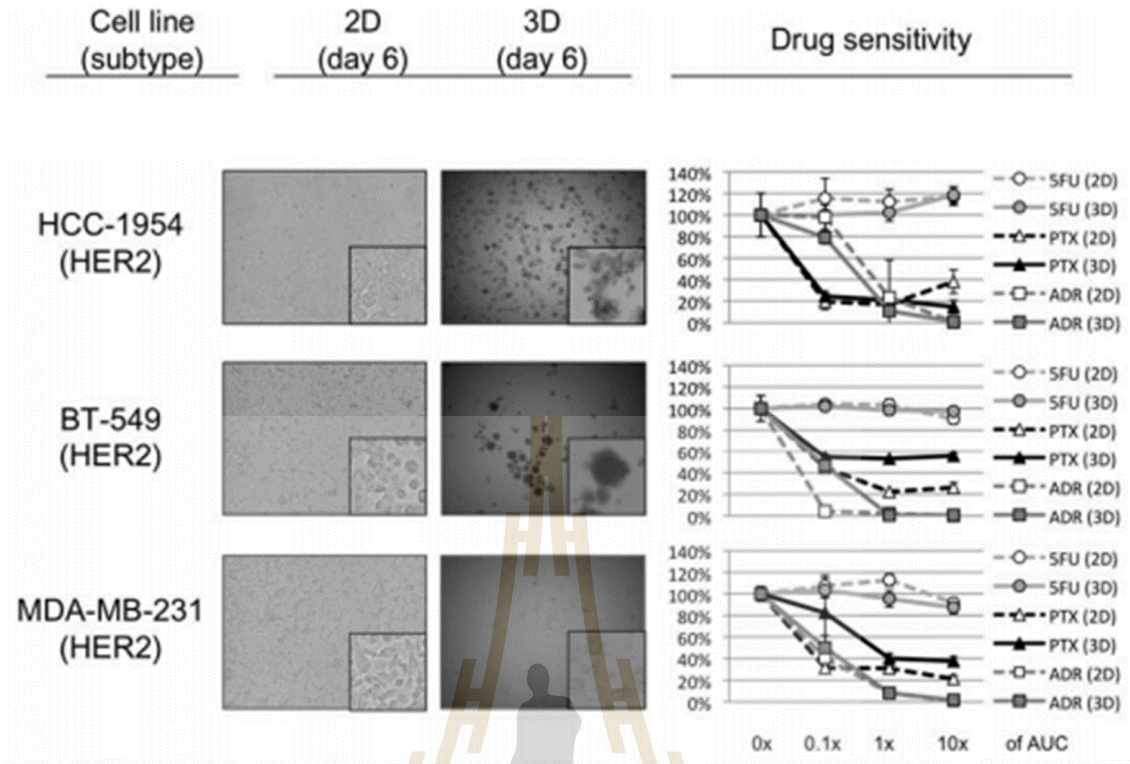


Figure 2.5 (Continued).

2.9.2 Stem cell modelling

Stem cells, particularly pluripotent stem cells (PSCs), have tremendous potential for generating pure populations of any cell type in the human body, and shed light on regenerative medicine. Pure populations of tissue-specific progenitors or terminally differentiated cells could be invaluable for enabling drug discovery, cell therapy and tissue regeneration. Major breakthroughs have been accomplished in the stem cell arena using 3D culture systems that replicate the *in vivo* development and temporal control of cellular signaling pathways (Sanyal, 2014). The development of induced pluripotent stem cells (iPSC) - derived human cardiomyocytes (CMs) by 3D cardiomyocyte spheroids was successfully demonstrated (Beauchamp et al., 2015). After four days of culture, the iPSC-derived CMs formed spheroidal cardiac microtissues (MTs), showing a homogeneous tissue structure with well-developed myofibrils with no necrotic core (Figure 2.6). Retinal ganglion cells (RGCs) differentiated into incisor dental pulp stem cells (DPSCs) when cultured in the

3D scaffolds. The 3D network of biocompatible fibrin hydrogel could resemble the natural tissue properties for effective generation of RGCs, which could be used to tackle neurodegenerative diseases such as glaucoma (Roozafzoon et al., 2015).

The advance in tissue engineering, cell biology and materials science has led to 3D bioprinting, which could create functional tissues or organ grafts by simulating their natural microenvironments. Although printing an intact organ still remains challenges, the 3D bioprinting of bladders, tracheal, bone, and cartilage has proved to be possible in animals and humans (Zhang et al., 2017). These printed organs can be used as assist organs or as viable replacements. For instance, Atala et al. (2006) engineered a human bladder by isolating autologous bladder urothelial and muscle cells from the bladder biopsy, prior to expanding and seeding the cells *in vitro* onto a biodegradable bladder-shaped scaffold. Seven weeks after the biopsy, the engineered bladders were used for reconstruction and implanted, either with or without an omental wrap. The 3D bioprinting technique has also been adopted to fabricate liver-like microstructures, exploiting 3D bioprinting of hepatoma cells and gelatin methacryloyl (GelMA) hydrogel (Bhise et al., 2016). The engineered hepatic constructs were still functional after 30 days, as assessed by the secretion of albumin, alpha-1 antitrypsin, transferrin and ceruloplasmin, as well as immunostaining of the hepatocyte markers, including cytokeratin 18, MRP2 and ZO-1. Besides, treatment with 15 mM acetaminophen induced a toxic response in the engineered hepatic construct, providing a proof-of-concept of using this artificial liver for toxicity assessment. A bioprinting strategy was used to print human umbilical vein endothelial cell (HUVEC) - laden bio-ink (predominantly alginate and gelatin) to form a multi-layered microfibrillar structure (Zhang et al., 2016). The bioprinted HUVECs migrated to the periphery and formed a confluent layer of endothelium. This 3D endothelial construct was then seeded with human iPSC-derived cardiomyocytes, fabricating an aligned myocardium that could spontaneously and synchronously contract. These organoids were then embedded into microfluidic perfusion

bioreactors to create an endothelialised-myocardium-on-chip platform that was used for cardiovascular toxicity evaluation. This highlighted the progress in human stem cell technology for cardiovascular disease modelling and testing of relevant drug. Another example of 3D culture and stem cell differentiation was presented by a 3D hydrogel that could promote the differentiation of human iPSCs into functional hepatocytes. The 3D conditions for hepatic differentiation of human iPSCs induced the expression of hepatocyte markers, functional maturation and metabolic activity. The generation of hepatocyte-like cells from human iPSCs provided the foundation for an artificial human liver, toxicity screening, and hepatocyte transplantation (Luo et al., 2018). Hydrogel encapsulation could also generate 3D neural tissues by co-culturing neuronal and astrocytic cells (Tekin et al., 2018). The transcriptomic profiles proposed that hydrogels could tune the expression patterns of the 3D brain organoids, correlating with those of specific brain regions and developmental stages.

The 3D cell culture systems present an increasingly importance in tumor and stem cell biology research. Due to the inherent differences in complexity and functionality, the choice of 3D cellular modeling is usually dependent on the application 3D culture, ranging from the simple cell spheroid model to the complex 3D bioprinting tissues. A wide range of 3D cell culture technologies has been developed in order to address the need of pharmaceutical industry. The 3D cell systems hold a great potential as a tool for drug discovery, disease modeling, cancer target identification as well as a novel source of tissue replacement materials. Future of 3D cell systems should validate with the pre-clinical outcomes, in order to reduce animal testing and clinical trials. The functional, safe, and transplantable index of the 3D cell cultures will be needed an intensive investigation for bringing toward clinical uses (Figure 2.7).

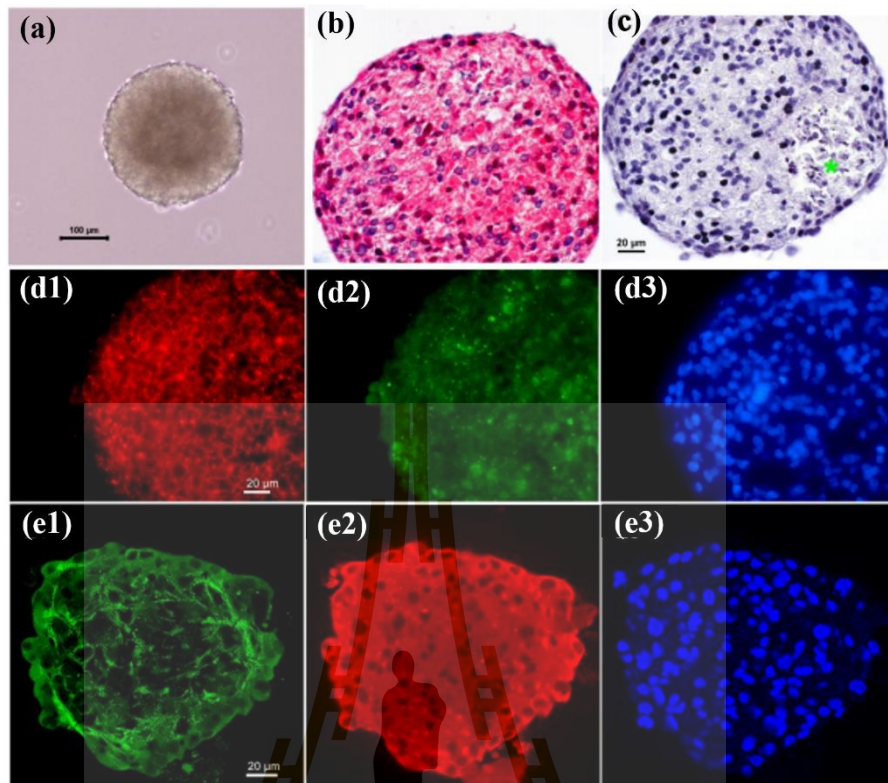


Figure 2.6 Demonstration of morphology and localization of typical proteins in cardiac microtissues using different techniques. Microtissues after 3 weeks in culture were fixed and processed for histology and immunohistochemistry. B- C: Paraffin-sections stained using hematoxylin-fuchsin (b) or Mayers Hemalaun (c). Green asterisk in c indicates cellular debris. d1-d3: Cryosections were stained for myomesin (d1), connexin-43 (d2) and for DNA (d3). e1-e3: A microtissue was permeabilized and immunostained as a whole-mount. Confocal images of single optical sections are shown for embryonic heart-myomesin (e1), cytoplasmic fibronectin (e2) and DNA (e3). **Source:** Beauchamp et al. (2015).

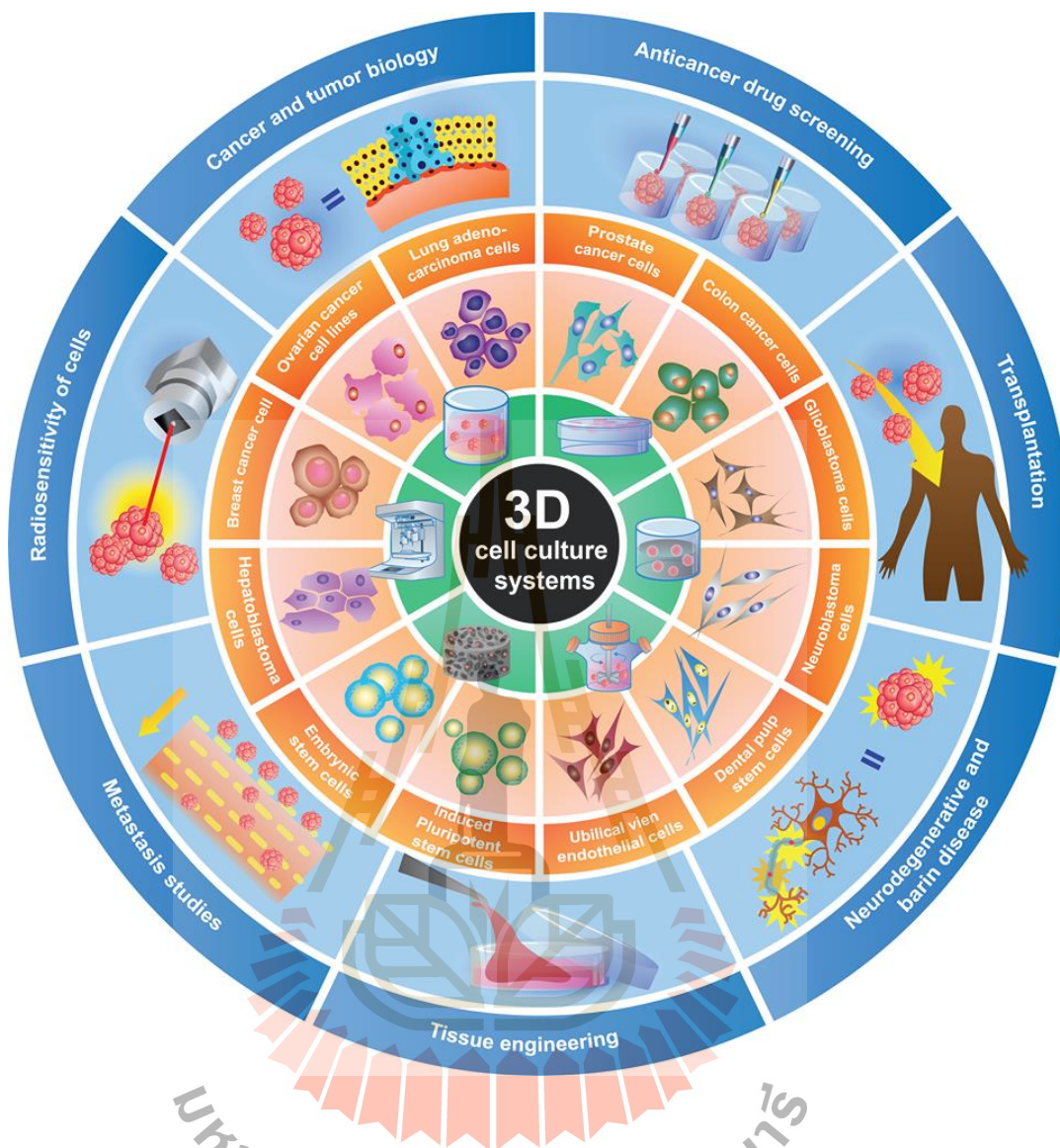


Figure 2.7 Potential applications of 3 D cell culture systems. **Graphic by:** Phongsakorn

Kunhorn

มหาวิทยาลัยเทคโนโลยีสุรนารี

2.10 References

- Abbott, A. (2003). Cell culture: biology's new dimension. **Nature**. 424(6951): 870-872.
- Aggarwal, B. B., Danda, D., Gupta, S., and Gehlot, P. (2009). Models for prevention and treatment of cancer: problems vs promises. **Biochemical pharmacology**. 78(9): 1083-1094.
- Ahn, Y.-J., Park, S.-J., Lee, S.-G., Shin, S.-C., and Choi, D.-H. (2000). Cordycepin: Selective Growth Inhibitor Derived from Liquid Culture of *Cordyceps militaris* against *Clostridium* spp. **Journal of agricultural and food chemistry**. 48(7): 2744-2748.
- Al-Shamkhani, A., and Duncan, R. (1995). Radioiodination of alginate via covalently-bound tyrosinamide allows monitoring of its fate *in vivo*. **Journal of bioactive and compatible polymers**. 10(1): 4-13.
- Andersen, T., Auk-Emblem, P., and Dornish, M. (2015). 3D cell culture in alginate hydrogels. **Microarrays**. 4(2): 133-161.
- Antoni, D., Burckel, H., Josset, E., and Noel, G. (2015). Three-dimensional cell culture: a breakthrough *in vivo*. **International journal of molecular sciences**. 16(3): 5517-5527.
- Arevalo, O., Valenzuela, R., Esquenazi, Y., et al. (2017). The 2016 World Health Organization Classification of Tumors of the Central Nervous System: A Practical Approach for Gliomas, Part 1. Basic Tumor Genetics. **Neurographics**. 7(5): 334-343.
- Atala, A., Bauer, S. B., Soker, S., Yoo, J. J., and Retik, A. B. (2006). Tissue-engineered autologous bladders for patients needing cystoplasty. **The Lancet**. 367(9518): 1241-1246.

- Beauchamp, P., Moritz, W., Kelm, J. M., et al. (2015). Development and characterization of a scaffold-free 3D spheroid model of induced pluripotent stem cell-derived human cardiomyocytes. **Tissue Engineering Part C: Methods**. 21(8): 852-861.
- Bhise, N. S., Manoharan, V., Massa, S., et al. (2016). A liver-on-a-chip platform with bioprinted hepatic spheroids. **Biofabrication**. 8(1): 014101.
- Bingel, C., Koeneke, E., Ridinger, J., et al. (2017). Three-dimensional tumor cell growth stimulates autophagic flux and recapitulates chemotherapy resistance. **Cell death & disease**. 8(8): e3013.
- Birgersdotter, A., Sandberg, R., and Ernberg, I. (2005). Gene expression *perturbation in vitro*-a growing case for three-dimensional (3D) culture systems. **Paper presented at the Seminars in cancer biology**. 405-412.
- Breslin, S., and O'Driscoll, L. (2016). The relevance of using 3D cell cultures, in addition to 2D monolayer cultures, when evaluating breast cancer drug sensitivity and resistance. **Oncotarget**. 7(29): 45745.
- Breslin, S., and O'Driscoll, L. (2013). Three-dimensional cell culture: the missing link in drug discovery. **Drug discovery today**. 18(5): 240-249.
- Bryukhovetskiy, I. S., Dyuzhen, I. V., Shevchenko, V. E., et al. (2016). Hematopoietic stem cells as a tool for the treatment of glioblastoma multiforme. **Molecular medicine reports**. 14(5): 4511-4520.
- Cahill, D. P., Sloan, A. E., Nahed, B. V., et al. (2015). The role of neuropathology in the management of patients with diffuse low grade glioma. **Journal of neuro-oncology**. 125(3): 531-549.

- Carlsson, J., and Yuhas, J. (1984). Liquid-overlay culture of cellular spheroids Spheroids in cancer research (pp. 1-23): **Springer**.
- Chen, C.-Y., Ke, C.-J., Yen, K.-C., et al. (2015). 3D porous calcium-alginate scaffolds cell culture system improved human osteoblast cell clusters for cell therapy. **Theranostics**. 5(6): 643.
- Chen, C-Y., Gao, D., Liu, H., Lin, S., and Jiang, Y. (2015). Drug cytotoxicity and signaling pathway analysis with three-dimensional tumor spheroids in a microwell-based microfluidic chip for drug screening. **Analytica chimica acta**. 898: 85-92.
- Choi, S., Lim, M.-H., Kim, K. M., et al. (2011). Cordycepin-induced apoptosis and autophagy in breast cancer cells are independent of the estrogen receptor. **Toxicology and applied pharmacology**. 257(2): 165-173.
- Costa, E. C., Gaspar, V. M., Coutinho, P., and Correia, I. J. (2014). Optimization of liquid overlay technique to formulate heterogenic 3D co-cultures models. **Biotechnology and bioengineering**. 111(8): 1672-1685.
- Cristalli, G., Costanzi, S., Lambertucci, C., et al. (2001). Adenosine deaminase: functional implications and different classes of inhibitors. **Medicinal research reviews**. 21(2): 105-128.
- Cui, X., Breitenkamp, K., Finn, M., Lotz, M., and D'Lima, D. D. (2012). Direct human cartilage repair using three-dimensional bioprinting technology. **Tissue engineering Part A**. 18(11-12): 1304-1312.
- Dai, X., Ma, C., Lan, Q., and Xu, T. (2016). 3D bioprinted glioma stem cells for brain tumor model and applications of drug susceptibility. **Biofabrication**. 8(4): 045005.

- Dolecek, T. A., Propp, J. M., Stroup, N. E., and Kruchko, C. (2012). CBTRUS statistical report: primary brain and central nervous system tumors diagnosed in the United States in 2005–2009. **Neuro-oncology**. 14(5): 1-49.
- Drury, J. L., and Mooney, D. J. (2003). Hydrogels for tissue engineering: scaffold design variables and applications. **Biomaterials**. 24(24): 4337-4351.
- Edmondson, R., Broglie, J. J., Adcock, A. F., and Yang, L. (2014). Three-dimensional cell culture systems and their applications in drug discovery and cell-based biosensors. **Assay and drug development technologies**. 12(4): 207-218.
- Fang, L., Zhao, J., Wang, D., et al. (2016). Jumonji AT-rich interactive domain 1B overexpression is associated with the development and progression of glioma. **International journal of molecular medicine**. 38(1): 172-182.
- Fang, Y., and Eglen, R. M. (2017). Three-dimensional cell cultures in drug discovery and development. **Slas discovery: Advancing Life Sciences R&D**. 22(5): 456-472.
- Feng, X., Zhou, Q., Liu, C., and Tao, M.-L. (2012). Drug screening study using glioma stem-like cells. **Molecular medicine reports**. 6(5): 1117-1120.
- Fitzgerald, K. A., Guo, J., Tierney, E. G., et al. (2015). The use of collagen-based scaffolds to simulate prostate cancer bone metastases with potential for evaluating delivery of nanoparticulate gene therapeutics. **Biomaterials**. 66: 53-66.
- Florczyk, S. J., Kievit, F. M., Wang, K., et al. (2016). 3D porous chitosan–alginate scaffolds promote proliferation and enrichment of cancer stem-like cells. **Journal of Materials Chemistry B**. 4(38): 6326-6334.
- Forsdahl, S., Kiselev, Y., Hogseth, R., Mjelle, J. E., and Mikkola, I. (2014). Pax6 regulates the expression of Dkk3 in murine and human cell lines, and altered responses to Wnt

signaling are shown in FlpIn-3T3 cells stably expressing either the Pax6 or the Pax6 (5a) isoform. **PloS one.** 9(7): e102559.

Frampton, J., Hynd, M., Shuler, M., and Shain, W. (2011). Fabrication and optimization of alginate hydrogel constructs for use in 3D neural cell culture. **Biomedical Materials.** 6(1): 015002.

Friedrich, J., Ebner, R., and Kunz-Schughart, L. A. (2007). Experimental anti-tumor therapy in 3-D: spheroids—old hat or new challenge?. **International journal of radiation biology.** 83(11-12): 849-871.

Friedrich, J., Seidel, C., Ebner, R., and Kunz-Schughart, L. A. (2009). Spheroid-based drug screen: considerations and practical approach. **Nature protocols.** 4(3): 309.

Giacomelli, E., Bellin, M., Sala, L., et al. (2017). Three-dimensional cardiac microtissues composed of cardiomyocytes and endothelial cells co-differentiated from human pluripotent stem cells. **Development.** 143438.

Godugu, C., Patel, A. R., Desai, U., et al. (2013). AlgiMatrix™ based 3D cell culture system as an *in-vitro* tumor model for anticancer studies. **PloS one.** 8(1): e53708.

Griffith, L. G., and Swartz, M. A. (2006). Capturing complex 3D tissue physiology *in vitro*. **Nature reviews Molecular cell biology.** 7(3): 211.

Gurski, L. A., Petrelli, N. J., Jia, X., and Farach-Carson, M. C. (2010). 3D matrices for anti-cancer drug testing and development. **Oncology Issues.** 25: 20-25.

Hao, X., Silva, E. A., Månsson-Broberg, A., et al. (2007). Angiogenic effects of sequential release of VEGF-A165 and PDGF-BB with alginate hydrogels after myocardial infarction. **Cardiovascular research.** 75(1): 178-185.

- Harrison, R. G. (1910). The outgrowth of the nerve fiber as a mode of protoplasmic movement. **Journal of Experimental Zoology Part A: Ecological Genetics and Physiology**. 9(4): 787-846.
- Harrison, R. G., Greenman, M., Mall, F. P., and Jackson, C. (1907). Observations of the living developing nerve fiber. **The Anatomical Record**. 1(5): 116-128.
- Heiland, D., Wörner, J., Haaker, J., et al. (2017). The integrative metabolomic-transcriptomic landscape of glioblastoma multiforme. **Oncotarget**. 8(30): 49178.
- Hickman, J. A., Graeser, R., de Hoogt, R., et al. (2014). Three-dimensional models of cancer for pharmacology and cancer cell biology: capturing tumor *complexity in vitro/ex vivo*. **Biotechnology journal**. 9(9): 1115-1128.
- Hoehner, J. C., Gestblom, C., Hedborg, F., et al. (1996). A developmental model of neuroblastoma: differentiating stroma-poor tumors' progress along an extra-adrenal chromaffin lineage. **Laboratory investigation; a journal of technical methods and pathology**. 75(5): 659-675.
- Hosseinkhani, H., Hosseinkhani, M., Hattori, S., Matsuoka, R., and Kawaguchi, N. (2010). Micro and nano-scale in vitro 3D culture system for cardiac stem cells. **Journal of biomedical materials research Part A**. 94(1): 1-8.
- Hughes, J. P., Rees, S., Kalindjian, S. B., and Philpott, K. L. (2011). Principles of early drug discovery. **British journal of pharmacology**. 162(6): 1239-1249.
- Hunt, N., Smith, A. M., Gbureck, U., Shelton, R., and Grover, L. (2010). Encapsulation of fibroblasts causes accelerated alginate hydrogel degradation. **Acta Biomaterialia**. 6(9): 3649-3656.

- Hutchinson, L., and Kirk, R. (2011). High drug attrition rates-where are we going wrong? : Nature Publishing Group.
- Imamura, Y., Mukohara, T., Shimono, Y., et al. (2015). Comparison of 2D-and 3D-culture models as drug-testing platforms in breast cancer. **Oncology reports**. 33(4): 1837-1843.
- Jaroonwichawan, T., Chaicharoenaudomrung, N., Namkaew, J., and Noisa, P. (2017). Curcumin attenuates paraquat-induced cell death in human neuroblastoma cells through modulating oxidative stress and autophagy. **Neuroscience Letters**. 636: 40-47.
- Jeong, J.-W., Jin, C.-Y., Kim, G.-Y., et al. (2010). Anti-inflammatory effects of cordycepin via suppression of inflammatory mediators in BV2 microglial cells. **International immunopharmacology**. 10(12): 1580-1586.
- Jessop, Z. M., Al-Sabah, A., Gardiner, M. D., et al. (2017). 3D bioprinting for reconstructive surgery: Principles, applications and challenges. **Journal of Plastic, Reconstructive & Aesthetic Surgery**. 70(9): 1155-1170.
- Jin, H.-J., Chen, J., Karageorgiou, V., Altman, G. H., and Kaplan, D. L. (2004). Human bone marrow stromal cell responses on electrospun silk fibroin mats. **Biomaterials**. 25(6): 1039-1047.
- Justice, B. A., Badr, N. A., and Felder, R. A. (2009). 3D cell culture opens new dimensions in cell-based assays. **Drug discovery today**. 14(1-2): 102-107.
- Kang, H.-W., Lee, S. J., Ko, I. K., et al. (2016). A 3D bioprinting system to produce human-scale tissue constructs with structural integrity. **Nature biotechnology**. 34(3): 312.

- Kelm, J. M., Timmins, N. E., Brown, C. J., Fussenegger, M., and Nielsen, L. K. (2003). Method for generation of homogeneous multicellular tumor spheroids applicable to a wide variety of cell types. **Biotechnology and bioengineering**. 83(2): 173-180.
- Khaitan, D., Chandna, S., Arya, M., and Dwarakanath, B. (2006). Establishment and characterization of multicellular spheroids from a human glioma cell line; Implications for tumor therapy. **Journal of translational medicine**. 4(1): 12.
- Kim, J. B. (2005). Three-dimensional tissue culture models in cancer biology. **Paper presented at the Seminars in cancer biology**. 365-377
- Kioi, M., Vogel, H., Schultz, G., et al. (2010). Inhibition of vasculogenesis, but not angiogenesis, prevents the recurrence of glioblastoma after irradiation in mice. **The Journal of clinical investigation**. 120(3): 694-705.
- Kleinman, H. K., Philp, D., and Hoffman, M. P. (2003). Role of the extracellular matrix in morphogenesis. **Current opinion in biotechnology**. 14(5): 526-532.
- Knowlton, S., Onal, S., Yu, C. H., Zhao, J. J., and Tasoglu, S. (2015). Bioprinting for cancer research. **Trends in biotechnology**. 33(9): 504-513.
- Krausz, E., de Hoogt, R., Gustin, E., et al. (2013). Translation of a tumor microenvironment mimicking 3D tumor growth co-culture assay platform to high-content screening. **Journal of biomolecular screening**. 18(1): 54-66.
- Kumbhar, S. G., and Pawar, S. (2016). Synthesis and characterization of chitosan-alginate scaffolds for seeding human umbilical cord derived mesenchymal stem cells. **Bio-medical materials and engineering**. 27(6): 561-575.

- Kurosawa, H. (2007). Methods for inducing embryoid body formation: in vitro differentiation system of embryonic stem cells. **Journal of bioscience and bioengineering**. 103(5): 389-398.
- Langer, R., and Tirrell, D. A. (2004). Designing materials for biology and medicine. **Nature**. 428(6982): 487-492.
- Leach, J. B., and Schmidt, C. E. (2005). Characterization of protein release from photocrosslinkable hyaluronic acid-polyethylene glycol hydrogel tissue engineering scaffolds. **Biomaterials**. 26(2): 125-135.
- Ledur, P. F., Onzi, G. R., Zong, H., and Lenz, G. (2017). Culture conditions defining glioblastoma cells behavior: what is the impact for novel discoveries? **Oncotarget**. 8(40): 69185.
- Lee, D.-H., Kim, H.-H., Cho, H.-J., et al. (2014). Cordycepin-Enriched WIB801C from *Cordyceps militaris* inhibits collagen-induced $[Ca^{2+}]_i$ mobilization via cAMP-dependent phosphorylation of inositol 1, 4, 5-trisphosphate receptor in human platelets. **Biomolecules & therapeutics**. 22(3): 223.
- Lee, H. H., Kim, S. O., Kim, G.-Y., et al. (2014). Involvement of autophagy in cordycepin-induced apoptosis in human prostate carcinoma LNCaP cells. **Environmental toxicology and pharmacology**. 38(1): 239-250.
- Lee, H. H., Park, C., Jeong, J.-W., et al. (2013). Apoptosis induction of human prostate carcinoma cells by cordycepin through reactive oxygen species-mediated mitochondrial death pathway. **International journal of oncology**. 42(3): 1036-1044.
- Lee, J., Cuddihy, M. J., and Kotov, N. A. (2008). Three-dimensional cell culture matrices: state of the art. **Tissue Engineering Part B: Reviews**. 14(1): 61-86.

- Lee, V., Singh, G., Trasatti, J. P., et al. (2013). Design and fabrication of human skin by three-dimensional bioprinting. **Tissue Engineering Part C: Methods**. 20(6): 473-484.
- Leong, D. T., and Ng, K. W. (2014). Probing the relevance of 3D cancer models in nanomedicine research. **Advanced drug delivery reviews**. 79: 95-106.
- Leor, J., Tuvia, S., Guetta, V., et al. (2009). Intracoronary injection of in situ forming alginate hydrogel reverses left ventricular remodeling after myocardial infarction in Swine. **Journal of the American College of Cardiology**. 54(11): 1014-1023.
- Li, Y., Li, R., Zhu, S., et al. (2015). Cordycepin induces apoptosis and autophagy in human neuroblastoma SK-N-SH and BE (2)-M17 cells. **Oncology letters**. 9(6): 2541-2547.
- Li, Z., and Guan, J. (2011). Hydrogels for cardiac tissue engineering. **Polymers**. 3(2): 740-761.
- Liao, Y., Ling, J., Zhang, G., et al. (2015). Cordycepin induces cell cycle arrest and apoptosis by inducing DNA damage and up-regulation of p53 in Leukemia cells. **Cell cycle**. 14(5): 761-771.
- Lim, F., and Sun, A. M. (1980). Microencapsulated islets as bioartificial endocrine pancreas. **Science**. 210(4472): 908-910.
- Lin, R. Z., and Chang, H. Y. (2008). Recent advances in three-dimensional multicellular spheroid culture for biomedical research. **Biotechnology journal**. 3(9-10): 1172-1184.
- Lodish, H., Berk, A., Zipursky, S. L., et al. (2000). Molecular cell biology 4th edition. National Center for Biotechnology Information, **Bookshelf**.

- London, W., Castleberry, R., Matthay, K., et al. (2005). Evidence for an age cutoff greater than 365 days for neuroblastoma risk group stratification in the Children's Oncology Group. **Journal of Clinical Oncology**. 23(27): 6459-6465.
- Louis, Perry, A., Reifenberger, G., et al. (2016). The 2016 World Health Organization classification of tumors of the central nervous system: a summary. **Acta neuropathologica**. 131(6): 803-820.
- Louis, D., Ohgaki, H., Wiestler, O., and Cavenee, W. (2007). WHO classification of tumours of the central nervous system. World Health Organization classification of tumours: World Health Organization.
- Louis, D., Ohgaki, H., Wiestler, O. D., et al. (2007). The 2007 WHO classification of tumours of the central nervous system. **Acta neuropathologica**. 114(2): 97-109.
- Luo, Y., Lou, C., Zhang, S., et al. (2018). Three-dimensional hydrogel culture conditions promote the differentiation of human induced pluripotent stem cells into hepatocytes. **Cytotherapy**. 20(1): 95-107.
- Lv, D., Yu, S.-c., Ping, Y.-f., et al. (2016). A three-dimensional collagen scaffold cell culture system for screening anti-glioma therapeutics. **Oncotarget**. 7(35): 56904.
- Ma, L., Zhang, B., Zhou, C., et al. (2018). The comparison genomics analysis with glioblastoma multiforme (GBM) cells under 3D and 2D cell culture conditions. **Colloids and Surfaces B: Biointerfaces**. 172: 665-673.
- Ma, N. K., Lim, J. K., Leong, M. F., et al. (2016). Collaboration of 3D context and extracellular matrix in the development of glioma stemness in a 3D model. **Biomaterials**. 78: 62-73.

- Mehta, G., Hsiao, A. Y., Ingram, M., Luker, G. D., and Takayama, S. (2012). Opportunities and challenges for use of tumor spheroids as models to test drug delivery and efficacy. **Journal of Controlled Release**. 164(2): 192-204.
- Metzger, W., Sossong, D., Bächle, A., et al. (2011). The liquid overlay technique is the key to formation of co-culture spheroids consisting of primary osteoblasts, fibroblasts and endothelial cells. **Cytotherapy**. 13(8): 1000-1012.
- Mikos, A. G., and Temenoff, J. S. (2000). Formation of highly porous biodegradable scaffolds for tissue engineering. **Electronic Journal of Biotechnology**. 3(2): 23-24.
- Müller, W. E., Seibert, G., Beyer, R., et al. (1977). Effect of cordycepin on nucleic acid metabolism in L5178Y cells and on nucleic acid-synthesizing enzyme systems. **Cancer research**. 37(10): 3824-3833.
- Murphy, S. V., and Atala, A. (2014). 3D bioprinting of tissues and organs. **Nature biotechnology**. 32(8): 773.
- Nakamura, K., Yoshikawa, N., Yamaguchi, Y., et al. (2006). Antitumor effect of cordycepin (3'-deoxyadenosine) on mouse melanoma and lung carcinoma cells involves adenosine A3 receptor stimulation. **Anticancer Research**. 26(1A): 43-47.
- Nicodemus, G. D., and Bryant, S. J. (2008). Cell encapsulation in biodegradable hydrogels for tissue engineering applications. **Tissue Engineering Part B: Reviews**. 14(2): 149-165.
- O'Brien, F. J., Harley, B. A., Yannas, I. V., and Gibson, L. (2004). Influence of freezing rate on pore structure in freeze-dried collagen-GAG scaffolds. **Biomaterials**. 25(6): 1077-1086.

- Omuro, A., and DeAngelis, L. M. (2013). Glioblastoma and other malignant gliomas: a clinical review. **Jama**. 310(17): 1842-1850.
- Pampaloni, F., Reynaud, E. G., and Stelzer, E. H. (2007). The third dimension bridges the gap between cell culture and live tissue. **Nature reviews Molecular cell biology**. 8(10): 839.
- Peela, N., Sam, F. S., Christenson, W., et al. (2016). A three dimensional micropatterned tumor model for breast cancer cell migration studies. **Biomaterials**. 81: 72-83.
- Ponten, J., and Westermarck, B. (1978). Properties of human malignant glioma cells in vitro. **Medical biology**. 56(4): 184-193.
- Raghavan, S., Ward, M. R., Rowley, K. R., et al. (2015). Formation of stable small cell number three-dimensional ovarian cancer spheroids using hanging drop arrays for preclinical drug sensitivity assays. **Gynecologic oncology**. 138(1): 181-189.
- Ravi, M., Paramesh, V., Kaviya, S., Anuradha, E., and Solomon, F. P. (2015). 3D cell culture systems: advantages and applications. **Journal of cellular physiology**. 230(1): 16-26.
- Ries, L. A. G., Smith, M. A., Gurney, J., et al. (1999). Cancer incidence and survival among children and adolescents: United States SEER Program. 1975-1995.
- Roofzafzoon, R., Lashay, A., Vasei, M., et al. (2015). Dental pulp stem cells differentiation into retinal ganglion-like cells in a three dimensional network. **Biochemical and biophysical research communications**. 457(2): 154-160.
- Ross, R. A., Spengler, B. A., and Biedler, J. L. (1983). Coordinate morphological and biochemical interconversion of human neuroblastoma cells. **Journal of the National Cancer Institute**. 71(4): 741-747.

- Sachlos, E., and Czernuszka, J. (2003). Making tissue engineering scaffolds work. Review: the application of solid freeform fabrication technology to the production of tissue engineering scaffolds. **European cells & materials**. 5(29): 39-40.
- Sanyal, S. (2014). Culture and assay systems used for 3D cell culture. *Corning*. 9: 1-18.
- Seçme, M., Eroğlu, C., Dodurga, Y., and Bağcı, G. (2016). Investigation of anticancer mechanism of oleuropein via cell cycle and apoptotic pathways in SH-SY5Y neuroblastoma cells. **Gene**. 585(1): 93-99.
- Senkowski, W., Jarvius, M., Rubin, J., et al. (2016). Large-scale gene expression profiling platform for identification of context-dependent drug responses in multicellular tumor spheroids. **Cell chemical biology**. 23(11): 1428-1438.
- Shelke, N. B., Lee, P., Anderson, M., et al. (2016). Neural tissue engineering: nanofiber-hydrogel based composite scaffolds. **Polymers for Advanced Technologies**. 27(1): 42-51.
- Shin, C., Kwak, B., Han, B., Park, K., and Panitch, A. (2014). 3D cancer tumor models for evaluating chemotherapeutic efficacy. **Biomaterials for Cancer Therapeutics**. 445-460.
- Siegel, R. L., Miller, K. D., and Jemal, A. (2017). Cancer statistics, 2017. **CA: a cancer journal for clinicians**. 67(1): 7-30.
- Simon, K. A., Mosadegh, B., Minn, K. T., et al. (2016). Metabolic response of lung cancer cells to radiation in a paper-based 3D cell culture system. **Biomaterials**. 95: 47-59.
- Sisson, K., Zhang, C., Farach-Carson, M. C., Chase, D. B., and Rabolt, J. F. (2010). Fiber diameters control osteoblastic cell migration and differentiation in electrospun gelatin. **Journal of biomedical materials research Part A**. 94(4): 1312-1320.

- Stummer, W., van den Bent, M. J., and Westphal, M. (2011). Cytoreductive surgery of glioblastoma as the key to successful adjuvant therapies: new arguments in an old discussion. **Acta neurochirurgica**. 153(6): 1211-1218.
- Stupp, R., Hegi, M. E., Mason, W. P., et al. (2009). Effects of radiotherapy with concomitant and adjuvant temozolomide versus radiotherapy alone on survival in glioblastoma in a randomised phase III study: 5-year analysis of the EORTC-NCIC trial. **The lancet oncology**. 10(5): 459-466.
- Sugar, A. M., and McCaffrey, R. P. (1998). Antifungal activity of 3'-deoxyadenosine (cordycepin). **Antimicrobial agents and Chemotherapy**. 42(6): 1424-1427.
- Sun, J., and Tan, H. (2013). Alginate-based biomaterials for regenerative medicine applications. **Materials**. 6(4): 1285-1309.
- Takai, A., Fako, V., Dang, H., et al. (2016). Three-dimensional organotypic culture models of human hepatocellular carcinoma. **Scientific reports**. 6: 21174.
- Tanner, K., and Gottesman, M. M. (2015). Beyond 3D culture models of cancer. **Science translational medicine**. 7(283): 283ps289-283ps289.
- Tao, X., Ning, Y., Zhao, X., and Pan, T. (2016). The effects of cordycepin on the cell proliferation, migration and apoptosis in human lung cancer cell lines A549 and NCI-H460. **Journal of Pharmacy and Pharmacology**. 68(7), 901-911.
- Tasoglu, S., and Demirci, U. (2013). Bioprinting for stem cell research. **Trends in biotechnology**. 31(1): 10-19.
- Tekin, H., Simmons, S., Cummings, B., et al. (2018). Effects of 3D culturing conditions on the transcriptomic profile of stem-cell-derived neurons. **Nature Biomedical Engineering**. 2(7), 540.

- Thoma, C. R., Zimmermann, M., Agarkova, I., Kelm, J. M., and Krek, W. (2014). 3D cell culture systems modeling tumor growth determinants in cancer target discovery. **Advanced drug delivery reviews**. 69: 29-41.
- Torsvik, A., Stieber, D., Enger, P. Ø., et al. (2014). U-251 revisited: genetic drift and phenotypic consequences of long-term cultures of glioblastoma cells. **Cancer medicine**. 3(4): 812-824.
- Verreault, M., Wehbe, M., Strutt, D., et al. (2015). Determination of an optimal dosing schedule for combining Irinophore C™ and temozolomide in an orthotopic model of glioblastoma. **Journal of Controlled Release**. 220: 348-357.
- Vinci, M., Gowan, S., Boxall, F., et al. (2012). Advances in establishment and analysis of three-dimensional tumor spheroid-based functional assays for target validation and drug evaluation. **BMC biology**. 10(1): 29.
- Wang, Yin, P., Lu, Y., et al. (2015). Cordycepin prevents oxidative stress-induced inhibition of osteogenesis. **Oncotarget**. 6(34): 35496.
- Westermarck, B., Ponten, J., and Hugosson, R. (1973). Determinants for the establishment of permanent tissue culture lines from human gliomas. **Acta Pathologica Microbiologica Scandinavica Section a Pathology**. 81(6): 791-805.
- Whang, K., Thomas, C., Healy, K., and Nuber, G. (1995). A novel method to fabricate bioabsorbable scaffolds. **Polymer**. 36(4): 837-842.
- Wu, X., Liu, Y., Li, X., et al. (2010). Preparation of aligned porous gelatin scaffolds by unidirectional freeze-drying method. **Acta Biomaterialia**. 6(3): 1167-1177.
- Yamada, K. M., and Cukierman, E. (2007). Modeling tissue morphogenesis and cancer in 3D. **Cell**. 130(4): 601-610.

- Yu, Y., Zhang, Y., Martin, J. A., and Ozbolat, I. T. (2013). Evaluation of cell viability and functionality in vessel-like bioprintable cell-laden tubular channels. **Journal of biomechanical engineering**. 135(9): 091011.
- Zhang, S., Xie, R., Wan, F., et al. (2013). Identification of U251 glioma stem cells and their heterogeneous stem-like phenotypes. **Oncology letters**. 6(6): 1649-1655.
- Zhang, Y. S., Arneri, A., Bersini, S., et al. (2016). Bioprinting 3D microfibrinous scaffolds for engineering endothelialized myocardium and heart-on-a-chip. **Biomaterials**. 110: 45-59.
- Zhang, Y. S., Yue, K., Aleman, J., et al. (2017). 3D bioprinting for tissue and organ fabrication. **Annals of biomedical engineering**. 45(1): 148-163.
- Zhao, Y., Yao, R., Ouyang, L., et al. (2014). Three-dimensional printing of Hela cells for cervical tumor model in vitro. **Biofabrication**. 6(3): 035001.
- Zhu, W., Holmes, B., Glazer, R. I., and Zhang, L. G. (2016). 3D printed nanocomposite matrix for the study of breast cancer bone metastasis. **Nanomedicine: Nanotechnology, Biology and Medicine**. 12(1): 69-79.
- Zimmermann, W. H., Fink, C., Kralisch, D., et al. (2000). Three-dimensional engineered heart tissue from neonatal rat cardiac myocytes. **Biotechnology and bioengineering**. 68(1): 106-114.
- Zustiak, S. P., Wei, Y., and Leach, J. B. (2012). Protein–hydrogel interactions in tissue engineering: Mechanisms and applications. **Tissue Engineering Part B: Reviews**. 19(2): 160-171.

CHAPTER III

CORDYCEPIN INDUCES APOPTOTIC CELL DEATH OF HUMAN NERVE-TISSUE CANCER THROUGH THE MODULATION OF AUTOPHAGY

3.1 Abstract

Nerve-tissue cancer, in particular glioblastoma and neuroblastoma, is a global challenge to human health. Cordycepin, extracted from *Cordyceps* ssp., has been revealed as a strong anticancer agent through several ways; however, the mechanism, by which cordycepin counteracts human nerve-tissue cancer, is still poorly understood. In this study, the underlying mechanisms of cordycepin against human nerve-tissue cancer cells were explored. U-251 and SH-SY5Y cell lines were being a model to represent human glioblastoma and neuroblastoma, respectively. Here, it was found that cordycepin inhibited cell growth, and induced apoptosis in a dose-dependent manner in both U-251 and SH-SY5Y cell lines. The expression of pro-apoptotic genes, including *P53*, *BAX*, *Caspase-3*, and *Caspase-9*, were upregulated, whereas the expression of anti-apoptotic gene, *BCL-2*, was suppressed. Besides, cordycepin induced the generation of reactive oxygen species (ROS) along with the suppression of antioxidant genes, including *GPX*, *SOD*, and *Catalase*. Importantly, cordycepin was shown to involve in the activation of autophagy, which was evidenced by the increment of *LC3II*. The combination of cordycepin with chloroquine, an autophagy inhibitor, further inhibited the growth, and enhanced the death of human nerve-tissue cancer cells. Altogether, this finding suggested that cordycepin induced apoptosis of human nerve-tissue cancer cells through mitochondrial-mediated intrinsic pathway and the

modulation of autophagy. Therefore, cordycepin could be a promising candidate for the development of anticancer drugs targeting human nerve-tissue cancer.

Keyword: Cordycepin, Apoptosis, Autophagy, Nerve-tissue cancer

3.2 Introduction

Glioblastoma is the most aggressive malignant primary human nerve-tissue cancer, originating from either glial cells or their precursors (Behin et al., 2003). Patients suffering from glioblastoma have a poor prognosis with a median survival rate of only 12-15 months for a newly diagnosed glioblastoma and 5-7 months for recurrent glioblastoma and occurrence of 3.19 per 100,000 people (Dolecek et al., 2012; Holland, 2000; Johnson and O'Neill, 2012; Louis et al., 2007). Glioblastoma is exacerbated by its rapid growth and highly diffused infiltration (Holland, 2000). Another nerve-tissue cancer is neuroblastoma that is the most predominant extracranial solid cancer in infancy and childhood (Brodeur, 2003). Despite the remarkable advances in glioblastoma and neuroblastoma therapy, such as neurosurgery, radiotherapy, and chemotherapy, the low median survival period is still a burden to society (Maris, 2010; Ohgaki and Kleihues, 2005). To date, anticancer agents extracted from natural sources have been widely applied to prevent and cure cancers (Mehta et al., 2010). Anticancer agents exerted their activity against cancer cells by inducing several mechanisms of cell death, including apoptosis (type I cell death) and autophagy (type II cell death) (Elmore, 2007). Cordycepin, a major bioactive component found in insect fungus, *Cordyceps* spp., exhibits significant anticancer potential (Tuli et al., 2013). Cordycepin is a derivative of the nucleoside adenosine, and its chemical formula is $C_{10}H_{13}N_5O_3$ with a molecular weight of 251.24 Da. The structure of cordycepin comprises an adenine nucleoside molecule, attached to a ribose sugar moiety via a β -N9-glycosidic bond (Tuli et al., 2013). The biological function of cordycepin has been explored for its anti-tumor and anti-inflammatory in several disease models (Kondrashov et al., 2012; Nakamura et al., 2006;

Wang et al., 2015). Besides, cordycepin possesses anticancer activities, such as anti-proliferation, anti-migration, apoptosis induction, and autophagy promotion (Choi et al., 2011; Li et al., 2015; Tao et al., 2016).

Although the anticancer activity of cordycepin has been tested in human glioblastoma and neuroblastoma cell lines (Baik et al., 2015; Li et al., 2015), the underlying mechanisms of cordycepin to encounter human glioblastomas and neuroblastomas have not yet been clearly explicated. In this report, the therapeutic effects of cordycepin on human nerve-tissue cancer cells were investigated, where its mechanisms of action were explored.

3.3 Materials and methods

3.3.1 Chemicals and reagents

Cordycepin (MW, 251.2; product no. C3394), 3-(4,5-dimethyl-2-thiazolyl)-2,5-diphenyl-2H-tetrazolium bromide (MTT), 4,6-diamidino-2-phenylindole (DAPI), N-acetyl-L-cysteine (NAC), dimethyl sulfoxide (DMSO), 2',7'-dichlorodihydrofluorescein diacetate (DCFH-DA), and chloroquine were purchased from Sigma-Aldrich Chemical Co. (St. Louis, MO). Dulbecco's Modified Eagle Medium (DMEM), and fetal bovine serum (FBS) were purchased from HyClone (HyClone, Logan, UT), while 0.05% Trypsin-EDTA, L-glutamax, and non-essential amino acids were obtained from Gibco (Gibco, CA, USA). Antibody against LC3-I/II was purchased from Merck (Merck KGaA, Darmstadt, Germany).

3.3.2 Cell culture

Human glioblastoma (U-251), human neuroblastoma (SH-SY5Y), human embryonic kidney 293 (HEK-293), human foreskin fibroblasts (HFF), and human hepatocellular carcinoma (HepG2) cell lines were obtained from the American Type Culture Collection (ATCC) (Manassas, VA, USA). Cells were cultured in DMEM medium, containing 10% (v/v) heat-inactivated FBS, 1% (v/v) nonessential amino acids, 1% (v/v)

L-glutamine, 1% (v/v) penicillin-streptomycin in a humidified incubator with 5% CO₂ atmosphere and 37 °C. The fresh complete medium was changed every other day.

3.3.3 MTT assay

The effect of cordycepin on cell viability was determined by the MTT colorimetric method. Briefly, cells were cultured in a 96-well plate with varying concentrations of cordycepin (0, 25, 50, 100, 200, 300, 400 and 500 µM) for 24 h. The MTT solution was added to cell culture media at 0.5 mg/ml final concentration, and incubated for 3 h at 37 °C in the dark. The media was removed, and the formazan crystal was solubilized in DMSO. The absorbance was measured at 570 nm, using a microplate reader (BMG Labtech, Ortenberg, Germany). The O.D. 570 nm in control cells was taken as 100% viability. The 50% inhibitory concentration (IC₅₀) was obtained from the dose-response curve of percent viability (Y) versus tested concentrations (X). IC₅₀ was calculated using linear regression analysis using Microsoft Excel.

3.3.4 Annexin V and 7-AAD staining

Cells were harvested and washed once with PBS. Cells were stained with Muse Annexin V/7-AAD & Dead Cell kit (MCH100105; Merck Millipore) for 20 min at room temperature in the dark. Live, apoptotic, and necrotic cells were analyzed by flow cytometry (Muse Cell Analyser; Merck Millipore, Billerica, MA, USA).

3.3.5 DAPI staining

The levels of nuclear condensation and fragmentation were observed by nucleic acid staining with DAPI. Cells were grown on a glass coverslip coated with Geltrex® (Gibco), and treated either with or without cordycepin for 48 h. Cells were washed twice with cold phosphate buffered saline (PBS), and fixed in 4% paraformaldehyde for 10 min at room temperature. The fixed cells were washed twice with PBS. DAPI stain solution (1.5 µg/ml) was dropped on a glass slide, and coverslip were placed on a glass slide prior to the observation by a laser scanning confocal microscope Nikon A1+ (Nikon, Tokyo, Japan).

3.3.6 RNA isolation and reverse transcription (RT)-PCR

Total RNA was isolated using NucleoSpin RNA kit (Macherey-Nagel, Dueren Germany), according to the manufacturer's protocol, and 1 µg of RNA was used for complementary DNA (cDNA) synthesis using 2-step RT-PCR Kit (Vivantis Technologies Sdn. Bhd, Malaysia). PCR was carried out in a Biorad/C1000Touch Thermocycle (Biorad, CA, USA) with specific primers. The amplified cDNA products were electrophoretically separated on 1% agarose gel and visualized by EtBr staining. The relative expression level of a target gene was quantified by normalization with the internal control *β-actin* gene. The expression level of *Caspase-3*, *Caspase-9*, *BAX*, *BCL-2*, *P53*, *SOD*, *GPX*, *Catalase* and *LC3I/II* were examined. The primers for the reference gene *β-actin* and the primers designed for the genes of interest are shown in Table 3.1

Table 3.1 The primer sequences used for RT-PCR.

	Forward (5'-3')	Reverse (5'-3')
<i>β-actin</i>	TCACCACCACGGCCGAGCG	TCTCCTTCTGCATCCTGTCTG
<i>Caspase-3</i>	TTTGTTTGTGTGCTTCTGAGCC	ATTCTGTTGCCACCTTTCGG
<i>Caspase-9</i>	AACAGGCAAGCAGCAAAGTT	TCCATCTGTGCCGTAGACAG
<i>BAX</i>	AGCTGAGCGAGTGTCTCAAGCG	TCCCGCCACAAAGATGGTCACG
<i>BCL-2</i>	CGCATCAGGAAGGCTAGAGT	AGCTTCCAGACATTCGGAGA
<i>P53</i>	CCCCTCCTGGCCCCTGTCATCTTC	GCAGCGCCTCACAACCTCCGTCAT
<i>SOD</i>	CTAGCGAGTTATGGCGAC	CATTGCCCAAGTCTCCAAC
<i>GPX</i>	CGCCAAGAACGAAGAGATTC	CAACATCGTTGCGACACAC
<i>Catalase</i>	TCCGGGATCTTTTTAACGCCATTG	TCGAGCACGGTAGGGACAGTTCAC
<i>LC3I/II</i>	CTTCGCCGACCGCTGTAA	GGTGCCTACGTTCTGATCTGTG

3.3.7 Measurement of intracellular ROS generation

The generation of ROS was evaluated by fluorescence microscopy and fluorescence-microplate reader. ROS level was measured using fluorescence associated oxidation of 2',7'-dichlorodihydrofluorescein diacetate (DCF-DA) to dichlorofluorescein

(DCF), as previously described (Huang et al., 2014; Kim et al., 2012). Cells were treated with or without cordycepin. Cells cultured on glass coverslips were rinsed with cold PBS, and incubated in 5 μM DCFH-DA for 15 min at 37 °C in the dark. Fluorescence was measured using a laser scanning confocal microscope Nikon A1+ (Nikon, Tokyo, Japan) at excitation and emission wavelengths of 485 and 530 nm for DCF fluorescence. In average, three microscope fields were quantified in three separate cultures per treatment condition. ImageJ was used to quantify fluorescence intensity. For fluorescence-microplate reader, cells were treated with cordycepin (0, 100, 200 and 400 μM) for 2 h. In another experiment, cells were pretreated either with or without 10 mM NAC for 1 h before being challenged with 200 μM cordycepin for another 2 h. Then the cells were incubated with 5 μM DCF-DA at 37 °C for 1 h in the dark, and washed twice with PBS. The fluorescence intensity of DCFH-DA was measured by a fluorescence-microplate reader (Thermo Scientific Varioskan, USA) at an excitation wavelength of 485 nm and an emission wavelength of 530 nm. Results were expressed as percentage of controls.

3.3.8 Immunofluorescence staining

Cells were cultured on coverslips and pretreated with 50 μM chloroquine for 2 h prior to treating with 200 μM cordycepin for another 24 h. Cells were then washed twice in PBS, fixed with 4% paraformaldehyde in PBS at room temperature for 30 min, washed 3 times for 5 min each, and permeabilized with 0.2% Triton X-100 in PBS for 20 min. After blocking with 10% FBS in PBS for 1 h, cells were incubated with LC3-I/II antibody overnight at 4 °C, washed three times in PBS, and incubated in FITC-conjugated anti-rabbit IgG for 1 h. Nuclei were counterstained using DAPI (Vector Laboratories), and the stained cells were observed under a laser scanning confocal microscope Nikon A1+. Images were analyzed using the ImageJ program (NIH).

3.3.9 Statistical analysis

All experiments were performed in triplicate and data were expressed as mean \pm standard deviation (SD). Statistical analysis was performed using SPSS (version 16.0, SPSS Inc., USA). Significant differences between treatment effects were determined by one-way ANOVA analysis, followed by Tukey's tests, and $p < 0.05$ was considered as statistically significant.

3.4 Results

3.4.1 Cordycepin inhibited the growth of human glioblastoma and neuroblastoma cell lines

To investigate the effect of cordycepin on the growth of human glioblastoma and neuroblastoma cell lines, SH-SY5Y and U-251 cell lines were cultured in the presence of various concentrations of cordycepin (0-500 μM) for 24 h, and cell viability was then assessed by using an MTT assay. The treatment of cordycepin for 24 h inhibited the growth of U-251 and SH-SY5Y cell lines in a dose-dependent manner, and their IC_{50} values were 250 and 175 μM , respectively (Figure 3.1a). Alternatively, cordycepin had less cytotoxicity to kidney cells (HEK-293), fibroblast cells (HFF), and liver cells (HepG2) as their IC_{50} values were 424, 419, and 484 μM , respectively (Figure 3.1b). This outcome suggested that cordycepin was more effective against nerve-tissue cancer cells than kidney cells (HEK-293), fibroblast cells (HFF), and liver cells (HepG2). Following the treatment of cordycepin, morphological changes of the U-251 and SH-SY5Y cell lines were observed by phase contrast microscopy, which appeared as cell shrinkage, increased cell floating, and reduced cell attachment, compared to the non-treated control cells, indicating that cordycepin reduced cell viability of both human nerve-tissue cancer cell lines (Figure 3.1c).

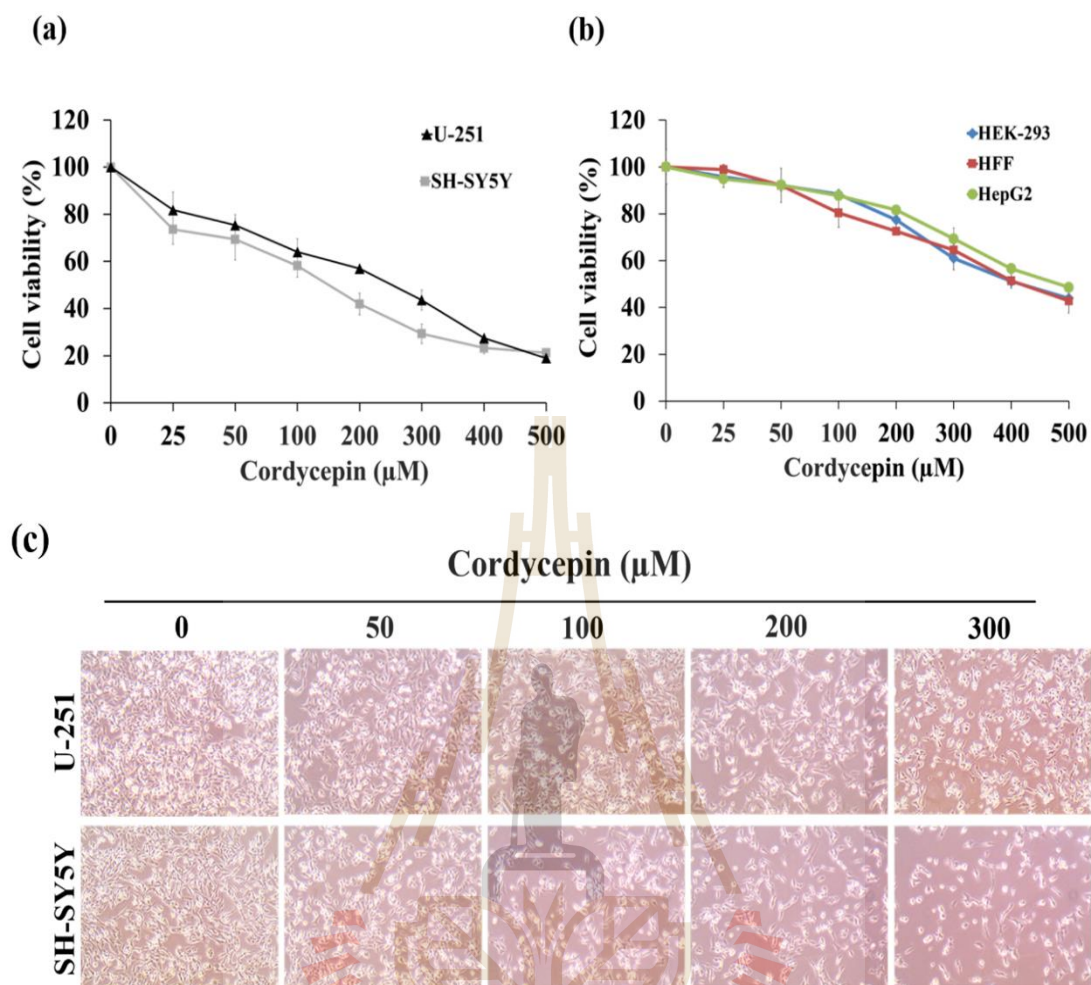


Figure 3.1 Cordycepin inhibited cell viability of human nerve-tissue cancer cell lines. (a) U-251 glioblastoma and SH-SY5Y neuroblastoma cell lines were treated with different concentrations of cordycepin (0, 25, 50, 100, 200, 300, 400 and 500 μM) for 24 h and assessed cell availability by MTT assays. (b) HEK-293, HFF, and HepG2 cells were treated under the same conditions as (A) and assessed cell availability by MTT assays. (c) Cellular morphology of SH-SY5Y and U-251 cells, treated with cordycepin at various concentrations for 24 h, was observed under phase contrast microscopy.

3.4.2 Cordycepin induced apoptotic cell death in human nerve-tissue cancer cells via caspase-dependent pathways

To determine whether the anti-proliferative effect of cordycepin was due to apoptosis, the apoptotic induction of cordycepin was examined by Annexin V/7-AAD staining and flow cytometry analysis. After the treatment of cordycepin at various concentrations (0, 100, 200, 300 μM) for 24 h, the percentage of U-251 and SH-SY5Y viable cells was shown to decrease, whereas the percentage of both early and late apoptotic cells significantly increased in a dose-dependent manner (Figure 3.2a). The treatment of 100, 200, and 300 μM cordycepin induced the early and late apoptotic cell death of U-251 cells at 26%, 29%, and 62%, respectively. Likewise, the treatment of 100, 200, and 300 μM cordycepin induced the early and late apoptotic cell death of SH-SY5Y cells at 50%, 57%, and 62%, respectively. The analysis of nuclear structure of cordycepin-treated U-251 and SH-SY5Y cells was performed by DAPI staining, and presented that the cells experienced apoptosis. This was evidently notified by chromatin condensation, nuclear shrinkage and fragmentation, as well as the aberrant of nuclear structure (Figure 3.2b). The expression of apoptosis-related genes (*P53*, *Caspase-9*, *Caspase-3*, *BAX*, and *BCL-2*) was measured by RT-PCR after the treatment with various concentrations of cordycepin for 24 h. The results revealed that cordycepin upregulated tumor suppressor gene *P53*, and pro-apoptotic genes, including *Caspase-9*, *Caspase-3*, and *BAX*, in a dose-dependent manner. Nevertheless, cordycepin significantly diminished the expression of anti-apoptotic gene, *BCL-2*, in both U-251 and SHSY5Y cells (Figure 3.2c and d). Taken together, these results indicated that cordycepin strongly induced apoptosis in both human nerve-tissue cancer cell lines by triggering the intrinsic apoptosis pathways, through *P53*, initiator caspase (*Caspase-9*), and executioner caspase (*Caspase-3*).

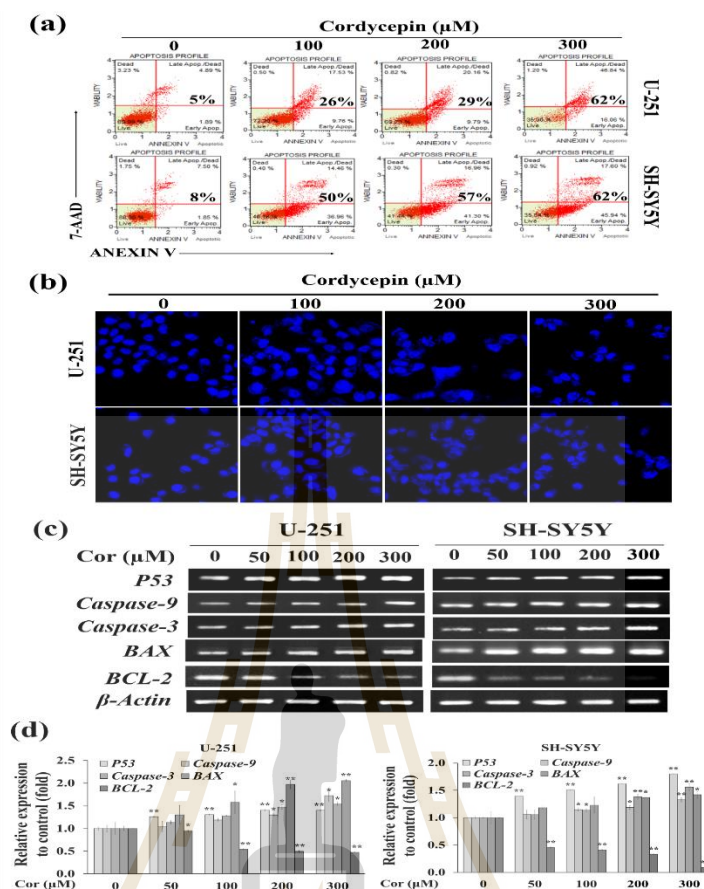


Figure 3.2 Cordycepin induced apoptotic cell death of human nerve-tissue cancer cells. (a) Cell apoptosis was determined by Annexin V/7-AAD flow cytometry analysis. U-251 and SH-SY5Y cells were treated with different concentrations of cordycepin (Cor) (0, 100, 200, 300 μM) for 24 h. (b) The nuclear structures of U-251 and SH-SY5Y cells were analyzed via fluorescence microscope. The cells were fixed and stained with DAPI solution for 10 min at room temperature. (c) The mRNA expression levels of apoptotic genes, *P53*, *Caspase-9*, *Caspase-3*, *BAX*, and *BCL-2*, were evaluated by semiquantitative RT-PCR. (d) The relative expression of *P53*, *Caspase-9*, *Caspase-3*, *BAX* and *BCL-2* were determined by using β -Actin as a reference gene. Values are expressed as mean \pm SD (n=3). * $p < 0.05$ and ** $p < 0.01$ versus control cells. (d) The relative expression of *P53*, *Caspase-9*, *Caspase-3*, *BAX* and *BCL-2* were determined by using β -Actin as a reference gene. Values are expressed as mean \pm SD (n=3). * $p < 0.05$ and ** $p < 0.01$ versus control cells.

3.4.3 Cordycepin-induced apoptosis was involved the generation of ROS in human nerve-tissue cancer cells

Since the intracellular reactive oxygen species (ROS) produced by the mitochondria is closely related to the induction of apoptosis in various cell types, ROS generation was investigated whether it involved in cordycepin-induced apoptosis (Fleury et al., 2002). Cordycepin-induced ROS was measured in U-251 and SH-SY5Y cell lines by using fluorescent dye DCF-DA. U-251 and SH-SY5Y cell lines were exposed to 200 μ M cordycepin for the various time periods (0, 0.5, 1, 2, 4 and 6 h), and found that the generation of ROS was initially observed at 0.5 h and the fluorescence levels were greatest at 2 h incubation prior to declining. In order to obtain the optimal value, various concentrations of cordycepin were subjected to both cell lines for 2 h, and data were collected. The treatment of cordycepin to both human nerve-tissue cancer cells resulted in a significant enhancement of intracellular ROS levels, compared to the non-treated control (Figure 3.3a and b). This cordycepin-induced ROS generation was confirmed by pre-treating the cells with the ROS scavenger NAC, and measured the relative fluorescence. As expected, the ROS scavenger NAC blocked the levels of intracellular ROS induced by cordycepin in both U-251 and SH-SY5Y cell lines. The pretreatment of NAC prior to cordycepin supplementation significantly reduced ROS generation, whereas the treatment of NAC alone did not alter ROS levels (Figure 3.3c). Besides, the cells were pretreated either with or without 10 mM NAC for 1 h before being challenged with cordycepin for another 24 h, and assessed cell viability by MTT assays. The result showed that NAC by itself had no effect on nerve-tissue cancer cell viability (Figure 3.3d). The pretreatment of NAC showed a significant reversal of cordycepin-induced cell death, suggesting that ROS plays an important role in cordycepin-induced apoptosis in human nerve-tissue cancer cells (Figure 3.3d). Furthermore, cordycepin treatment significantly decreased the expression of antioxidant genes, including *GPX*, *SOD*, and *Catalase*, in a dose-dependent manner for both cell lines (Figure 3.3e and f). Altogether, these data supported that cordycepin induced apoptosis in human nerve-tissue cancer cells through ROS-dependent mechanisms.

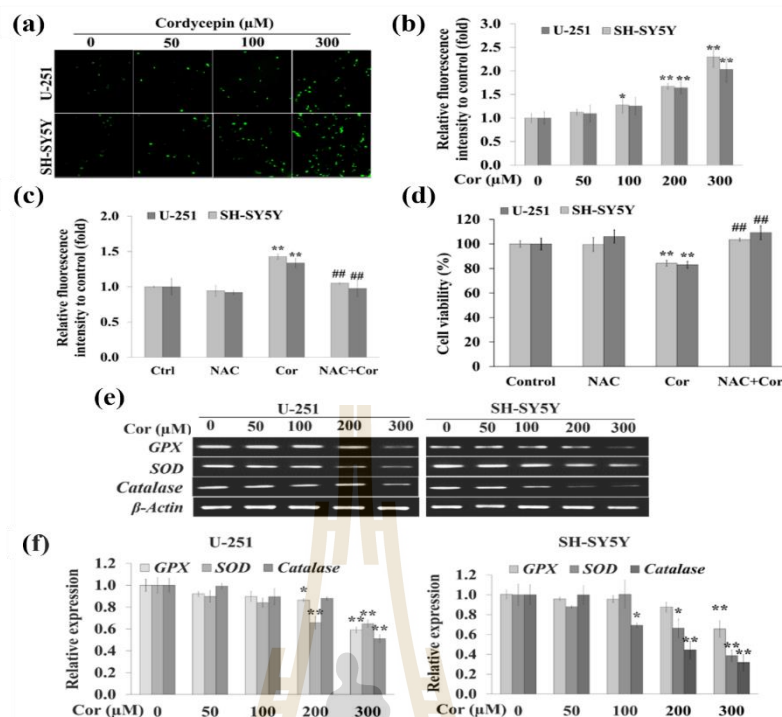


Figure 3.3 Cordycepin-induced apoptosis associated with ROS generation in human nerve-tissue cancer cells. (a) Intracellular ROS levels of U-251 and SH-SY5Y cell lines under 0, 100, 200, 300 μM cordycepin (Cor) exposures for 2 h were determined by DCF fluorescence. (b) Relative DCF fluorescence was quantitatively analyzed by fluorescence-microplate reader, and expressed as fold of DCF fluorescence over the control. (c) Cells were pretreated with or without NAC (10 mM) for 1 h before being challenged with 200 μM of cordycepin for another 2 h. The relative fluorescence intensity was analyzed by fluorescence-microplate reader. (d) NAC rescued nerve-tissue cancer cell death by cordycepin as determined by the MTT assay. Data were shown as mean ± SD. * $p < 0.05$ and ** $p < 0.01$ versus control cells. (e) The mRNA expression levels of antioxidant genes, *Superoxide dismutase (SOD)*, *Glutathione peroxidase (GPX)*, and *Catalase*, were evaluated using semiquantitative RT-PCR. (f) The relative expression of *Catalase*, *SOD*, and *GPX* were determined by using β -Actin as a reference gene. Data were presented as mean ± SD. * $p < 0.05$, ** $p < 0.01$ versus control cells and ## $p < 0.01$ versus cordycepin-treated cells.

3.4.4 Cordycepin induced autophagy in human nerve-tissue cancer cells

As the sophistication of autophagy-apoptosis axis, the crosstalk between autophagy and apoptotic cell death was previously examined in various cancer cell types (Geng et al., 2010; Liu et al., 2016). To investigate whether cordycepin could modulate autophagy in U-251 and SH-SY5Y cell lines, the formation of *LC3I/II*, a key protein of aggresome complex, was determined after the treatment of cordycepin. Following the treatment of 200 and 300 μM cordycepin for 24 h, both U-251 and SH-SY5Y cell lines exhibited a significant increase of LC3I/II protein, compared to the non-treated control cells (Figure 3.4a). In addition, cordycepin treatment significantly enhanced the expression of *LC3I/II* gene, as determined by RT-PCR (Figure 3.4b and c). It was proved that cordycepin activated autophagy of human nerve-tissue cancer cells, and, thereafter, triggered apoptotic cell death.

3.4.5 Autophagy involved in cordycepin-induced apoptosis of human nerve-tissue cancer cells

Autophagy has been proposed as survival mechanisms of cancer cells upon cancer drug treatment, and the inhibition of autophagy lead to cancer cell death (Lee et al., 2014). To investigate whether the interference of autophagy influenced cordycepin-induced apoptosis of human nerve-tissue cancer cells, chloroquine, an autophagy inhibitor, was used for preventing the degradation of LC3I/II and inhibiting lysosome fusion (Zaidi et al., 2001). The upsurge of LC3I/II accumulation was marked by fluorescence dot after chloroquine treatment (Figure 3.5a). Compared to chloroquine alone, the post-treatment of cordycepin after chloroquine refined the accumulation of LC3I/II in both cell lines (Figure. 5a). The apoptotic cell death and cell survival of U-251 and SH-SY5Y cell lines were then examined by flow cytometry analysis and MTT assays, respectively, in conditions with or without chloroquine pretreatment. The results presented that, upon chloroquine pretreatment, the apoptosis of both cell lines was enhanced, and the survival rate was declined

(Figure 3.5b and c). This result indicated that autophagy served as a survival mechanism of human nerve-tissue cancer and the suppression of autophagy by chloroquine improved chemosensitivity of nerve-tissue cancer cells to cordycepin. Taken together, these results demonstrated that the inhibition of autophagy promoted cordycepin-induced apoptosis in human glioblastoma and neuroblastoma cells. The activation of autophagy by cordycepin was the underlying mechanisms to trigger the death of nerve-tissue cancer cells.



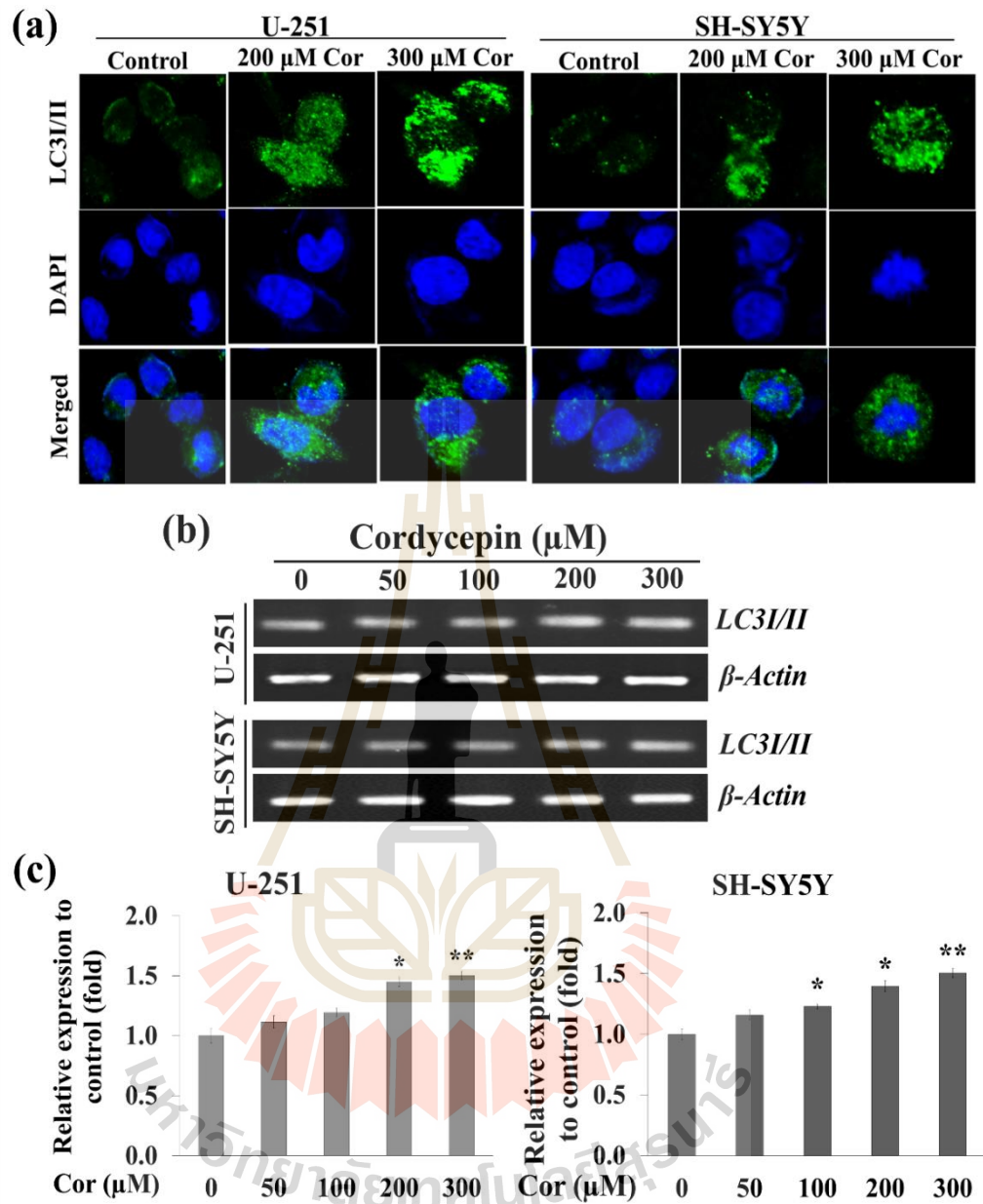


Figure 3.4 Cordycepin (Cor) induced autophagy in human nerve-tissue cancer cells by the upregulation of LC3I/II. (a) Confocal microscopic images showed the increase of LC3I/II protein when high concentration of cordycepin was applied to the cells as stained by a specific antibody. (b) The mRNA expression levels of *LC3I/II* were positively correlated to the concentration of cordycepin as evaluated by using semiquantitative RT-PCR. (c) The relative expression of *LC3I/II* was relatively quantified by using β -Actin as a reference gene. Data were presented as mean \pm SD. * $p < 0.05$ and ** $p < 0.01$ versus control cells.

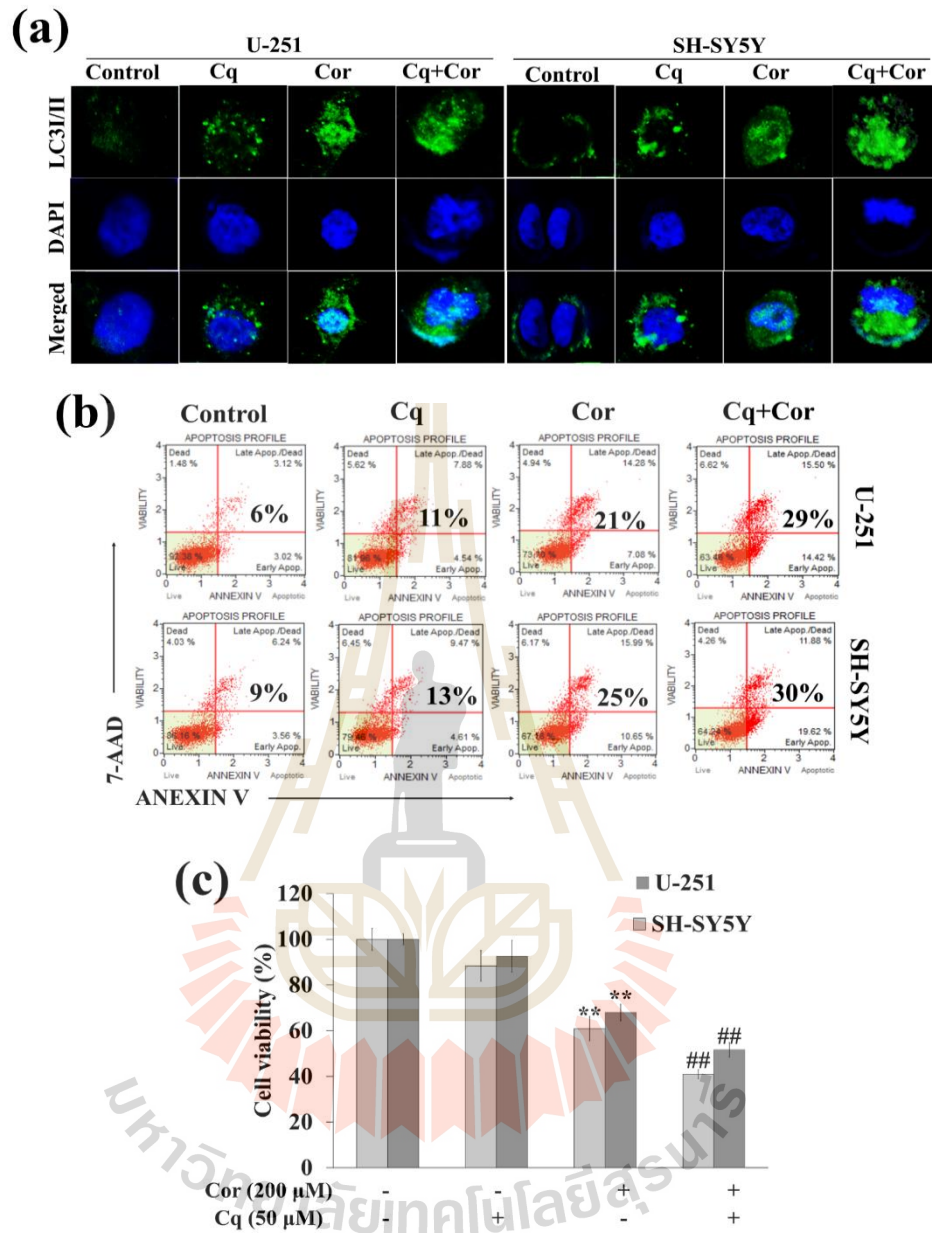


Figure 3.5 Inhibition of autophagy promoted cordycepin-induced apoptosis in nerve-tissue cancer cells. (a) Cells were pretreated with 50 μ M chloroquine (Cq) for 2 h prior to the treatment of 200 μ M cordycepin (Cor) for 24 h. After 24-h incubation, the level of LC3I/II was visualized by fluorescence microscopy after immunostaining with LC3I/II antibody. (b) Apoptotic cell death was evaluated by Annexin V/7-AAD flow cytometry analysis. (c) Cell viability was determined by the MTT assay after 24-h incubation. Data were presented as mean \pm SD. * $p < 0.05$, ** $p < 0.01$ versus control cells, and ## $p < 0.01$ versus cordycepin-treated cells.

3.5 Discussion

Glioblastoma is the most aggressive malignant primary human nerve-tissue cancer, originating from either glial cells or their precursors (Behin et al., 2003), has a low survival rate despite extensive efforts to develop new treatments (Shergalis et al., 2018). Another nerve-tissue cancer is neuroblastoma that is the most predominant extracranial solid cancer in infancy and childhood, representing 8%-10% of all childhood cancer (Brodeur, 2003; Park et al., 2008). Despite the remarkable advances in glioblastoma and neuroblastoma therapy, such as neurosurgery, radiotherapy, and chemotherapy, the low median survival period is still a burden to society (Maris, 2010; Ohgaki and Kleihues, 2005). Cordycepin is a major bioactive component found in insect fungus, *Cordyceps* spp., and exhibits a significant therapeutic potential (Tuli et al., 2013). It was presented in this study that cordycepin, also termed 3'-deoxyadenosine, could inhibit cancer cell growth, induce apoptosis, generate ROS, and activate autophagy in U-251 and SH-SY5Y human nerve-tissue cancer cell lines. The growth inhibition of cordycepin against nerve-tissue cancer cells in this study was a dose-dependent manner (Figure 3.1a and b). Other studies reported that cordycepin inhibited the growth of various cancer cell types. For example, cordycepin inhibited the growth of NB-4 and U937 leukemic cells at IC_{50} 73.2 μ M and 90.4 μ M, respectively (Liao et al., 2015). Cordycepin also significantly induced apoptosis in oral squamous cancer cells at IC_{50} ranging from 100 μ M to 1 mM, while IC_{50} of HepG2 cells was 1990 μ M (Lu et al., 2014; Yu X. et al., 2017). Notably, IC_{50} of HepG2 in this study was 484 μ M, differing from the previous report, which should due to the 4-fold less cell seeding number (Lu et al., 2014). The diverse specificity of cordycepin against cancer cells might rely not only on the tissues of origin, but also cell density, source of cordycepin (natural or synthesis) and purity of cordycepin (Osieka et al., 1984). While the anticancer activity of cordycepin against nerve-tissue cancer cells was shown higher than HEK-293, HFF, and HepG2 cells, it is important to evaluate the cytotoxicity of cordycepin against non-tumor derived neuronal cells in my next study to

verify cancer specificity. Several healthy neuronal cell types are currently used as models to evaluate neurotoxic chemotherapy, such as stem cell-derived neuronal cells and primary neurons, which will be further implemented (Daub et al., 2009; Wing et al., 2017). Since the structure of cordycepin is very similar to nucleoside, adenosine and acts like a nucleoside analogue (Li G. et al., 2015), which is able to be involved in the actions of DNA and/or RNA polymerases (Kuchta, 2010). During the process of RNA synthesis (transcription), some enzymes are not able to distinguish between an adenosine and cordycepin which leads to incorporation of cordycepin to induce premature termination of transcription (Chen et al., 2008). Cancer cells can divide without receiving the all-clear signal. While normal cells will stop division in the presence of genetic (DNA) damage, cancer cells will continue to divide (Urry et al., 2017). Therefore, cancer cells have a proliferation rate more than normal cells as results cordycepin was more effective against nerve-tissue cancer cells than normal cells.

The pharmacokinetic study demonstrated that cordycepin has a short half-life and is rapidly metabolized in blood plasma. The half-life of cordycepin in rat blood was 1.6 ± 0.0 min after the administration, and the measurable concentration of cordycepin was vanished within 30 min (Tsai et al., 2010). It was noted that the unidentified metabolites of cordycepin detected in the blood and liver of rat for over 2 h, which might have certain biological activities within the body (Tsai et al., 2010). However, the structure and function of cordycepin-derived metabolites is needed further investigation. Recent report explicated the anti-migratory effects of cordycepin in human glioblastoma using mouse xenografts. Glioblastoma-bearing mice treated with 5 mg/kg of cordycepin significantly reduced the brain tumor size at day 14 postimplantation (Hueng et al., 2017). Cordycepin has also been studied in numerous cancer cell lines, including oral cancer, cervical, breast, and leukemias (Thomadaki et al., 2005; Wu et al., 2007). Despite these promising results, the limitation of cordycepin in clinical application is that it requires the co-administration of ADA inhibitors, such as deoxycoformycin (dCF). The continuous co-administration of dCF with cordycepin

caused the adverse effects, such as severe gastrointestinal toxicity (Rodman et al., 1997). The used dosages of cordycepin might vary due to diseased etiology, for instance 1 mg/kg for depression and 5 mg/kg for parasitic infections. No human toxicity report was found and even animal models were failed to determine median lethal dose. Cordyceps dosage up to 80 g/kg body weight/day for 7 days was injected intraperitoneally in mice and even then it did not cause any fatality (Li et al., 2006). Although there is no direct translation of *in vitro* exposure to *in vivo* treatment of cordycepin against brain cancers, the outcomes of cellular assays could inform the potential pharmacological benefits of cordycepin (Tuli et al., 2014). The administered cordycepin was able to transport from peripheral blood to the brain via an adenosine transporter across the blood-brain barrier, and exhibited neuroprotective functions in the brain (Li et al., 2016; Rottenberg et al., 2005). Additional information of human blood-brain barrier reacting to cordycepin is needed to establish a greater accuracy of brain cancer therapy.

Accumulating evidence has demonstrated the role of cordycepin in the induction of nerve-tissue cancer cell apoptosis. For example, cordycepin induced apoptosis by increasing the protein expression level of total P53 and phosphorylated P53, cleaved caspase-7, and poly (ADP-ribose) polymerase (PARP) pathway (Chen et al., 2014). Cordycepin-mediated apoptosis was observed in neuroblastoma SK-N-SH and BE(2)-M17 cells by increasing the levels of cleaved caspase-3 and PARP (Li et al., 2015). Human glioblastoma U87MG cells could be induced to cell death by cordycepin through the extrinsic pathway, including the upregulation of Fas/FasL, downregulation of anti-apoptotic Bcl-2, and activation of initiator caspase-8 as well as executor caspase-3 (Baik et al., 2016). Here, we demonstrated that apoptotic cell death of SH-SY5Y and U-251 cells associated with the upregulation of tumor suppressor gene *P53* and pro-apoptotic genes, *BAX*, *Caspase-9*, and *Caspase-3*, in a dose-dependent manner of cordycepin. The anti-apoptotic gene, *BCL-2*, was decreased upon cordycepin treatment, implying that cordycepin strongly induces apoptosis in human

nerve-tissue cancer cells by triggering the intrinsic pathways (Figure 3.2 c, d). In addition to apoptosis, ROS are known as a key mediator of intracellular signaling cascades, including mitochondrial-mediated apoptosis pathway (Chakraborti et al., 1999). ROS has the potential to induce the collapse of mitochondrial membrane potential, and, consequently, trigger the release of mitochondrial factors to activate caspase cascade, and, eventually, apoptosis (Fiers et al., 1999; Fleury et al., 2002; Jeong et al., 2011; Zhou et al., 2009). To our finding, cordycepin-treated U-251 and SH-SY5Y cells overproduced intracellular ROS levels superior to the control cells (Figure 3.3a and b). The pretreatment of cells with the ROS scavenger, NAC, effectively blocked ROS generation and rescued cell death, implicating that cordycepin-induced apoptosis is through a mitochondrial-mediated intrinsic pathway of human nerve-tissue cancer cells (Figure 3.3c and d). Under normal circumstance, ROS, which is produced by the mitochondrial respiratory chain, is scavenged by the endogenous antioxidant enzymes, including superoxide dismutase (SOD), catalase, and glutathione peroxidase (GPX) (Liou and Storz, 2010). Superoxide dismutases (SOD) are metalloenzymes, which catalyzes the dismutation of superoxide radical anion (O_2^-) to oxygen and hydrogen peroxide H_2O_2 and dioxygen (Copin et al., 2000). Catalase (CAT) facilitates the decomposition of hydrogen peroxide (H_2O_2) to water (H_2O) and oxygen (O_2), while hydrogen peroxide (H_2O) can be reduced to water (H_2O) by glutathione peroxidases (GPX) (Figure 3.6) (Hashimoto and Hayashi, 1990). Remarkably, cordycepin significantly decreased the expression of antioxidant genes, including *GPX*, *SOD*, and *Catalase*, in SH-SY5Y and U-251 cells (Figure 3.3e and f). These results suggested that cordycepin enhanced ROS production by interference the cellular antioxidant machinery, and directed nerve-tissue cancer cells to mitochondria-mediated program cell death.

autophagy in yeast and mammalian cells (Yu et al., 2017). Several studies revealed that numbers of anticancer agents directly activate autophagy and promote apoptotic cell death in cancer cells, such as breast, prostate, and melanoma cancer, and the addition of autophagy inhibitors prevents the death of cancer cells (Ahmed et al., 2017; Bursch et al., 2008; Wang et al., 2017). On the other hand, under the aggressive stress environments, the autophagy levels of cancer cells are higher than normal and, therefore, the disruption of this increased autophagy interferes the adaptation of cancer cells to extreme environments and, therefore, contributes to cancer cell death (Carew et al., 2007). Likewise, the blockage of autophagic flux by chloroquine resulted in the enhanced anticancer activity of cordycepin against U-251 and SH-SY5Y cell lines, verifying that the inhibition of autophagy enhances the sensitivity of nerve-tissue cancer to anticancer agents and improves apoptosis (Figure 3.6b and c) (Liu et al., 2016). The dual roles of autophagy, either survival or death signaling pathways, depend on the extent of cell degradation products as well as the nature and intensity of the stimulus (Dalby et al., 2010; Motyl et al., 2006). This study reflects the importance of autophagy in chemosensitizing of human nerve-tissue cancer cells to anticancer agents, and, in the near future, cordycepin could be implemented in a combination with conventional anticancer drugs to augment the treatment efficacy against nerve-tissue cancers (Du et al., 2016).

3.6 Conclusion

In conclusion, cordycepin could effectively inhibit the proliferation and induce apoptotic cell death of human nerve-tissue cancer cells through the generation of reactive oxygen species and modulation of autophagy. The control of autophagy activity within cells by small molecules might be an alternative approach for a better treatment of human nerve-tissue cancer. Importantly, this finding revealed the mechanisms of action of cordycepin, which is a foundation to study other relevant mechanistic insights into the mysterious

potential of cordycepin. Future studies should focus on the enhancement of cordycepin absorption and bioavailability, and targeted-tissue delivery strategies using nanoparticles.

3.7 References

- Ahmed, R., Begam, K., Kanduluru, A. K., et al. (2017). Antitumor agent 25-epi Ritterostatin GN1N induces endoplasmic reticulum stress and autophagy mediated cell death in melanoma cells. **International journal of oncology**. 50(5): 1482-1490.
- Baik, J.-S., Mun, S.-W., Kim, K.-S., et al. (2016). Apoptotic effects of cordycepin through the extrinsic pathway and p38 MAPK activation in human glioblastoma U87MG cells. **Journal of Microbiology and Biotechnology**. 26(2): 309-314.
- Behin, A., Hoang-Xuan, K., Carpentier, A. F., and Delattre, J.-Y. (2003). Primary brain tumours in adults. **The Lancet**. 361(9354): 323-331.
- Brodeur, G. M. (2003). Neuroblastoma: biological insights into a clinical enigma. **Nature reviews cancer**. 3(3): 203.
- Bursch, W., Karwan, A., Mayer, M., et al. (2008). Cell death and autophagy: cytokines, drugs, and nutritional factors. **Toxicology**. 254(3): 147-157.
- Carew, J. S., Nawrocki, S. T., and Cleveland, J. L. (2007). Modulating autophagy for therapeutic benefit. **Autophagy**. 3(5): 464-467.
- Chakraborti, T., Das, S., Mondal, M., Roychoudhury, S., and Chakraborti, S. (1999). Oxidant, mitochondria and calcium: an overview. **Cellular signalling**. 11(2): 77-85.
- Chen, L. S., Stellrecht, C. M., and Gandhi, V. (2008). RNA-directed agent, cordycepin, induces cell death in multiple myeloma cells. **British journal of haematology**. 140(6): 682-391.
- Chen, Y., Yang, S.-H., Hueng, D.-Y., et al. (2014). Cordycepin induces apoptosis of C6 glioma cells through the adenosine 2A receptor-p53-caspase-7-PARP pathway. **Chemico-biological interactions**. 216: 17-25.

- Choi, K. S. (2012). Autophagy and cancer. **Experimental & molecular medicine**. 44(2): 109-120.
- Choi, S., Lim, M.-H., Kim, K. M., et al. (2011). Cordycepin-induced apoptosis and autophagy in breast cancer cells are independent of the estrogen receptor. **Toxicology and applied pharmacology**. 257(2): 165-173.
- Copin, J.-C., Gasche, Y., and Chan, P. H. (2000). Overexpression of copper/zinc superoxide dismutase does not prevent neonatal lethality in mutant mice that lack manganese superoxide dismutase. **Free Radical Biology and Medicine**. 28(10): 1571-1576.
- Dalby, K., Tekedereli, I., Lopez-Berestein, G., and Ozpolat, B. (2010). Targeting the pro-death and pro-survival functions of autophagy as novel therapeutic strategies in cancer. **Autophagy**. 6(3): 322-329.
- Daub, A., Sharma, P., and Finkbeiner, S. (2009). High-content screening of primary neurons: ready for prime time. **Current opinion in neurobiology**. 19(5): 537-543.
- Dolecek, T. A., Propp, J. M., Stroup, N. E., and Kruchko, C. (2012). CBTRUS statistical report: primary brain and central nervous system tumors diagnosed in the United States in 2005–2009. **Neuro-oncology**. 14(suppl 5): v1-v49.
- Du, Y., Yu, J., Du, L., Tang, J., and Feng, W. H. (2016). Cordycepin enhances Epstein-Barr virus lytic infection and Epstein-Barr virus-positive tumor treatment efficacy by doxorubicin. **Cancer Lett**. 376(2): 240-248. doi: 10.1016/j.canlet.2016.04.001
- Elmore, S. (2007). Apoptosis: a review of programmed cell death. **Toxicologic pathology**. 35(4): 495-516.
- Fiers, W., Beyaert, R., Declercq, W., and Vandenabeele, P. (1999). More than one way to die: apoptosis, necrosis and reactive oxygen damage. **Oncogene**. 18(54): 7719-7730.
- Fleury, C., Mignotte, B., and Vayssière, J.-L. (2002). Mitochondrial reactive oxygen species in cell death signaling. **Biochimie**. 84(2): 131-141.
- Geng, Y., Kohli, L., Klocke, B. J., and Roth, K. A. (2010). Chloroquine-induced autophagic

- vacuole accumulation and cell death in glioma cells is p53 independent. **Neuro-oncology**. 12(5): 473-481.
- Gozuacik, D., and Kimchi, A. (2007). Autophagy and cell death. **Current topics in developmental biology**. 78: 217-245.
- Hashimoto, F., and Hayashi, H. (1990). Significance of Catalase in Peroxisomal Fatty Acyl-CoA β -Oxidation NADH Oxidation by Acetoacetyl-CoA and H₂O₂. **Journal of biochemistry**. 108(3): 426-431.
- Holland, E. C. (2000). Glioblastoma multiforme: the terminator. **Proceedings of the National Academy of Sciences**. 97(12): 6242-6244.
- Huang, J., Xu, J., Tian, L., and Zhong, L. (2014). A thioredoxin reductase and/or thioredoxin system-based mechanism for antioxidant effects of ambroxol. **Biochimie**. 97: 92-103.
- Hueng, D.-Y., Hsieh, C.-H., Cheng, Y.-C., Tsai, W.-C., and Chen, Y. (2017). Cordycepin inhibits migration of human glioblastoma cells by affecting lysosomal degradation and protein phosphatase activation. **The Journal of nutritional biochemistry**. 41: 109-116.
- Jeong, J. W., Jin, C. Y., Park, C., et al. (2011). Induction of apoptosis by cordycepin via reactive oxygen species generation in human leukemia cells. **Toxicology in Vitro**. 25(4): 817-824.
- Jiang, X., Overholtzer, M., and Thompson, C. B. (2015). Autophagy in cellular metabolism and cancer. **The Journal of Clinical Investigation**. 125(1): 47-54.
- Johnson, D. R., and O'Neill, B. P. (2012). Glioblastoma survival in the United States before and during the temozolomide era. **Journal of neuro-oncology**. 107(2): 359-364.
- Kanzawa, T., Germano, I., Komata, T., et al. (2004). Role of autophagy in temozolomide-induced cytotoxicity for malignant glioma cells. **Cell Death & Differentiation**. 11(4): 448-457.

- Kanzawa, T., Kondo, Y., Ito, H., Kondo, S., and Germano, I. (2003). Induction of autophagic cell death in malignant glioma cells by arsenic trioxide. **Cancer research**. 63(9): 2103-2108.
- Kim, S. M., Chung, M. J., Ha, T. J., et al. (2012). Neuroprotective effects of black soybean anthocyanins via inactivation of ASK1–JNK/p38 pathways and mobilization of cellular sialic acids. **Life sciences**. 90(21-22): 874-882.
- Kondrashov, A., Meijer, H. A., Barthelet-Barateig, A., et al. (2012). Inhibition of polyadenylation reduces inflammatory gene induction. **Rna**. 18(12): 2236-2250.
- Kuchta, R. D. (2010). Nucleotide Analogues as Probes for DNA and RNA Polymerases. **Current protocols in chemical biology**. 2(2): 111-124.
- Lee, H. H., Kim, S. O., Kim, G.-Y., et al. (2014). Involvement of autophagy in cordycepin-induced apoptosis in human prostate carcinoma LNCaP cells. **Environmental toxicology and pharmacology**. 38(1): 239-250.
- Li, B., Hou, Y., Zhu, M., et al. (2016). 3'-deoxyadenosine (cordycepin) produces a rapid and robust antidepressant effect via enhancing prefrontal AMPA receptor signaling pathway. **International Journal of Neuropsychopharmacology**. 19(4).
- Li, G., Nakagome, I., Hirono, S., Itoh, T., and Fujiwara, R. (2015). Inhibition of adenosine deaminase (ADA)-mediated metabolism of cordycepin by natural substances. **Pharmacology research & perspectives**. 3(2): e00121.
- Li, S., Yang, F., and Tsim, K. W. (2006). Quality control of *Cordyceps sinensis*, a valued traditional Chinese medicine. **Journal of Pharmaceutical and Biomedical Analysis**. 41(5): 1571-1584.
- Li, Y., Li, R., Zhu, S., et al. (2015). Cordycepin induces apoptosis and autophagy in human neuroblastoma SK-N-SH and BE (2)-M17 cells. **Oncology letters**. 9(6): 2541-2547.
- Liang, J., Shao, S. H., Xu, Z.-X., et al. (2007). The energy sensing LKB1–AMPK pathway regulates p27kip1 phosphorylation mediating the decision to enter autophagy or

- apoptosis. **Nature cell biology**. 9(2): 218-224.
- Liao, Y., Ling, J., Zhang, G., et al. (2015). Cordycepin induces cell cycle arrest and apoptosis by inducing DNA damage and up-regulation of p53 in Leukemia cells. **Cell cycle**. 14(5): 761-771.
- Liou, G.-Y., and Storz, P. (2010). Reactive oxygen species in cancer. **Free radical research**. 44(5): 479-496.
- Liu, X., Sun, K., Wang, H., and Dai, Y. (2016). Inhibition of autophagy by chloroquine enhances the antitumor efficacy of sorafenib in glioblastoma. **Cellular and molecular neurobiology**. 36(7): 1197-1208.
- Lockshin, R. A., and Zakeri, Z. (2004). Apoptosis, autophagy, and more. **The international journal of biochemistry & cell biology**. 36(12): 2405-2419.
- Louis, D. N., Ohgaki, H., Wiestler, O. D., et al. (2007). The 2007 WHO classification of tumours of the central nervous system. **Acta Neuropathol**. 114(2): 97-109. doi: 10.1007/s00401-007-0243-4
- Lu, H., Li, X., Zhang, J., et al. (2014). Effects of cordycepin on HepG2 and EA. hy926 cells: Potential antiproliferative, antimetastatic and anti-angiogenic effects on hepatocellular carcinoma. **Oncology letters**. 7(5): 1556-1562.
- Maris, J. M. (2010). Recent advances in neuroblastoma. **New England Journal of Medicine**. 362(23): 2202-2211.
- Mehta, R. G., Murillo, G., Naithani, R., and Peng, X. (2010). Cancer chemoprevention by natural products: how far have we come? **Pharmaceutical research**. 27(6): 950-961.
- Motyl, T., Gajkowska, B., Zarzynska, J., Gajewska, M., and Lamparska-Przybysz, M. (2006). Apoptosis and autophagy in mammary gland remodelling and breast cancer chemotherapy. **Journal of physiology and pharmacology**. 57: 17.
- Nakamura, K., Yoshikawa, N., Yamaguchi, Y., et al. (2006). Antitumor effect of cordycepin (3'-deoxyadenosine) on mouse melanoma and lung carcinoma cells involves adenosine

- A3 receptor stimulation. **Anticancer Research**. 26(1A): 43-47.
- Nikoletopoulou, V., Markaki, M., Palikaras, K., and Tavernarakis, N. (2013). Crosstalk between apoptosis, necrosis and autophagy. **Biochimica et Biophysica Acta (BBA)-Molecular Cell Research**. 1833(12): 3448-3459.
- Ohgaki, H., and Kleihues, P. (2005). Epidemiology and etiology of gliomas. **Acta neuropathologica**. 109(1): 93-108.
- Osieka, R., Seeber, S., and Schmidt, C. (1984). Predictive tests in cancer chemotherapy a reappraisal. **Klinische Wochenschrift**. 62(5): 203-212.
- Park, J. R., Eggert, A., and Caron, H. (2008). Neuroblastoma: biology, prognosis, and treatment. **Pediatric clinics of North America**. 55(1): 97-120.
- Rodman, L. E., Farnell, D. R., Coyne, J. M., et al. (1997). Toxicity of cordycepin in combination with the adenosine deaminase inhibitor 2'-deoxycoformycin in beagle dogs. **Toxicology and applied pharmacology**. 147(1): 39-45.
- Rottenberg, M. E., Masocha, W., Ferella, M., et al. (2005). Treatment of African trypanosomiasis with cordycepin and adenosine deaminase inhibitors in a mouse model. **Journal of Infectious Diseases**. 192(9): 1658-1665.
- Shergalis, A., Bankhead, A., Luesakul, U., Muangsin, N., and Neamati, N. (2018). Current challenges and opportunities in treating glioblastoma. **Pharmacological reviews**. 70(3): 412-445.
- Tao, X., Ning, Y., Zhao, X., and Pan, T. (2016). The effects of cordycepin on the cell proliferation, migration and apoptosis in human lung cancer cell lines A549 and NCI-H460. **Journal of Pharmacy and Pharmacology**.
- Thomadaki, H., Tsiapalis, C. M., and Scorilas, A. (2005). Polyadenylate polymerase modulations in human epithelioid cervix and breast cancer cell lines, treated with etoposide or cordycepin, follow cell cycle rather than apoptosis induction. **Biological chemistry**. 386(5): 471-480.

- Tsai, Y.-J., Lin, L.-C., and Tsai, T.-H. (2010). Pharmacokinetics of adenosine and cordycepin, a bioactive constituent of *Cordyceps sinensis* in rat. **Journal of agricultural and food chemistry**. 58(8): 4638-4643.
- Tuli, H. S., Sandhu, S. S., and Sharma, A. (2014). Pharmacological and therapeutic potential of *Cordyceps* with special reference to Cordycepin. **3 Biotech**. 4(1): 1-12.
- Tuli, H. S., Sharma, A. K., Sandhu, S. S., and Kashyap, D. (2013). Cordycepin: a bioactive metabolite with therapeutic potential. **Life sciences**. 93(23): 863-869.
- Urry, L. A., Cain, M. L., Wasserman, S. A., Minorsky, P. V., and Reece, J. B. (2017). *Campbell biology*: Pearson Education, **Incorporated**.
- Wang, B., Lu, D., Xuan, M., and Hu, W. (2017). Antitumor effect of sunitinib in human prostate cancer cells functions via autophagy. **Experimental and therapeutic medicine**. 13(4): 1285-1294.
- Wang, F., Yin, P., Lu, Y., et al. (2015). Cordycepin prevents oxidative stress-induced inhibition of osteogenesis. **Oncotarget**. 6(34): 35496.
- Wing, C., Komatsu, M., Delaney, S. M., et al. (2017). Application of stem cell derived neuronal cells to evaluate neurotoxic chemotherapy. **Stem cell research**. 22: 79-88.
- Wu, W.-C., Hsiao, J.-R., Lian, Y.-Y., Lin, C.-Y., and Huang, B.-M. (2007). The apoptotic effect of cordycepin on human OEC-M1 oral cancer cell line. **Cancer Chemotherapy and Pharmacology**. 60(1): 103-111.
- Yu, S., Yin, Y., Zhu, J., et al. (2010). A modulatory bifunctional artificial enzyme with both SOD and GPx activities based on a smart star-shaped pseudo-block copolymer. **Soft Matter**. 6(21): 5342-5350.
- Yu, X., Ling, J., Liu, X., et al. (2017). Cordycepin induces autophagy-mediated c-FLIPL degradation and leads to apoptosis in human non-small cell lung cancer cells. **Oncotarget**. 8(4): 6691.
- Zaidi, A. U., McDonough, J. S., Klocke, B. J., et al. (2001). Chloroquine-induced neuronal

cell death is p53 and Bcl-2 family-dependent but caspase-independent. **Journal of Neuropathology & Experimental Neurology.** 60(10): 937-945.

Zhou, H., Liu, X., Liu, L., et al. (2009). Oxidative stress and apoptosis of human brain microvascular endothelial cells induced by free fatty acids. **The Journal of International Medical Research.** 37(6): 1897-1903.



CHAPTER IV

FABRICATION OF 3D CALCIUM-ALGINATE SCAFFOLDS FOR HUMAN GLIOBLASTOMA MODELING AND ANTICANCER DRUG RESPONSE EVALUATION

4.1 Abstract

The three-dimensional (3D) cell culture model has been increasingly used to study cancer biology and screen for anticancer agents due to its close mimicry to *in vivo* tumor biopsies. In this study, 3D calcium (Ca)-alginate scaffolds were developed for human glioblastoma cell culture and an investigation of the responses to two anticancer agents, temozolomide, doxorubicin and cordycepin. Compared to the 2D monolayer culture, glioblastoma cells cultured on these 3D Ca-alginate scaffolds showed reduced cell proliferation, increased tumor spheroid formation, enhanced expression of cancer stem cell genes (*CD133*, *SOX2*, *Nestin*, and *Musashi-1*), and improved expression of differentiation potential-associated genes (*GFAP* and *β -tubulin III*). Additionally, the vascularization potential of the 3D glioblastoma cells was increased, as indicated by a higher expression of tumor angiogenesis biomarker (VEGF) than in the cells in 2D culture. To highlight the application of Ca-alginate scaffolds, the 3D glioblastomas were treated with anticancer agents, including temozolomide, doxorubicin and cordycepin. The results demonstrated that the 3D glioblastomas presented a greater resistance to the tested anticancer agents than that of the cells in 2D culture. In summary, the 3D Ca-alginate scaffolds for glioblastoma

cell line that were developed in this study offer a promising platform for anticancer agent screening and the discovery of drug-resistant mechanisms of cancer.

Keyword: 3D nerve-tissue cancer, 3D calcium-alginate scaffolds, anticancer drug screening, nerve-tissue cancer model, glioblastoma

4.2 Introduction

Glioblastoma is the most aggressive malignant primary human nerve-tissue cancer, originating from either glial cells or their precursors (Behin et al., 2003). Patients suffering from glioblastoma have a poor prognosis with a median survival rate of only 12–15 months for a newly diagnosed glioblastoma and 5-7 months for recurrent glioblastoma (Johnson and O'Neill, 2012). Currently, chemotherapy is one of the most effective treatments for glioblastoma nerve-tissue cancer, which require high-efficiency drug screening methods to provide highly predictable results for the *in vivo* tests. Currently, cell-based assays are widely used as an *in vitro* model for improving our understanding of cell biology and the mechanisms of diseases, and for the drug discovery processes. Additionally, *in vitro* cell platforms can provide convenient and cost-effective means to avoid ethical concerns and large budget requirement of animal and clinical testing (Kapałczyńska et al., 2016). Traditional two-dimensional (2D) cell culture models have been used for cell culture studies because of their simplicity, convenience, and high cell viability. However, an emerging view is that, due to its simplicity, the 2D cell culture model cannot accurately simulate the three-dimensional (3D) environment in which cancer cells reside within the body. Since *in vivo* cells are encompassed by other cells and an extracellular matrix (ECM) in the 3D model, the 2D cell culture does not sufficiently reflect the natural 3D environment of the cells. This leads to high differences in anticancer drug sensitivities between *in vitro* tests and *in vivo* clinical assessments (Shoemaker, 2006). Hence, there is a growing demand for developing 3D *in vitro* tumor models, which can simulate the tumor microenvironment, mimic *in vivo*

cell behaviors, and provide comparable results to *in vivo* assays. In addition, 3D *in vitro* models have the potential to bridge the gap between traditional 2D cultures and animal models (Pampaloni et al., 2007). The 3D culture models have increased the understanding of cancer stem cell properties and differentiation potential, and anticancer drug screening (Chen et al., 2012; Dhiman et al., 2005; Lv et al., 2016). Over the past few decades, sodium alginate has been used as a biomaterial in tissue engineering (Wang et al., 2003). Alginate is approved by the Food and Drug Administration (FDA) for broad tissue engineering applications because of its biocompatibility, biodegradability, and limited immunogenicity (Rinaudo, 2008). Alginate is a family of natural polysaccharides composed of different lengths of G (α -L-glucuronate), M (β -D-mannuronate), and GM alternating blocks. Alginate can form noncovalent crosslinks through interaction with bivalent metal ions, such as calcium ions (Shull, 2012). Hydrophilic alginate hydrogels have been used as an artificial ECM to provide temporary supports for many kinds of cell types, including chondrocytes (Awad et al., 2004), osteoblasts (Kuo and Ma, 2001), fibroblasts (Hunt et al., 2010) and embryonic stem cells (Hwang et al., 2009). Alternatively, alginate scaffolds can be generated through a freeze drying process (Shapiro and Cohen, 1997). The porosity and pore interconnectivity of alginate scaffolds benefits the exchange of oxygen and nutrients, and waste elimination from the cells. Nowadays, the commercial porous alginate scaffold has been available on the market such as AlgiMatrix™. The AlgiMatrix™ 3D alginate scaffold is product of Life Technologies Corporation Company, which is ready-to-use for the development cell culture models that are more predictive of disease states and drug responses. Its sponge was made from lyophilized alginate gel which nontoxic, biodegradable and is stable at room temperature. AlgiMatrix™ alginate scaffolds has been used for 3D culture for various cell type, including human embryonic stem cells (Gerecht et al., 2004), human osteoblast (Chen et al., 2015), non-small cell lung cancer (NSCLC) (Godugu et al., 2013), U87 glioblastoma and C6 glioma cell lines (Sams et al., 2009). Moreover, Godugu et al. (2013), AlgiMatrix™

3D alginate scaffold was used for *in vitro* tumor model for anticancer drug screening. They found that cancer cells can grow and form multicellular spheroids in 6 and 96 well AlgiMatrix™ scaffolds. Different marketed anticancer drugs were screened cytotoxicity of cells on AlgiMatrix™ system compared to the 2D monolayer cultures. IC₅₀ values for anticancer drugs were significantly higher in AlgiMatrix™ systems compared to 2D culture models. The results from their studies are strongly support that the 3D alginate scaffold may be used as an *in vitro* tumor model. It is possible to predict the anticancer effect of various drugs and formulations in a better model than 2D monolayer cultures. As a result, the ability to predict outcomes in preclinical animal models and clinical trials can be better understood because the positive anticancer effects observed in 2D cultures often fail during *in vivo* testing. However, the price of AlgiMatrix™ quite expensive (17,000 baht/24 well plate) and require other solution (AlgiMatrix™ Firming Buffer and AlgiMatrix™ Dissolving Buffer) to support sponges.

In this study, I modified the 3D Ca-alginate scaffolds via a freeze-drying technique and applied this to human glioblastoma U-251 cell line. Then, the growth characteristics, stemness, and differentiation properties of cells in the Ca-alginate scaffold system were verified, in comparison with the 2D monolayer culture. Finally, to verify whether the 3D Ca-alginate scaffolds can act as a potential platform for screening new anti-glioblastoma agents, the sensitivity of anticancer agents (temozolomide, doxorubicin and cordycepin) on glioblastoma cells in the 3D Ca-alginate scaffolds was evaluated and compared to the cells in the 2D culture. Consequently, the 3D Ca-alginate scaffolds can be cost-effective, low - cost, easy-to-use method, availability, suitability, reproducibility and can also practical in anti-glioblastoma drug screening.

4.3 Materials and methods

4.3.1 Chemicals and reagents

Sodium alginate (A0682), resazurin sodium salt (R7017), arginine-glycine-aspartate (RGD; A8052), calcium chloride (449709), temozolomide (T2577), doxorubicin (D1515) and cordycepin (C3394) were purchased from Sigma-Aldrich Chemical Co. (St. Louis, MO). 4, 6-Diamidino-2-phenylindole (DAPI), calcein-AM and propidium iodide (PI) were purchased from Life Technologies Inc. (Carlsbad, CA). Ethanol and isopropanol were purchased from Fisher Scientific (Pittsburgh, PA). Glutaraldehyde was purchased from Loba-Chemie (Mumbai, India) and Osmium tetroxide (OsO_4) was purchased from Acros Organics (Morris Plains, NJ). Antibodies against Nestin, CD133, β -tubulin III, GFAP, and vascular endothelial growth factor (VEGF) were purchased from Merck (Merck KGaA, Darmstadt, Germany). The human glioblastoma (U-251) cell line was obtained from the European Collection of Authenticated Cell Cultures (ECACC; Salisbury, UK). Human cerebral microvascular endothelial cell line (hCMEC/D3) was obtained from Dr. Oratai Weeranantanapan (Institute of Science, Suranaree University of Technology). EGM-2 (Lonza), EBM-2 medium (serum free, growth-factor free), human fibroblast growth factor-B (hFGF-B), human epidermal growth factor (hEGF), human vascular endothelial cell growth factor (hVEGF), long R insulin-like growth factor-1 (R3-IGF-1), ascorbic acid, hydrocortisone, and heparin (complete media) were obtained from Merck (Merck KGaA, Darmstadt, Germany). Dulbecco's modified Eagle's medium (DMEM) and fetal bovine serum (FBS) were purchased from HyClone (HyClone, Logan, UT), while 0.5% trypsin-ethylenediaminetetraacetic acid (EDTA), L-glutamax, and nonessential amino acids (NEAA) were obtained from Gibco (GIBCO, Carlsbad, CA).

U-251 cell line were cultured in complete medium with DMEM medium, 10% (v/v) FBS, 1% NEAA, 1% (v/v) L-glutamine, and 1% (v/v) penicillin–streptomycin. Cells

were incubated at 37°C in a humidified incubator atmosphere with 5% CO₂: 95% air. The fresh complete medium was changed every 2 days.

hCMEC/D3 cell line were maintained in a specific endothelial cell growth medium EGM-2 (Lonza) that contained EBM-2 medium (serum free, growth-factor free), supplemented with 2% fetal bovine serum (FBS), human fibroblast growth factor-B (hFGF-B), human epidermal growth factor (hEGF), human vascular endothelial cell growth factor (hVEGF), long R insulin-like growth factor-1 (R3-IGF-1), ascorbic acid, hydrocortisone, and heparin (complete media). The cells were incubated at 37°C in a humidified atmosphere of 5% CO₂. The fresh complete medium was changed every 2 days.

4.3.2 Calcium-alginate scaffold fabrication and preparation

The Ca-alginate scaffolds were prepared as previously reported (Shapiro & Cohen, 1997), with slight modifications. A 2% sodium alginate was dissolved in sterile deionized (DI) water, shaken in the incubator shaker for 6 h at 37°C and refrigerated at 4°C for 24 h to remove bubbles. Sodium alginate solution (400 µl) was injected into each 48-well culture plate, frozen at -20°C for 24 h and lyophilized for 8 h. The scaffolds were cross-linked with 2% calcium chloride solution for 1 h, washed three times with sterile DI water, then sterilized with 75% alcohol overnight, and stored at room temperature until use. Before the scaffolds were used, the scaffolds were washed three times with sterile DI water, immersed in arginine-glycine-aspartate (RGD) peptide solution (100 mg/L of DMEM complete medium; Sigma-Aldrich), and incubated for 24 h at 37°C under an atmosphere of 5% CO₂.

4.3.3 Ca-alginate scaffold characterization

A modified liquid displacement method was used for the measurement of porosity in the Ca-alginate scaffold. Isopropanol was utilized as the displacement liquid (Kirdponpattara et al., 2015). Briefly, weight (W_i) and volume (V_i) of the dry scaffold were measured. Isopropanol, with a known density, (ρ_i), was used to immerse scaffolds for 15

min; the scaffolds were weighed (W_f) after removal from the isopropanol. The porosity was calculated by the following equation: $\left[\frac{(W_f - W_i) \times \rho_i}{V_i}\right] \times 100\%$ ($n = 10$).

Mechanical properties of the scaffolds, after being cultured for 0, 7, 14, and 21 days were measured using a texture analyzer (TA.XT Plus Texture Analyzer; Stable Micro Systems, Surrey, UK). Scaffolds were compressed at a rate of 0.4 mm/min until at least 70% strain was attained ($n = 10$). Young's modulus was obtained by calculating the linear regions of the stress-strain graph. Scaffolds were coated with gold sputtering and then placed under a scanning electron microscope (FIB-SEM; Carl Zeiss, Dresden, Germany) to observe the pore structure of the Ca-alginate scaffolds.

4.3.4 Cell seeding on Ca-alginate scaffolds

Human glioblastoma cells (U-251) were seeded onto the scaffolds in 24-well plates at 1×10^6 cells/ml in 50 μ l complete medium per scaffold. Cells were permitted to penetrate the scaffold for 1 h, then 1 ml complete medium was added to each well. For 2D cell cultures, a cell concentration of 50,000 cells in complete medium was added into each 24-well plate. The cells were grown in a humidified incubator at 37°C under an atmosphere of 5% CO₂. The complete medium was changed every 2 days.

4.3.5 Live/dead staining

Live/dead cell fluorescent double staining was used to assess the viability of cells inside the Ca-alginate scaffolds. U-251 spheroids inside the Ca-alginate scaffolds were stained with 4 μ M calcein AM and 4 μ M of propidium iodide (PI) for 30 min at room temperature and protected from light. Calcein AM and PI were used to stain live cells (green fluorescence) and dead cells (red fluorescence), respectively. Live/dead cells were imaged with a fluorescence microscope (ZOETM Fluorescent Cell Imager, Bio-Rad Laboratories, Hercules, CA). Five fields were counted randomly from each image at a magnification of 100x using the ImageJ program (NIH).

4.3.6 Scanning electron microscopy

The morphology of U-251 spheroids inside the Ca-alginate scaffolds and glioblastomas in the 2D culture (on coverslips) were observed using a scanning electron microscope (FIB-SEM, Carl Zeiss). The cells inside the Ca-alginate scaffolds and the 2D culture were fixed with 4% glutaraldehyde overnight at 4°C and 2% osmium tetroxide (OsO₄) solution for 2 h at room temperature. All the samples were dehydrated in a graded series of ethanol (0%, 30%, 50%, 70%, 85%, 95%, and 100%), each step lasting 15 min, and dried by critical-point drying (CPD; Leica EM CPD300; Leica Microsystems (SEA) Pte Ltd, Singapore). The sample was sputter-coated (Sputter Coater Leica EM ACE600, Leica Microsystems (SEA) Pte Ltd) with gold to produce a thick film before observation under a scanning electron microscope (FIB-SEM, Carl Zeiss).

4.3.7 Cell proliferation analysis

Cell proliferation analysis The proliferation of cells cultured on the 3D Ca-alginate scaffolds and the 2D culture was determined using a resazurin assay, as reported previously (Perrot et al., 2003). Briefly, 1 ml of resazurin solution (25 µg resazurin per 1 ml fully complete medium) was added to each well after washing with phosphate buffered saline (PBS) and incubated at 37°C for 30 min. The resazurin solution was transferred to a black 96-well plate to read the fluorescence values on a microplate reader (Varioskan, Thermo Fisher Scientific, Waltham, MA) at an excitation wavelength of 530 nm and an emission wavelength of 590 nm. Cells were washed three times with PBS to remove resazurin solution, then the fresh complete medium was added. This procedure was repeated every 2 days for 21 days. Results were expressed as relative fluorescent units (RFU).

4.3.8 Cell size distribution

After U-251 cells were cultured for 1, 2, and 3 weeks in the 3D Ca-alginate scaffolds, 50 mM EDTA solution was added and incubated for 5 min at 37°C to release the U-251 spheroids from the scaffolds. The U-251 spheroids were washed with PBS, centrifuged briefly, and then fixed for 15 min at room temperature in 4% paraformaldehyde

(PFA). The average diameters of the spheroids were measured with a light microscope (ECLIPSE Ts2; Nikon Instruments Inc.), and the data were calculated with iworks software (Pixera Corporation, Santa Clara, CA).

4.3.9 Quantitative real-time polymerase chain reaction quantification

The U-251 cells inside the Ca-alginate scaffolds were extracted with a 50 mM EDTA solution. The cells inside the Ca-alginate scaffolds were washed with PBS and dissolved in 50 mM EDTA solution at 37°C for 5 min, then the cells were collected by centrifugation at 200 rpm for 3 min. Total RNA from the cells after 7, 14, and 21 days in the 3D and 2D cultures were isolated using a NucleoSpin RNA Kit (Macherey-Nagel, Dueren, Germany), according to the manufacturer's instructions. The total RNA was converted into complementary DNA (cDNA) using a 2-step RT-PCR Kit (Vivantis Technologies Sdn. Bhd, Selangor Darul Ehsan, Malaysia). Quantitative polymerase chain reaction (qPCR) experiments were performed using the QuantStudio 5 Real- Time PCR System (Thermo Fisher Scientific), which were conducted in 96-well plates. To monitor cDNA amplification, qPCR BioSyGreen Mix Low-Rox (PCR BIOSYSTEMS, London, UK) was used in a 20 μ l reaction volume. Cycling conditions according to the specific SYBRGreen protocol were: 95°C for 30 s, 60°C for 30 s, and 72°C for 45 s (40 cycles). A melting curve analysis of the PCR products was performed by heating at 60°C for 60 s, 95°C for 15 s, and continuous measurement of the fluorescence to verify the PCR product.

Glyceraldehyde-3-phosphate dehydrogenase (*GAPDH*) was used as the endogenous housekeeping gene. The expression level of *Nestin*, *CD133*, *Musashi-1*, *Sox2*, *β III-Tubulin*, glial fibrillary acidic protein (*GFAP*), and *VEGF* were examined. The primers for the reference gene *GAPDH* and the primers designed for the genes of interest are

shown in Table 4.1 Relative expression was determined by the $2^{-\Delta\Delta C_t}$ method, and each target gene was normalized against *GAPDH* and the 2D culture condition.

Table 4.1 The primer sequences used for real-time RT-PCR.

	Forward	Reverse
<i>GAPDH</i>	5'- CTCTGCTCCTCCTGTTCGAC-3'	5'- TTAAAAGCAGCCCTGGTGAC-3'
<i>CD133</i>	5'- ACTCCCATAAAGCTGGACCC-3'	5'- TCAATTTTGGATTCATATGCCTT-3'
<i>Musashi-1</i>	5'- ACAGCCCAAGATGGTGACTC -3'	5'- TGGTTTTGTCAAACATCAGCA-3'
<i>Sox2</i>	5'- GCGAACCATCTCTGTGGTCT-3'	5'- GGAAATTTGGGATCGAACAA-3'
<i>Nestin</i>	5'-GGAGAAACAGGGCCTACAGA -3'	5'- GGGAGTTCTCAGCCTCCAG-3'
<i>GFAP</i>	5'-ATCGAGATCGCCACCTACAG-3'	5'- CACCACGATGTTCTCTTGA-3'
<i>βIII-tubulin</i>	5'- CGCCCAGTATGAGGGAGAT-3'	5'- AGTCGCCCACGTAGTTGC -3'
<i>VEGF</i>	5'- AGGGCAGAATCATCACGAAG-3'	5'- CACACAGGATGGCTTGAAGA-3'

GAPDH : Glyceraldehyde 3-phosphate dehydrogenase; *GFAP*: Glial fibrillary acidic protein; *VEGF*: vascular endothelial growth factor;

4.3.10 Immunofluorescence staining

Human glioblastoma cell line (U-251) were cultured either with 2D culture or 3D Ca-alginate scaffolds for 14 days. The cells were washed with PBS two times, fixed for 1 h in 4% PFA, washed three times with PBS, permeated for 20 min in 0.2% Triton X-100 in PBS and blocked with 4% BSA in PBS for 1 hour. Anti-nestin, anti-CD133, anti-βIII-tubulin, anti-GFAP, and anti-VEGF antibodies were added into the blocking buffer and then incubated at 4°C overnight. The cells were washed with PBS three times, then incubated with secondary antibody for 1 h in the dark. After washing with PBS, the nuclei of the cells were stained with DAPI and observed using a fluorescence microscope (ZOE™ Fluorescent Cell Imager, Bio-Rad Laboratories).

4.3.11 Combination of 3D U-251 and 2D hCMEC/D3 cell lines

U-251 cells were seeded onto the Ca-alginate scaffolds in 24-well plates at 1×10^6 cells/ml in 50 μl complete medium per scaffold. After 14 days in 3D Ca-alginate scaffold, U-251 spheroid were extracted with a 50 mM EDTA solution and cultivated on the hCMEC/D3 layer on 2D glass coverslips in the medium constituted of 50% U-251 medium and 50% hCMEC/D3 medium. After 7 and 14 days, the morphology of 3D U-251 and 2D

hCMEC/D3 were observed using a scanning electron microscope (FIB-SEM, Carl Zeiss) and angiogenesis markers (VEGF and collagen IV) were stained using immunofluorescence assay.

For U-251 and hCMEC/D3 monolayer cells were cultured on 2D glass coverslips in complete medium. At days 14 the morphology of hCMEC/D3 monolayer cells were observed using a scanning electron microscope (FIB-SEM, Carl Zeiss) and angiogenesis markers (VEGF and collagen IV) of both cells were stained using immunofluorescence assay.

4.3.12 Cytotoxicity of anticancer agents

The cytotoxicity of temozolomide, doxorubicin and cordycepin was compared between the 2D culture and the 3D Ca-alginate glioblastomas. To examine anticancer agent sensitivity, U-251 cells (5×10^5 cells/well) were seeded into 24-well plates (2D) and 3D Ca-alginate scaffolds for 14 days. The most common cancer chemotherapy drug, temozolomide (Khasraw et al., 2009), doxorubicin (Rivankar, 2014) and potential candidate, cordycepin were selected for this test. The cells were treated with varying concentrations of temozolomide (15-500 $\mu\text{g/ml}$) or doxorubicin (2.5-40 $\mu\text{g/ml}$) or cordycepin (12.5-400 $\mu\text{g/ml}$). Cell viability was examined 48 hours after treatment via a resazurin assay, as described above, and reported as the fluorescence intensity value of viable cells relative to the untreated control. Live and dead cells were assessed by a fluorescent live/dead viability assay, as described above, and cell survival was observed by a fluorescence microscope (ZOE™ Fluorescent Cell Imager Bio-Rad Laboratories) after the cells were treated with 100 $\mu\text{g/ml}$ temozolomide or 200 $\mu\text{g/ml}$ cordycepin. The cells were treated with 10 $\mu\text{g/ml}$ doxorubicin, and live/dead cells were stained with 4 μM calcein AM and 4 μM of DAPI; since the spectral ranges of PI and doxorubicin overlapped, PI was substituted with DAPI. Images were obtained using a fluorescence microscope (ZOE™ Fluorescent Cell Imager, Bio-Rad Laboratories).

4.3.13 Statistical analysis

All the results were expressed as means \pm standard deviations. Statistical analysis was performed using a Student's t test (SPSS version 16.0, SPSS Inc., Hong Kong, China) to compare means from two independent sample groups. $p < 0.05$ were considered statistically significant.

4.4 Results

The 3D Ca-alginate scaffold cell culture systems are a suitable growth environment for cells or tissues. In this study, the 3D Ca-alginate scaffold cell culture system was used as a model to create micro tumor spheroids (Figure 4.1). First, the 3D Ca-alginate scaffolds were fabricated using a freeze-drying technique (Step 1a). U-251 human glioblastoma cells were then seeded into the 3D Ca-alginate scaffolds (Step 2a) or onto the 2D cell culture plates (Step 2b). Glioblastoma cells could be cultured in a 2D monolayer environment, but the 2D cell culture did not sufficiently accurately mimic the natural 3D environment of the cells in which cancer cells reside, limiting the potential of the cells to proliferate and differentiate, and to the loss of their phenotype (Step 3b). Meanwhile, the 3D Ca-alginate scaffolds exhibited a highly porous structure and created an environment permissive for glioblastoma cell ingrowth and spheroid formation (Step 3a). After 14 days of incubation, chemotherapy drug resistance assays of the 3D U-251 glioblastoma cells were performed and compared to the 2D culture (Step 4a). In the future, the 3D Ca-alginate scaffolds could potentially be a platform for studies of glioblastomagenesis, cancer biology, as well as mechanisms of cancer drug resistance.

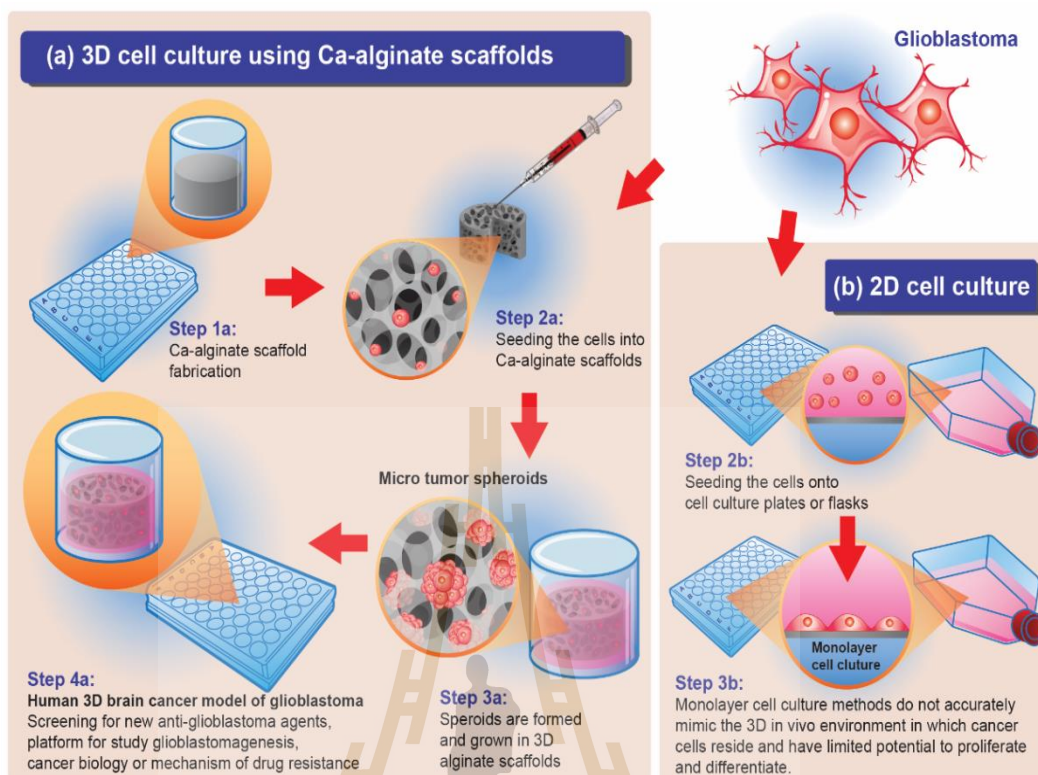


Figure 4.1 Schematic illustration of the platform for drug screening of nerve-tissue cancer in the 3D human glioblastoma cell culture system. Briefly, step 1 was to prepare the 3D calcium-alginate scaffold by using freeze-drying technique. Next step was to seed human glioblastoma U-251 cells into the Ca-alginate scaffolds (Step 2a) or onto the cell culture plates (Step 2b). Step 3b was to culture cells as the 2D monolayer, which did not accurately mimic the 3D *in vivo* environment. Cancer cells were limited their potential to proliferate, differentiate, and loose phenotype, while micro-tumor spheroids were formed and grown in the 3D alginate scaffold (Step 3a). At the end of this study, to verify whether the 3D Ca-alginate scaffolds were capable as an *in vitro* research platform for screening a potent anti-glioblastoma agent, chemotherapy drug resistance assay of the 3D Ca-alginate were determined (Step 4a).

4.4.1 Ca-alginate scaffold properties

The Ca-alginate scaffolds were fabricated and their structural and mechanical properties were evaluated, determining the relation to cancer biopsies of the human body (Figure 4.2). The morphology of the Ca-alginate scaffold is shown in Figure 4.2a. After freeze-drying, the Ca-alginate scaffold was 10 mm in diameter and 4 mm in height. The internal structure of the scaffolds was shown in the SEM images, which exhibited an even spread of pores with an approximate diameter of 100-400 μm (Figure 4.2b). The interconnected pores were found inside the scaffolds, despite the presence of some closed-wall pores. The Ca-alginate scaffolds presented a porosity of 89.5% (Figure 4.2c). The mechanical properties of the Ca-alginate scaffolds after 7, 14, and 21 days of U-251 cell culture were assessed with compression testing (Figure 4.2d-g). The Young's modulus was 131.0 ± 16.2 , 100.6 ± 9.6 , 73.2 ± 2.1 , and 27.8 ± 7.4 kPa for Ca-alginate scaffolds after 0, 7, 14, and 21 days of culture, respectively. The Young's modulus of the scaffolds was found to decrease with time, which was closer to that of nerve-tissue cancer cancer tissue (~ 7 kPa) (Yu et al., 2011) than cell cultures on polystyrene plates (2-4 GPa) (Florczyk et al., 2016).

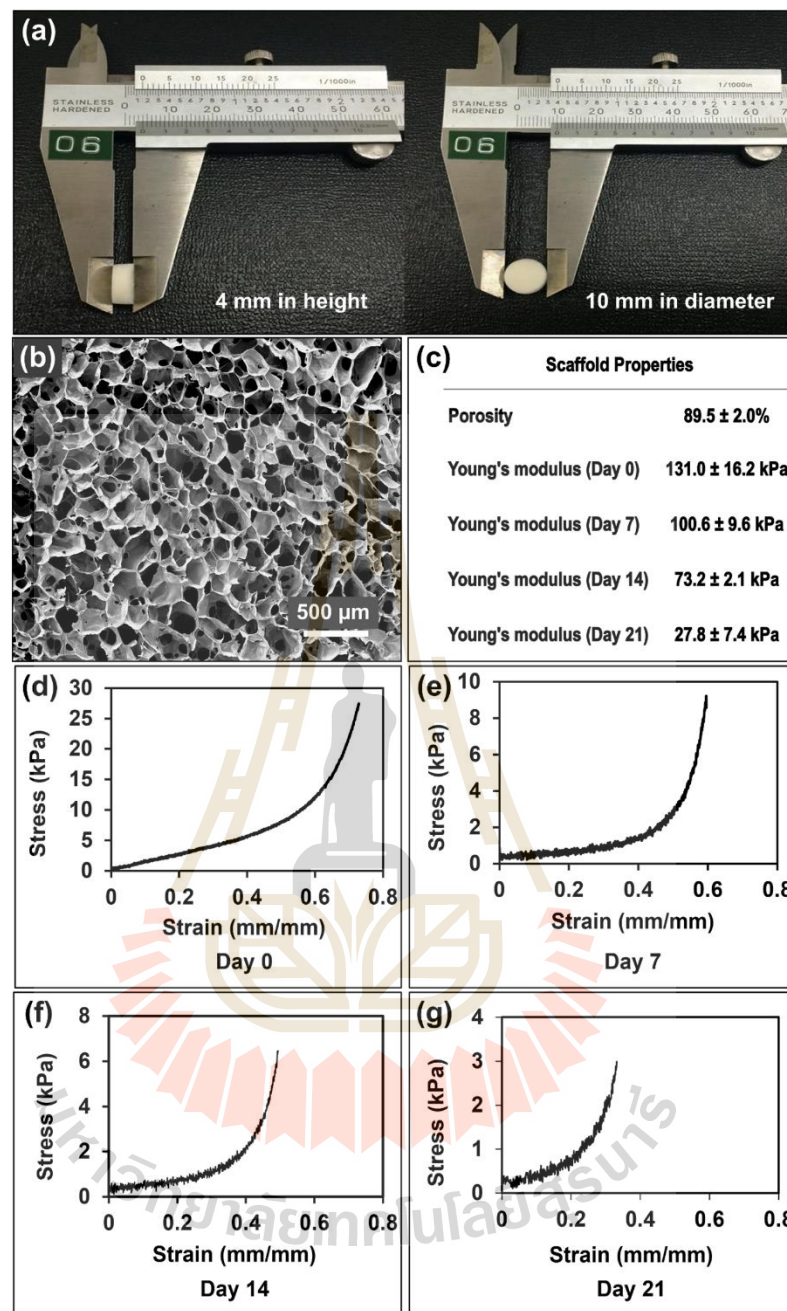
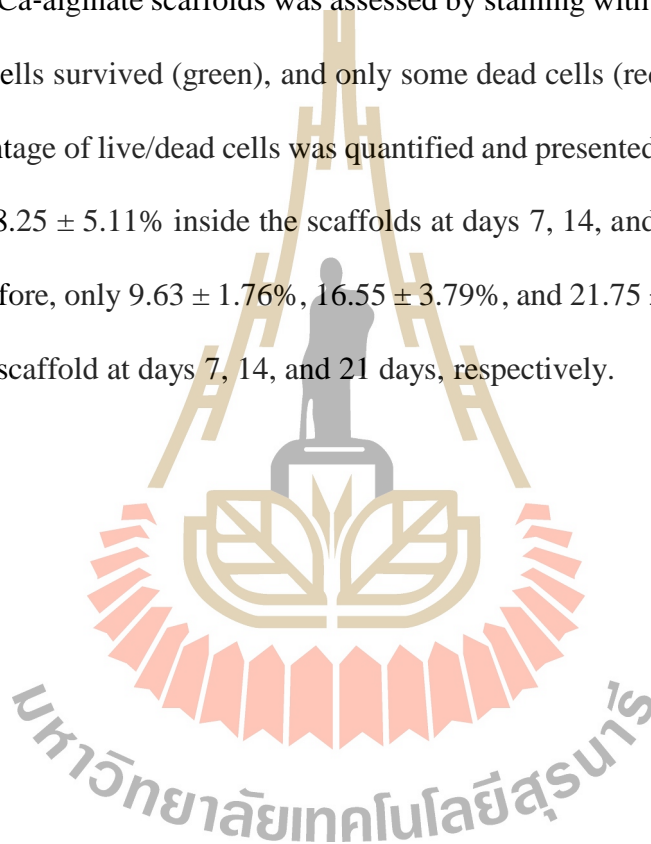


Figure 4.2 Ca-alginate scaffold morphology and properties. (a) Ca-alginate scaffolds were shown with 4 mm in height and 10 mm in diameter in a cylinder-shaped after lyophilization. (b) SEM images of the Ca-alginate scaffold exhibiting pore morphology (c) Physical properties of Ca-alginate scaffolds (d-g) Stress- strain plot of Ca-alginate scaffolds before and after 7, 14, and 21 days of U-251 cell culture.

4.4.2 Live/dead glioblastoma cells inside the Ca-alginate scaffolds

To investigate the effect of the Ca-alginate scaffolds on human glioblastoma cell viability, U-251 cells were seeded onto the scaffolds in 24-well plates at 50,000 cells per scaffold and cultured for 7, 14, and 21 days. During the culture period, glioblastoma cells tended to grow as cellular aggregates/spheroids (Figure 4.3a1-c1). The viability of U-251 cells within the Ca-alginate scaffolds was assessed by staining with fluorescent dyes (calcein AM/PI). Most cells survived (green), and only some dead cells (red) were observed (Figure 4.3). The percentage of live/dead cells was quantified and presented as $90.37 \pm 1.76\%$, $83.45 \pm 3.79\%$, and $78.25 \pm 5.11\%$ inside the scaffolds at days 7, 14, and 21, respectively (Figure 4.3a5-c5); therefore, only $9.63 \pm 1.76\%$, $16.55 \pm 3.79\%$, and $21.75 \pm 5.11\%$ of the cells were dead inside the scaffold at days 7, 14, and 21 days, respectively.



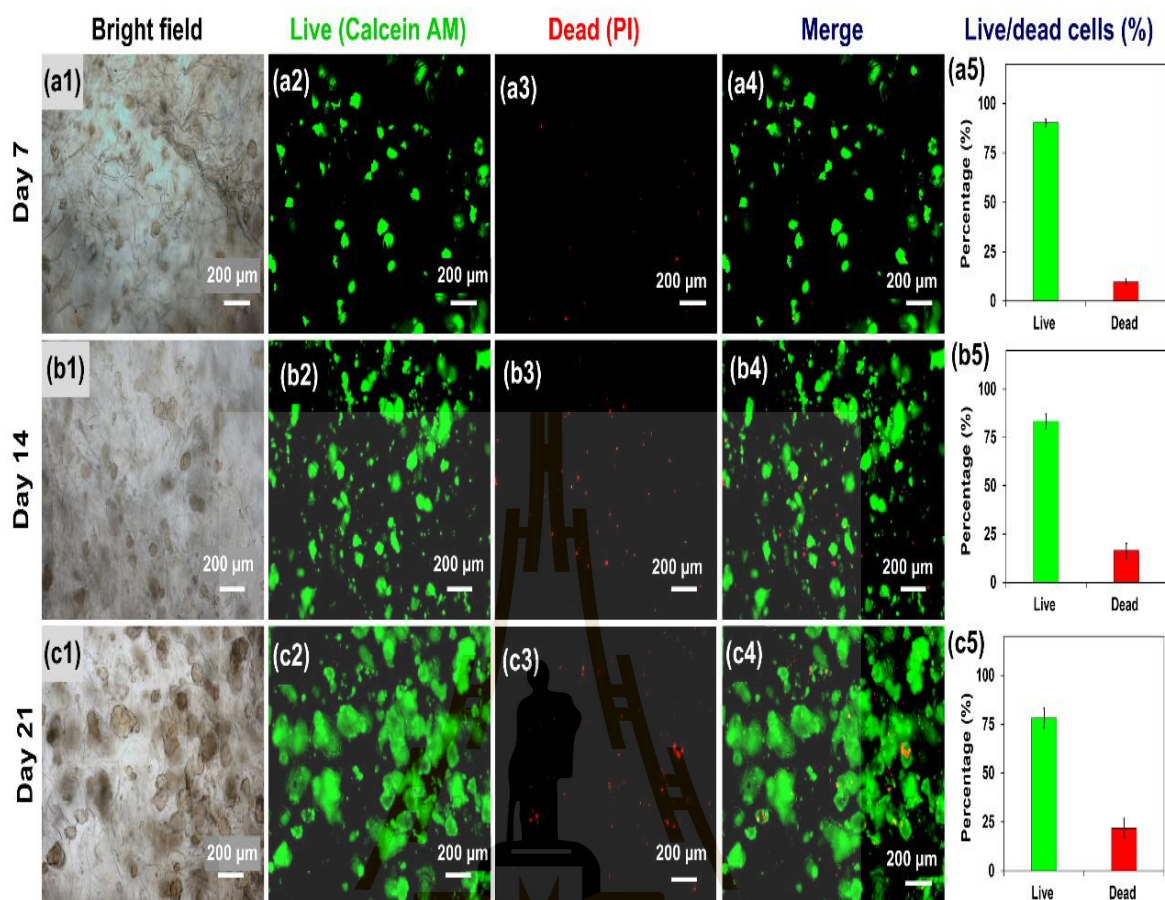


Figure 4.3 The influence of Ca-alginate scaffolds on glioblastoma stem cells U-251 viability at 7, 14, and 21 days culture was determined by fluorescence live/dead staining. (a1, b1, and c1) showed the U-251 spheroid within Ca-alginate scaffold in bright field; (a2, b2, and c2) in green represented the live cells of U-251 spheroid with calcein AM dye; (a2, b3, and c3) in red (PI) indicated dead cells; (a4, b4, and c4) were the merge images; (a5, b5, and c5) displayed the percentage of live and dead cells.

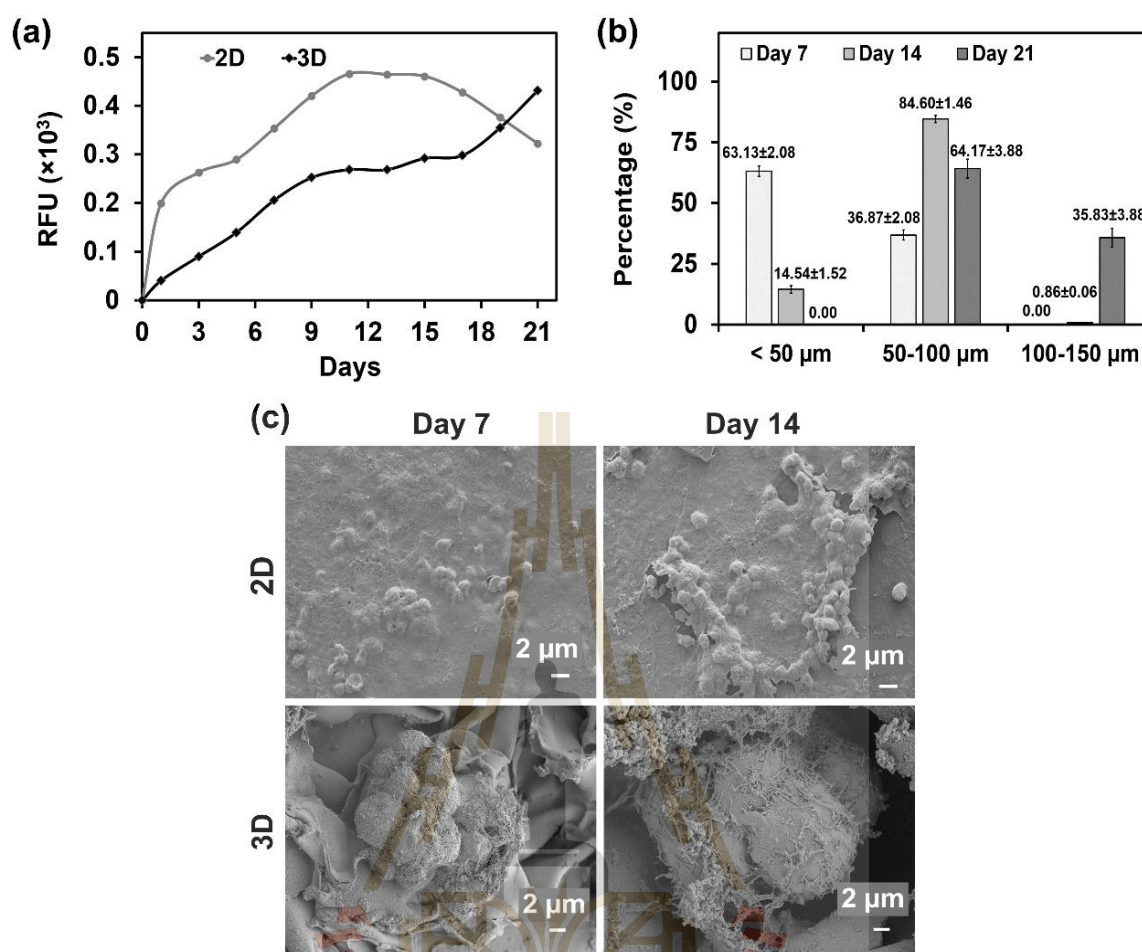


Figure 4.4 Cell proliferation, spheroids size distribution, and morphology of glioblastoma spheroids. (a) Cell proliferation of U-251 cells cultured on the 2D culture and in the Ca-alginate scaffolds was determined by resazurin assay. (b) The spheroids diameter histograms presented the size distribution of U-251 spheroids in the 3D Ca-alginate scaffolds after 7, 14, and 21 days of the culture. (c) SEM images of glioblastoma U-251 cells growing on the 2D culture and inside the 3D Ca-alginate scaffolds for 7 and 14 days, respectively.

4.4.3 Characterization of U-251 glioblastoma cells inside the Ca-alginate scaffolds

The proliferation capacity of cells in the 2D culture and 3D Ca-alginate scaffold culture were measured using a resazurin assay every 2 days for 21 days. (Figure 4.4a). For the first 14 days, cells in the 2D condition grew rapidly, and then the cell population decreased at the 15-day time point. On the other hand, the 3D glioblastoma grew slowly at

the beginning of the culture, but the growth rate increased gradually, which lasted for 21 days of the culture. After 7 days of 3D cell culture, over half of the spheroids were under 50 μm in diameter; then, up to 85% and 100% of spheroids became larger than 50 μm in diameter on Days 14 and 21, respectively (Figure 4.4b). These results suggest that the Ca-alginate scaffolds supported the continuous culture, proliferation, and spheroid formation of U-251 human glioblastoma cells. The morphology of the U-251 cells in the 2D and 3D Ca-alginate scaffold culture was shown under a SEM images (Figure 4.4c). The SEM images indicated that the cell culture environment affected cell morphology. Cells in the 2D condition grew as flat sheets with microstructures that were similar to those in the 3D condition, but they were unable to form spheroids (Figure 4.4c).

4.4.4 Stemness, differentiation, and angiogenesis properties of glioblastoma cells in both culture conditions

To compare the expression of stemness, differentiation, proliferation, and angiogenesis genes in the 2D and 3D glioblastoma cells, the expression of marker genes in cells from both conditions was measured using real-time polymerase chain reaction. Here, *Nestin*, *CD133*, *SOX2*, and *Musashi-1* were used as markers of cancer stem cells. Results showed that *CD133*, *Nestin*, *SOX2*, and *Musashi-1* mRNAs were significantly increased in the culture of the Ca-alginate scaffolds (Figure 4.5a-d). The stemness markers, including *CD133*, *Nestin*, *SOX2*, and *Musashi-1*, were upregulated by 2.3-, 2.2-, 2.6-, and 2.4- fold, respectively, in the 3D glioblastoma cells cultured on Day 21, compared to the 2D culture. In addition, the expression of CD133 and Nestin protein in glioblastoma cells was confirmed by immunofluorescent staining. After 2 weeks of culture, the expression of CD133 and Nestin significantly increased in the 3D glioblastoma cells, compared to the 2D culture (Figure 4.5h). These data indicate that the 3D Ca-alginate scaffolds maintained and enriched the cancer stemness of human glioblastoma cells.

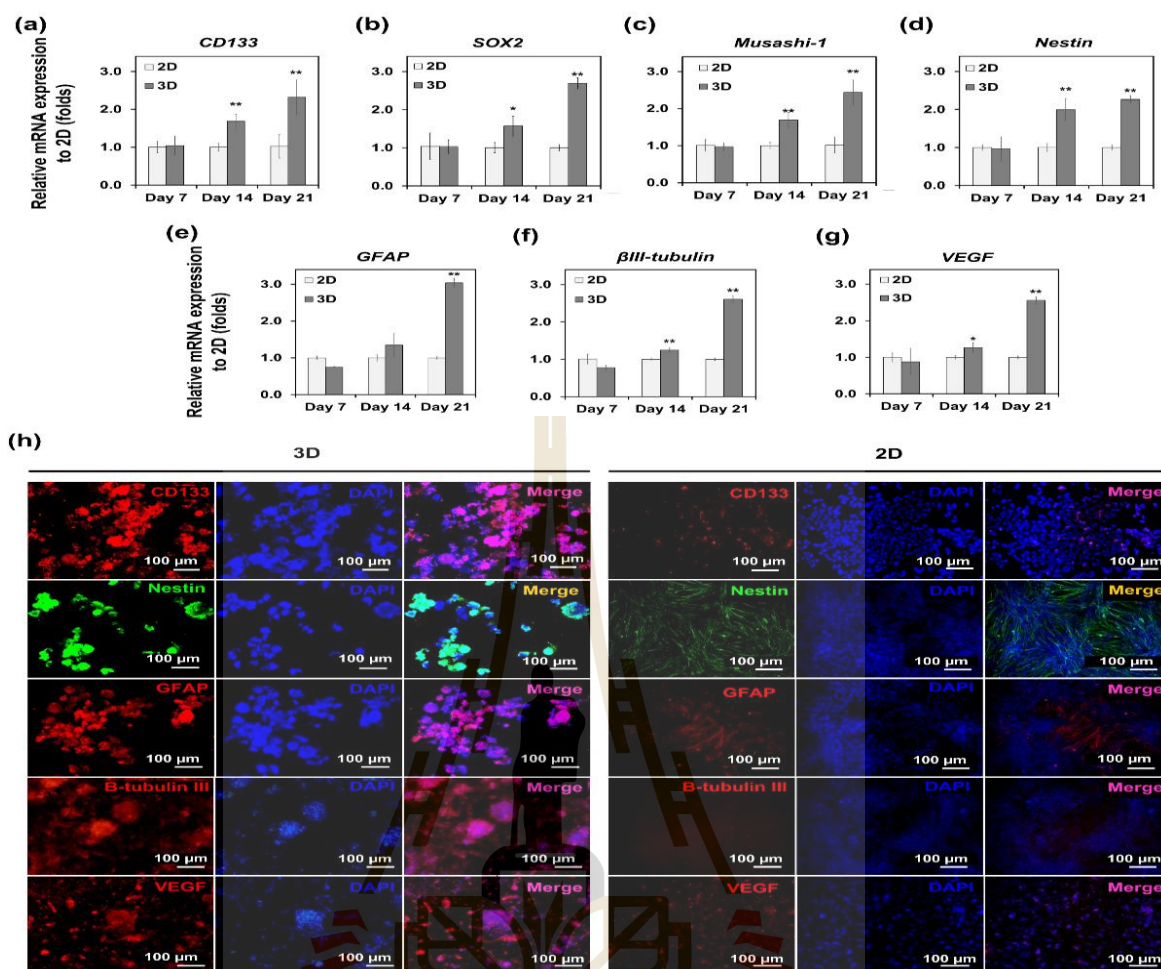


Figure 4.5 Gene expression levels and protein expression of glioblastoma U-251 cells growing on the 2D and inside the 3D Ca-alginate scaffolds. (a, b, c, and d) Expression of stemness genes (*CD133*, *SOX2*, *Nestin*, and *Musashi-1*), (e,f) differentiation-related genes (*β -Tubulin III* and *GFAP*), (g) angiogenesis factor (*VEGF*) were quantified by qRT-PCR. The relative mRNA expression was calculated following $2^{-\Delta\Delta C(T)}$ method, and each target gene was normalized against *GAPDH* and the 2D culture condition. Cells were grown on the 2D well plate and in the 3D Ca-Alginate scaffolds for 7, 14, and 21 days prior to collection and analysis. Asterisks indicated statistical significance as determined by the Student's t-test: * $p < 0.05$ and ** $p < 0.01$. Data represent the means \pm SD (n=3). (h) Immunofluorescence images of glioblastoma U-251 cells growing on the 2D and inside the 3D Ca-Alginate scaffolds for 14 days stained with CD133, Nestin, β -Tubulin III, GFAP, VEGF, and DAPI.

The expression of GFAP and β III-tubulin, the differentiation potential markers, was investigated at both the mRNA and protein levels. It was apparent that, after 3 weeks of culture, the expression of *GFAP* and *β -Tubulin III* genes was significantly increased in the 3D glioblastoma cells. Likewise, at Week 2, the expression of GFAP and β -Tubulin III protein was increased in the U-251 cells cultured in the 3D condition (Figure 4.5h). These results suggest that the 3D Ca-alginate scaffolds promoted the differentiation potential of human glioblastoma cells. Angiogenesis potential was also observed by determining the expression of *VEGF*. At weeks, U-251 human glioblastoma in the 3D Ca-alginate scaffolds expressed a 2.5-fold upregulation of *VEGF*, compared with the 2D culture (Figure 4.5g). Similarly, the fluorescence intensity of the VEGF protein was higher in the 3D Ca-alginate scaffolds than in the 2D culture (Figure 4.5h). These results imply that the 3D Ca-alginate scaffolds can mimic the *in vivo* tumor microenvironment to support angiogenesis in human glioblastoma, which is important for tumor progression.

4.4.5 Characterization of combination 3D U-251 and 2D hCMEC/D3

To confirm whether U-251 cell in 3D Ca-alginate scaffolds induce vascularization and can be applied as an *in vitro* 3D vascularized tumor model, we cultured hCMEC/D3 on coverslips and co-cultured with U-251 spheroid cultured for 14 days in 3D Ca-alginate scaffolds. As shown in microscopic images (Figure 4.6a-c), U-251 spheroid, accumulated on top of the endothelial cells grew in 2D monolayer, proliferated, spread rapidly, and covered almost the entire surface of hCMEC/D3 (Figure 4.6 b and c). At day 7 and 14 of co-culture, U-251 spheroids (3D) and hCMEC/D3 (2D) monolayer culture could proliferated as usual. Moreover, hCMEC/D3 endothelial cells entered self-organization and began to form vascular-like structures which connected and infiltrated to U-251 spheroids as shown by scanning electron microscopy (SEM) in Figure 4.6e, f, h and i. To explore the mechanism related to the formation of vascular-like structures, we studied expression of VEGF (vascular endothelial growth factor), well-known angiogenesis stimulator,

of 3D U-251 and 2D hCMEC/D3 after 14 days of co-culture using immunofluorescence staining. VEGF protein expression was increased in the co-culture but obviously decreased in each individual culture at 14 days (Figure 4.7a-e). To ensure that the vascular-like structures possessed endothelial property, we observed the expression of collagen IV, a specific marker of the vessel basal membrane using immunostaining comparing the co-culture with each type of individual culture. At day 14 of culture, collagen IV expression was dramatically upregulated in the combined 3D U-251 and 2D hCMEC/D3 (Figure 4.7f-j). These results indicate that the combination of 3D U-251 glioblastoma and 2D hCMEC/D3 endothelial cells could induce the formation of vascular-like structures corresponding to tumor angiogenesis.

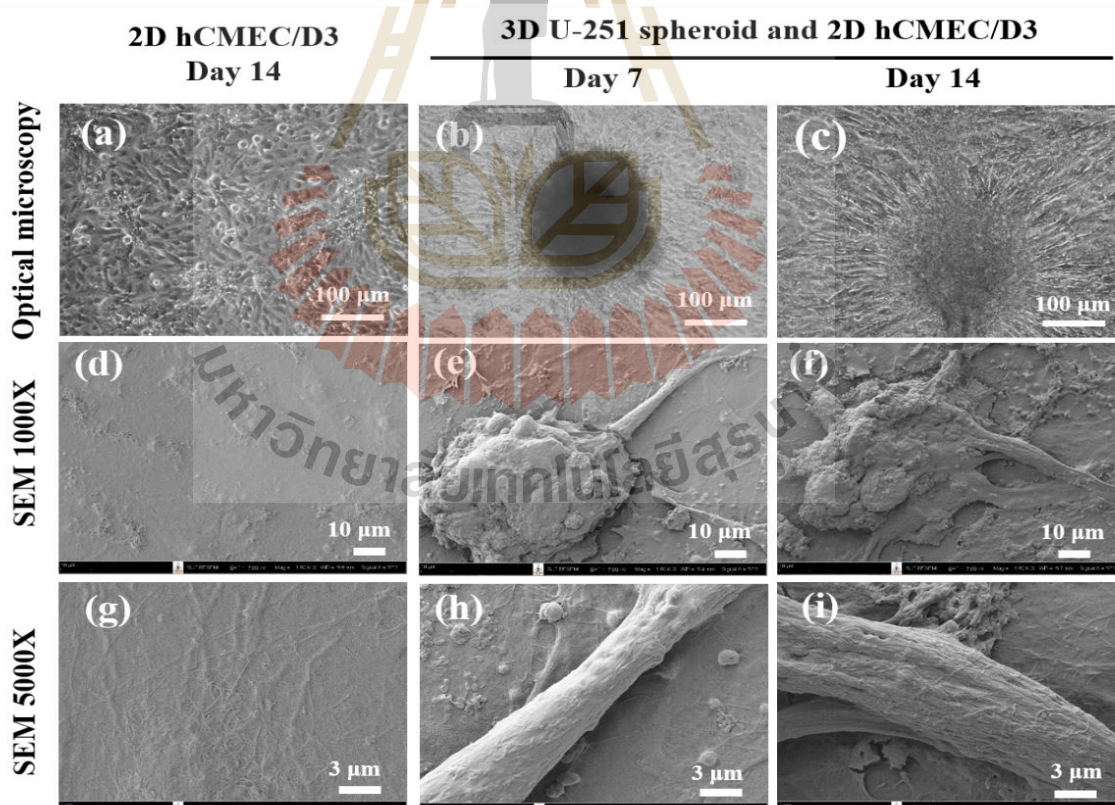


Figure 4.6 (a-c) Optical microscopy and (d-i) scanning electron microscopy of combined cultures of U-251 cultivated for 14 days in Ca-alginate scaffold and U-251 spheroid deposited on hCMEC/D3 endothelial cells on glass coverslips for 7 and 14 days.

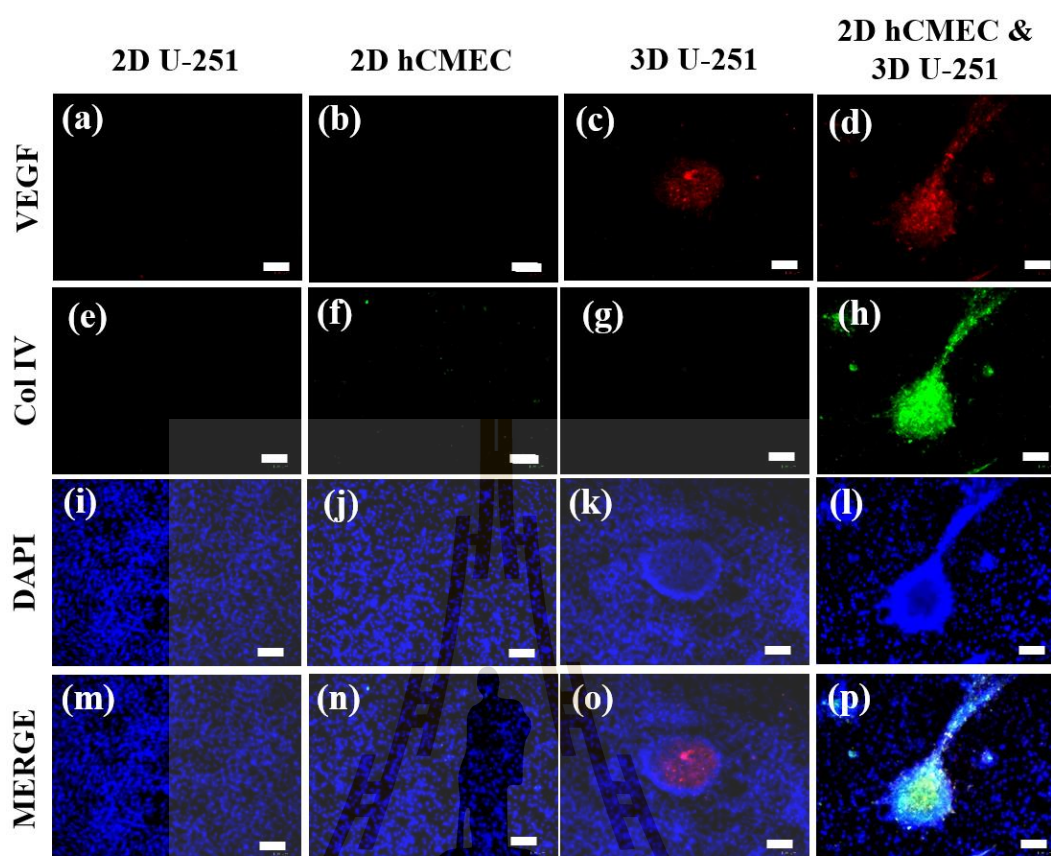
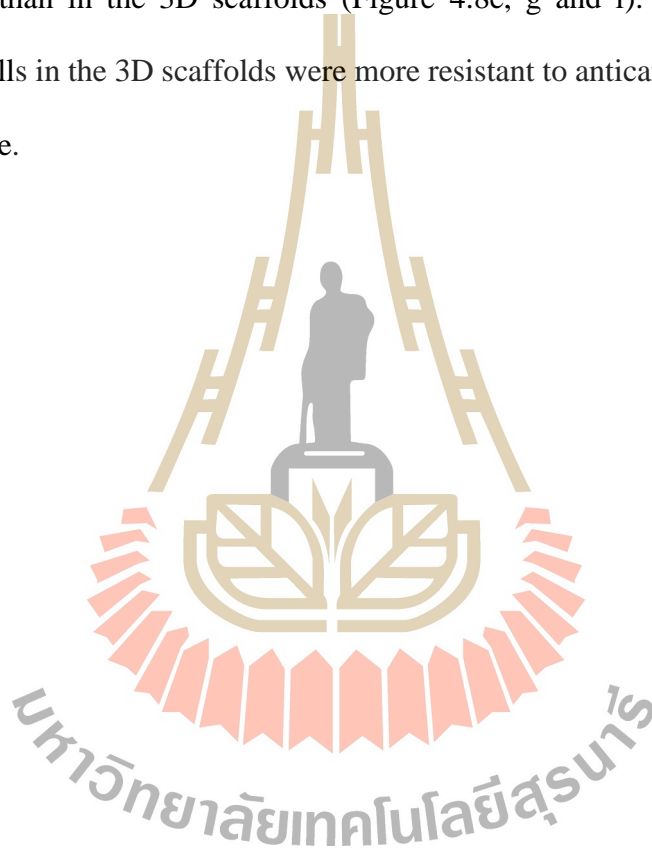


Figure 4.7 Immunofluorescence for VEGF and Collagen IV of combined 3D U-251 and 2D hCMEC/D3 culture at day 14 compared to each type of cells cultured in 2D monolayer. Scale bars is 100 μm

4.4.6 Effect of anticancer agents on glioblastoma cells in both culture conditions

To verify whether the 3D Ca-alginate scaffolds contain the potential to be an *in vitro* research platform for drug screening, the 3D Ca-alginate glioblastoma cells were treated with anticancer agents, and cell viability was compared to that in the 2D culture. The cells in the 3D Ca-alginate were more resistant to both agents than those in the 2D culture condition (Figure 4.8a-b). The half-maximal inhibitory concentrations (IC_{50}) of temozolomide in the 2D and 3D Ca-alginate cultures were 30.07 ± 1.40 and 169.40 ± 8.85 $\mu\text{g/ml}$, respectively, while, the IC_{50} values of doxorubicin in the 2D and 3D Ca-alginate cultures were 1.98 ± 0.01 and 10.00 ± 1.0 $\mu\text{g/ml}$, respectively. Additionally, the IC_{50} values of cordycepin were 103.66 ± 10.26 and 207.33 ± 16.62 $\mu\text{g/ml}$ for the 2D and 3D Ca-

alginate cultures, respectively. The high IC_{50} values of 3D glioblastomas highlighted that the biochemical nature of the 3D Ca-alginate scaffold closely mimicked the natural tumor environment, which possibly enhanced drug resistance in the cancer cells in the 3D culture. After 48 h of treatment with either 100 $\mu\text{g}/\text{ml}$ temozolomide or 10 $\mu\text{g}/\text{ml}$ doxorubicin or 200 $\mu\text{g}/\text{ml}$ cordycepin, a higher number of dead cells were observed in the 2D culture (Figure 4.8d, f and h) than in the 3D scaffolds (Figure 4.8e, g and i). These data suggest that glioblastoma cells in the 3D scaffolds were more resistant to anticancer agents than the cells in the 2D culture.



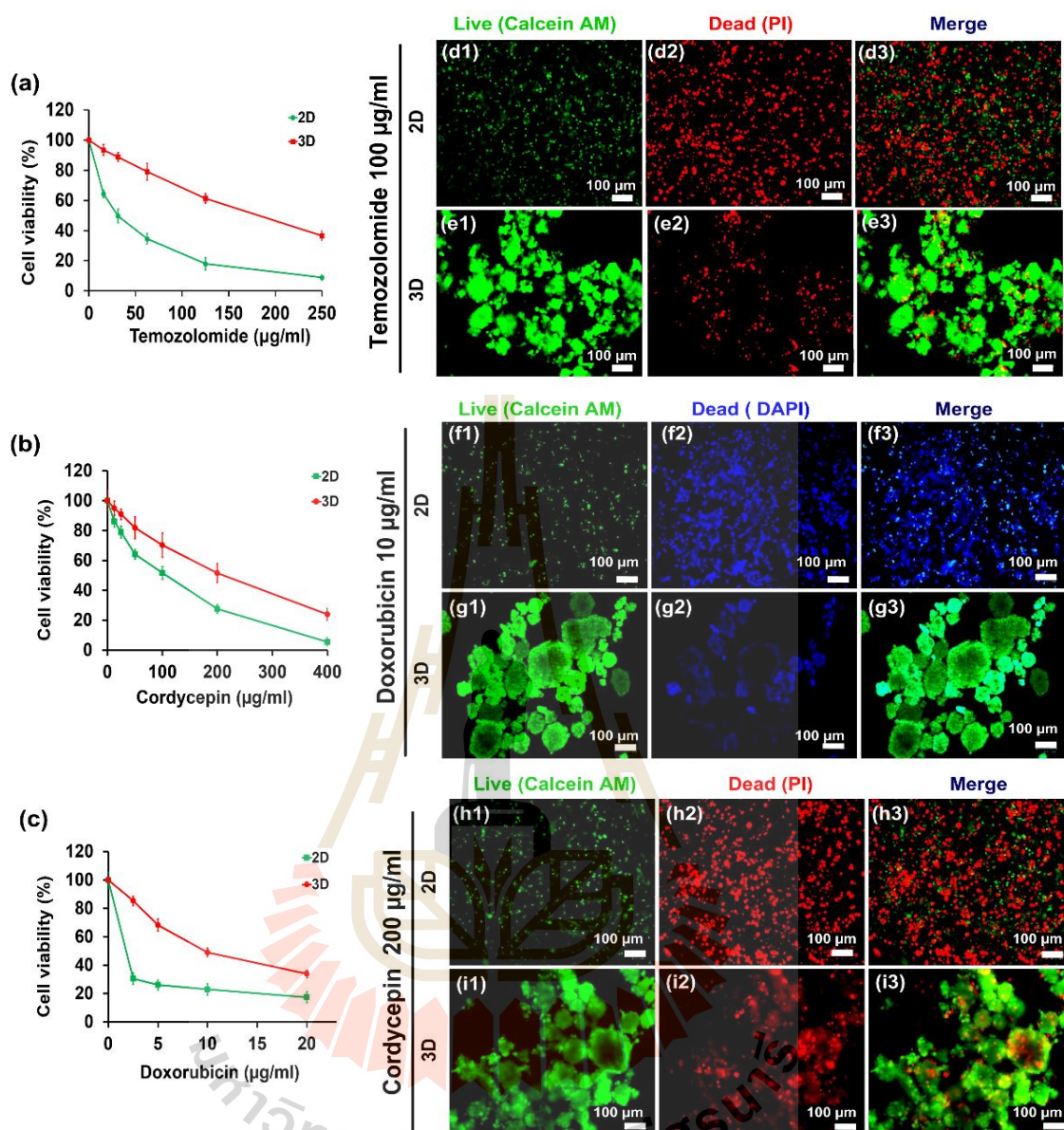


Figure 4.8 Glioblastoma cells responded to anticancer agents. U-251 cell viability in the 2D and 3D culture conditions after the exposure to temozolomide (a) doxorubicin (b) and cordycepin (c) for 48 hours. Data represented the mean percentage viability \pm SD normalized against the untreated control cells. (d) and (e): temozolomide treated U-251 in the 2D and 3D at 100 μ g/ml for 48 h; (f) and (g): doxorubicin treated U-251 in the 2D and 3D at 10 μ g/ml for 48 h; (h) and (i): cordycepin treated U-251 in the 2D and 3D at 200 μ g/ml for 48 h.

4.5 Discussion

Direct clinical trials for tumorigenesis and the development of anticancer agents without the approval of the responsible organizations are prohibited due to controversial ethical issues and safety restrictions (Ulrich et al., 2016). This gives rise to alternative cell based studies, which are potentially used as preclinical procedures to provide reliable information about both tumorigenesis and anticancer agents. Traditionally, cell-based *in vitro* assays for the screening of anticancer drugs have relied on 2D cell cultures, which have recently been considered to not be reflective of the natural microenvironment of the tumor, making the 2D culture unable to precisely select clinically active drugs (Shoemaker, 2006). Therefore, 3D culture models were developed and expected to be a better alternative for the simulation of human tumor tissues *in vitro* (Pampaloni et al., 2007). The previously reported 3D glioblastoma culture systems were hydrogel-based, which exhibited good biocompatibility and biodegradability and were suitable for studies of cell invasion, migration, motility or specific signaling pathways (Huang et al., 2018; Koh et al., 2018). However, cell viability tests, such as 3-(4,5-dimethylthiazol-2-yl)-2,5-diphenyltetrazolium bromide, resazurin, or the Alamar blue assay, were difficult to test in the hydrogel. Therefore, the 3D scaffold systems are considered a suitable platform for studying glioblastomagenesis and for screening potent anticancer agents.

In this study, Ca-alginate scaffolds were fabricated by the freeze-drying of formulated alginate solution. Spontaneous sublimation directly from the solid to the gas phase caused natural freezing and the formation of pores within synthetically polymeric materials (Sachlos and Czernuszka, 2003); this particular process consequently resulted in porous alginate scaffolds that were crosslinked with calcium ions, which exhibited excellent physicochemical and biological properties, similar to the detailed scaffold characterization reported previously (Chen et al., 2015). The Ca-alginate scaffold was cylinder-shaped. Internally, porous structures were shown on the SEM images, demonstrating evenly

distributed pores throughout the scaffold. The porous structures were beneficial for nutrient storage and provided a 3D platform for cell proliferation and differentiation (Zhou et al., 2016). Plus, the porosity of the Ca-alginate scaffolds also provided a larger surface area for cell/tissue expansion than that of the 2D culture system. Stiffness (or rigidity) was another parameter of the Ca-alginate scaffolds that indicated the ability of the scaffolds to resist mechanical force; this parameter could be quantitatively identified by plotting the stress-strain curves of the scaffolds under mechanical pressure and calculating the slope of the curve, known as Young's modulus E (Jhala and Vasita, 2015). In this study, the mechanical properties, mainly Young's modulus, of the Ca-alginate scaffolds during the culture of U-251 cells for 7, 14, and 21 days were assessed with compression testing. The Young's modulus is usually used to estimate the mechanical (stiffness) properties of biomaterials (Jhala and Vasita, 2015). The Young's modulus of the scaffolds was found to decrease with time, which was closer to that of brain cancer tissue (~ 7 kPa) (Yu et al., 2011) than cell cultures on polystyrene plates (2-4 GPa) (Florczyk et al., 2016). The Young's modulus is an important parameter of biomaterials, which can affect cell proliferation and the direction of cell differentiation (Banerjee et al., 2009).

To closely mimic the *in vivo* tumor microenvironment in the 3D scaffold cell culture models, a synthetic ECM is crucial for supporting stem cells during the differentiation process and for integration into the surrounding tissues. Alginate is a family of natural polysaccharides, composed of β -D-mannuronate and α -L-glucuronate, which has been widely used as a material for extracellular matrix construction in tissue engineering (Shull, 2012). To investigate the effect of the Ca-alginate scaffolds on glioblastoma cell viability, U-251 cells were cultured in both the 2D and 3D Ca-alginate scaffold systems, and cell viability was then assessed using a resazurin assay. During the culture period, glioblastoma cells tended to grow as cellular aggregates or spheroids. Cell viability of the U-251 cells was detected after culture for 3 weeks, and a high survival rate (78.25%) was observed. The death

of 21.75% of the total cells inside the scaffold may have been a result of the development of necrotic regions inside the spheroid due to insufficient oxygen diffusion rather than a negative effect of the alginate. This results showed that Ca-alginate scaffolds could also mimic the microenvironment suitable for the growth and spheroid formation of glioblastoma cells.

Before clinical trials, *in vitro* trials are widely used to elucidate the behavior of cancer cells and the cellular mechanism that controls their behavior, providing clues for potential clinical treatments. Many of these trials are conducted with cells cultured on 2D surfaces (polystyrene tissue culture plates or wells). With 2D cell cultures, inconsistencies in the cellular response can be found when applied to an *in vivo* system because of the difference between the 2D and 3D environments (Hutmacher et al., 2010). The integration of 3D structures into *in vitro* trials as an artificial 3D environment allows for a more reliable and applicable model of the *in vivo* system and increases the chances of success in the later, costlier stages of clinical trials. Here, an equal number of U-251 human glioblastoma cells were seeded directly into 24-well plates (2D condition) or Ca-alginate scaffolds (3D condition) to verify the ability of Ca-alginate scaffolds to support cell proliferation. The relative proliferation of the cells in each culture environment was then comparatively evaluated. Results showed that the cells in the 2D condition rapidly grew, faster than those in the 3D condition at the beginning of the culture period, followed by a drastic decrease in the cell population at the 15-day time point. The rapid growth of cells in the 2D condition caused cells to become overgrown to reach the maximum capacity of the 2D surface and require subculturing. On the other hand, cells in the 3D condition grew slower over the first few days, but then the growth rate increased gradually. Therefore, this 3D Ca-alginate culture system could last longer, up to 21 days *in vitro*.

Previous studies showed that the 3D microenvironment provided by porous scaffolds promotes a greater malignancy of tumor cells (Kievit et al., 2010). The morphology of U-

251 cells in two different culture environments was investigated by SEM. Glioblastoma cells were found to spherically aggregate within the scaffold pores, but not on the 2D flat surface, indicating that the 3D environment promoted tumor spheroid formation. Spheroids more closely imitated the model of the *in vivo* tumor structure (Benton et al., 2011; Hutmacher et al., 2010). This finding suggests that the 3D Ca-alginate scaffolds more effectively mimic the *in vivo* microenvironment than the 2D cultures. To distinguish the cellular properties of glioblastoma cells in both culture conditions, cell proliferation, stemness, differentiation potential, and angiogenesis of the U-251 cells in the 3D Ca-alginate scaffolds were sequentially verified and compared with the 2D cell culture. The difference in the relative proliferation from the resazurin assay was influenced by the confinement of the 2D culture environment. Moreover, the expression of glioblastoma stem cells markers (CD133 and Nestin) and differentiation markers (GFAP and β III-tubulin) was significantly increased in the Ca-alginate scaffold culture. The difference in the expression level of these biomarkers demonstrated the inconsistency of cellular phenomena between the 2D and 3D culture systems, which may produce misleading data in cancer cell studies. Angiogenesis is known to be one of the essential processes of tumor growth and metastasis *in vivo* (Lopes-Bastos et al., 2016). Glioblastoma cells have been previously reported to transdifferentiate into tumor endothelial cells for vasculogenic mimicry in the *in vivo* condition, highlighting characteristics of cancer stem cell biology (Dai et al., 2016; Scully et al., 2012). We observed a higher expression of VEGF, the potent angiogenic factor, in the culture of our 3D Ca-alginate scaffolds, suggesting that 3D Ca-alginate scaffolds could mimic the *in vivo* tumor microenvironment to a degree that is suitable for vessel formation. However, there are a few *in vitro* studies that model brain tumor angiogenesis or vascularization, either using 3D aggregates of brain derived vascular cells (but without co-culture features) (Juillerat-Jeanneret et al., 2003), or with co-cultures in a 2D configuration (McLaughlin et al., 2006). Chaddad et al. (2017) demonstrated that 3D culture of osteosarcoma cells (MG-63) deposited

on 2D endothelial cells (HUVEC) grown in monolayer were able to form a well-organized network, and that tubule-like structures corresponding to new vessels infiltrate tumor spheroids. Thus, in this study, we combined cultures of U-251 cultivated for 14 days in 3D Ca-alginate scaffold and U-251 spheroid deposited on 2D hCMEC/D3 endothelial cells as a model to confirm vascular-like structures. After 7 and 14 days of combined 3D U-251 and 2D hCMEC/D3 cell culture, both cells formed vascular-like structures as observed by SEM. We have also observed that tubule-like structures of endothelial cells seemed to grow over the time and varied from 3 to 10 μm . Moreover, the combination of 3D U-251 glioblastoma and 2D hCMEC/D3 promoted the expression of VEGF angiogenic factor. Furthermore, after 14 days of combined combined 3D U-251 and 2D hCMEC/D3 endothelial cells organized in tubules-like, secreted collagen IV, a specific marker of the basal membrane. A possible explanation for this might be that U-251 spheroids can secrete both exosomes and extracellular vesicles in their surrounding microenvironment (Chistiakov and Chekhonin, 2014; Godlewski et al., 2014; Van et al., 2011) supporting tumor progression by several mechanisms, including angiogenesis stimulation (Skog et al., 2008). Exosomes contain a plethora of angiogenic molecules such as angiogenin, IL-6 and IL-8, and vascular endothelial growth factor (VEGF) (Skog et al., 2008). Both exosomes and extracellular vesicles from U-251 cells convey messages to other tumor cells, create a microenvironment that supports cancer growth and progression and are implicated in drug resistance. They are also involved in angiogenesis stimulation, inducing endothelial cells proliferation, and other pro-angiogenic activities (Giusti et al., 2016). By using this combined 3D U-251 and 2D hCMEC/D3 model, we have confirmed that 3D Ca-alginate scaffolds were able to form vascular-like structures and might be used as an *in vitro* 3D vascularized tumor model for assessment of therapeutic.

For drug discovery and development, or the evaluation of drug efficacy, sequential processes are conducted, from 2D cell culture-based tests, followed by animal model tests,

to clinical trials (Dai et al., 2016). However, 2D cell culture-based tests often fail to provide accurate and reliable data that can be applied to further *in vivo* tests because of large deviations in drug sensitivities (Birgersdotter et al., 2005; Shoemaker, 2006), leading to failures in the predictions of chemotherapy tolerance. Even with the same anticancer drugs, tumor cells in 2D and 3D models tend to exhibit different responses (Godugu et al., 2013). Data from animal model tests may also not accurately reflect observations in clinical trials because of species differences. As a result, only about 10% of drugs are effectively applicable in both animals and humans, and the rest end up as failures during clinical trials (Levinger et al., 2014). The 3D Ca-alginate scaffolds may be practical in anti-cancer drug screening.

In this study, a 3D Ca-alginate scaffold cell culture system was fabricated, mainly for use in drug studies, I try to test the sensitivity of anticancer agents on glioblastoma cell line in the 3D Ca-alginate scaffolds compared to the cells in 2D culture. Temozolomide was primarily selected for the tests; it is the major chemotherapy utilized for glioblastoma, an alkylating agent prodrug which delivering a methyl group to purine bases of DNA (O⁶-guanine; N⁷-guanine and N³-adenine) (Lee, 2016). I found that glioblastoma cells in the 3D system were more resistant to temozolomide at high concentrations (between 15-500 µg/ml) compared with the cells in the 2D culture. Another chemotherapeutic drug is doxorubicin, it is a potent chemotherapeutic drug that shows strong activity against many different types of cancers, via intercalation within DNA molecules (MacDiarmid et al., 2016; Rivankar, 2014). As expected, we found that glioblastoma cells in the 3D system were more resistant to doxorubicin at high concentrations (between 2.5-40 µg/ml) compared with the cells in the 2D culture. The 3D Ca-alginate scaffolds were then applied to an evaluation of a natural bioactive compound. Cordycepin, a major bioactive component found in the entomopathogenic fungus *Cordyceps* spp., was selected as a potential candidate. This derivative of adenosine was previously reported to exhibit various biological and pharmacological functions, such as anti-inflammatory (Choi et al., 2014), neuroprotection

(Olatunji et al., 2016), analgesic (Ashraf et al., 2017), antioxidant (Wang et al., 2015) and importantly anticancer properties, including antiglioblastoma (Chaicharoenaudomrung et al., 2018). However, all of these studies were based on traditional *in vitro* 2D culture models or *in vivo* animal tests. To the best of my knowledge, there is no previously reported study of cordycepin in a 3D culture model, and this particular study is the first to compare and contrast the cellular toxicity of cordycepin to glioblastoma in both 2D and 3D conditions. In the same manner as temozolomide and doxorubicin, a higher cordycepin resistance was also found in glioblastoma cells in the 3D system, at concentrations between 12.5-400 $\mu\text{g/ml}$. The low sensitivity of 3D-cultured cells to anticancer agents is consistent with reports in the literature (Dai et al., 2016; Godugu et al., 2013; Gong et al., 2011), and maybe possibly due to differences in the stemness property, which were previously verified. The overexpression of CD133 is reported to cause significant resistance to doxorubicin in glioma cells via the suppression of apoptosis (Angelastro and Lame, 2010). The upregulation of Nestin in 3D Ca-alginate scaffolds may also involve drug resistance. Nestin was found to be upregulated in a chemoresistant hepatocellular carcinoma cell line and induced epithelial-mesenchymal transition (Zhang et al., 2016).

Taken together, I expected to be the 3D Ca-alginate scaffold can be cost-effective, low-cost, easy-to-use method, availability, suitability, reproducibility and can also practical in anti-cancer drug screening, in order to reduce animal testing and clinical trials and novel molecular target identification for the treatment of human glioblastoma.

4.6 Conclusion

In conclusion, this study presented the development of an *in vitro* 3D glioblastoma cell culture system using Ca-alginate scaffolds. This system mimicked the nerve-tissue cancer tumor microenvironment, with high cell viability and proliferation. In the 3D Ca-alginate

scaffolds, human glioblastoma U-251 cells can proliferate, retain characteristics of cancer stem cells, as well as exhibit differentiation potential. Moreover, combination of 3D U-251 glioblastoma and 2D hCMEC/D3 endothelial cells were able to form vascular-like structures corresponding to new vessels infiltrate tumor spheroids. These confirmed that 3D Ca-alginate scaffolds might be used as an *in vitro* 3D vascularized tumor model. In addition, the 3D glioblastoma cell culture system showed more resistance to the anticancer agents, temozolomide, doxorubicin and cordycepin, compared with the 2D culture system. I findings suggest that 3D Ca-alginate scaffolds are promising *in vitro* research platforms for the screening of antiglioblastoma therapeutic agents.

4.7 References

- Angelastro, J. M., and Lame, M. W. (2010). Overexpression of CD133 promotes drug resistance in C6 glioma cells. **Molecular Cancer Research**. 8(8): 1105-1115.
- Ashraf, S., Burston, J., Chapman, V., and de Moor, C. (2017). OP0183 Cordycepin, a novel compound, reduces knee joint pathology and pain in the monosodium iodoacetate (MIA) rat model of osteoarthritis. **Annals of the Rheumatic Diseases**. 76: 127.
- Awad, H. A., Wickham, M. Q., Leddy, H. A., Gimble, J. M., and Guilak, F. (2004). Chondrogenic differentiation of adipose-derived adult stem cells in agarose, alginate, and gelatin scaffolds. **Biomaterials**. 25(16): 3211-3222.
- Banerjee, A., Arha, M., Choudhary, S., et al. (2009). The influence of hydrogel modulus on the proliferation and differentiation of encapsulated neural stem cells. **Biomaterials**. 30(27): 4695-4699.
- Behin, A., Hoang-Xuan, K., Carpentier, A. F., and Delattre, J.-Y. (2003). Primary brain tumours in adults. **The Lancet**. 361(9354): 323-331.

- Benton, G., Kleinman, H. K., George, J., and Arnaoutova, I. (2011). Multiple uses of basement membrane-like matrix (BME/Matrigel) *in vitro* and *in vivo* with cancer cells. **International journal of cancer**. 128(8): 1751-1757.
- Birgersdotter, A., Sandberg, R., and Ernberg, I. (2005). Gene expression perturbation in vitro-a growing case for three-dimensional (3D) culture systems. **Paper presented at the Seminars in cancer biology**. 405-412.
- Chaddad, H., Kuchler-Bopp, S., Fuhrmann, G., et al. (2017). Combining 2D angiogenesis and 3D osteosarcoma microtissues to improve vascularization. **Experimental cell research**. 360(2): 138-145.
- Chaicharoenaudomrung, N., Jaroonwichawan, T., and Noisa, P. (2018). Cordycepin induces apoptotic cell death of human brain cancer through the modulation of autophagy. **Toxicology in Vitro**. 46: 113-121.
- Chen, C.-Y., Ke, C.-J., Yen, K.-C., et al. (2015). 3D porous calcium-alginate scaffolds cell culture system improved human osteoblast cell clusters for cell therapy. **Theranostics**. 5(6): 643.
- Chen, L., Xiao, Z., Meng, Y., et al. (2012). The enhancement of cancer stem cell properties of MCF-7 cells in 3D collagen scaffolds for modeling of cancer and anti-cancer drugs. **Biomaterials**. 33(5): 1437-1444.
- Chistiakov, D. A., and Chekhonin, V. P. (2014). Extracellular vesicles shed by glioma cells: pathogenic role and clinical value. **Tumor Biology**. 35(9): 8425-8438.
- Choi, Y. H., Kim, G.-Y., and Lee, H. H. (2014). Anti-inflammatory effects of cordycepin in lipopolysaccharide-stimulated RAW 264.7 macrophages through Toll-like receptor 4-mediated suppression of mitogen-activated protein kinases and NF- κ B signaling pathways. **Drug design, development and therapy**. 8: 1941.
- Dai, X., Ma, C., Lan, Q., and Xu, T. (2016). 3D bioprinted glioma stem cells for brain tumor model and applications of drug susceptibility. **Biofabrication**. 8(4): 045005.

- Dhiman, H. K., Ray, A. R., and Panda, A. K. (2005). Three-dimensional chitosan scaffold-based MCF-7 cell culture for the determination of the cytotoxicity of tamoxifen. **Biomaterials**. 26(9): 979-986.
- Florczyk, S. J., Kievit, F. M., Wang, K., et al. (2016). 3D porous chitosan-alginate scaffolds promote proliferation and enrichment of cancer stem-like cells. **Journal of Materials Chemistry B**. 4(38): 6326-6334.
- Gerecht, S., Cohen, S., Ziskind, A., and Itskovitz-Eldor, J. (2004). Three-dimensional porous alginate scaffolds provide a conducive environment for generation of well-vascularized embryoid bodies from human embryonic stem cells. **Biotechnology and bioengineering**. 88(3): 313-320.
- Giusti, I., Delle Monache, S., Di Francesco, M., et al. (2016). From glioblastoma to endothelial cells through extracellular vesicles: messages for angiogenesis. **Tumor Biology**. 37(9): 12743-12753.
- Godlewski, J., Krichevsky, A. M., Johnson, M. D., Chiocca, E. A., and Bronisz, A. (2014). Belonging to a network—microRNAs, extracellular vesicles, and the glioblastoma microenvironment. **Neuro-oncology**. 17(5): 652-662.
- Godugu, C., Patel, A. R., Desai, U., et al. (2013). AlgiMatrix™ based 3D cell culture system as an in-vitro tumor model for anticancer studies. **PloS one**. 8(1): e53708.
- Gong, X., Schwartz, P. H., Linskey, M. E., and Bota, D. A. (2011). Neural stem/progenitors and glioma stem-like cells have differential sensitivity to chemotherapy. **Neurology**. 76(13): 1126-1134.
- Huang, Y., Tong, L., Yi, L., et al. (2018). Three-dimensional hydrogel is suitable for targeted investigation of amoeboid migration of glioma cells. **Molecular medicine reports**. 17(1): 250-256.

- Hunt, N., Smith, A. M., Gbureck, U., Shelton, R., and Grover, L. (2010). Encapsulation of fibroblasts causes accelerated alginate hydrogel degradation. **Acta Biomaterialia**. 6(9): 3649-3656.
- Hutmacher, D. W., Loessner, D., Rizzi, S., et al. (2010). Can tissue engineering concepts advance tumor biology research? **Trends in biotechnology**. 28(3): 125-133.
- Hwang, Y.-S., Cho, J., Tay, F., et al. (2009). The use of murine embryonic stem cells, alginate encapsulation, and rotary microgravity bioreactor in bone tissue engineering. **Biomaterials**. 30(4): 499-507.
- Jhala, D., and Vasita, R. (2015). A review on extracellular matrix mimicking strategies for an artificial stem cell niche. *Polymer Reviews*. 55(4): 561-595.
- Johnson, D. R., and O'Neill, B. P. (2012). Glioblastoma survival in the United States before and during the temozolomide era. **Journal of neuro-oncology**. 107(2): 359-364.
- Juillerat-Jeanneret, L., Monnet-Tschudi, F., Zurich, M.-G., et al. (2003). Regulation of peptidase activity in a three-dimensional aggregate model of brain tumor vasculature. **Cell and tissue research**. 311(1): 53-59.
- Kapałczyńska, M., Kolenda, T., Przybyła, W., et al. (2016). 2D and 3D cell cultures—a comparison of different types of cancer cell cultures. **Archives of medical science**. 14(4): 910.
- Khasraw, M., Bell, D., and Wheeler, H. (2009). Long-term use of temozolomide: could you use temozolomide safely for life in gliomas? **Journal of Clinical Neuroscience**. 16(6): 854-855.
- Kievit, F. M., Florczyk, S. J., Leung, M. C., et al. (2010). Chitosan–alginate 3D scaffolds as a mimic of the glioma tumor microenvironment. **Biomaterials**. 31(22): 5903-5910.
- Kirdponpattara, S., Khamkeaw, A., Sanchavanakit, N., Pavasant, P., and Phisalaphong, M. (2015). Structural modification and characterization of bacterial cellulose-alginate composite scaffolds for tissue engineering. **Carbohydrate polymers**. 132: 146-155.

- Koh, I., Cha, J., Park, J., et al. (2018). The mode and dynamics of glioblastoma cell invasion into a decellularized tissue-derived extracellular matrix-based three-dimensional tumor model. **Scientific reports**. 8(1): 4608.
- Kuo, C. K., and Ma, P. X. (2001). Ionically crosslinked alginate hydrogels as scaffolds for tissue engineering: part 1. Structure, gelation rate and mechanical properties. **Biomaterials**. 22(6): 511-521.
- Lee, S. Y. (2016). Temozolomide resistance in glioblastoma multiforme. **Genes & diseases**. 3(3): 198-210.
- Levinger, I., Ventura, Y., and Vago, R. (2014). Life is Three Dimensional-As *In Vitro* Cancer Cultures Should Be. **Advances in cancer research**. 121: 383-414.
- Lopes-Bastos, B. M., Jiang, W. G., and Cai, J. (2016). Tumour-Endothelial Cell Communications: Important and Indispensable Mediators of Tumour Angiogenesis. **Anticancer research**. 36(3): 1119-1126.
- Lv, D., Yu, S.-c., Ping, Y.-f., et al. (2016). A three-dimensional collagen scaffold cell culture system for screening anti-glioma therapeutics. **Oncotarget**. 7(35): 56904.
- MacDiarmid, J. A., Langova, V., Bailey, D., et al. (2016). Targeted doxorubicin delivery to brain tumors via minicells: proof of principle using dogs with spontaneously occurring tumors as a model. **PloS one**. 11(4): e0151832.
- McLaughlin, N., Annabi, B., Kim, K. S., et al. (2006). The response to brain tumor-derived growth factors is altered in radioresistant human brain endothelial cells. **Cancer biology & therapy**. 5(11): 1539-1545.
- Olatunji, O. J., Feng, Y., Olatunji, O. O., et al. (2016). Cordycepin protects PC12 cells against 6-hydroxydopamine induced neurotoxicity via its antioxidant properties. **Biomedicine & Pharmacotherapy**. 81: 7-14.

- Pampaloni, F., Reynaud, E. G., and Stelzer, E. H. (2007). The third dimension bridges the gap between cell culture and live tissue. **Nature reviews Molecular cell biology**. 8(10): 839.
- Perrot, S., Dutertre-Catella, H., Martin, C., Warnet, J. M., and Rat, P. (2003). A new nondestructive cytometric assay based on resazurin metabolism and an organ culture model for the assessment of corneal viability. **Cytometry Part A: The Journal of the International Society for Analytical Cytology**. 55(1): 7-14.
- Rinaudo, M. (2008). Main properties and current applications of some polysaccharides as biomaterials. **Polymer International**. 57(3): 397-430.
- Rivankar, S. (2014). An overview of doxorubicin formulations in cancer therapy. **Journal of cancer research and therapeutics**. 10(4): 853.
- Sachlos, E., and Czernuszka, J. (2003). Making tissue engineering scaffolds work. Review: the application of solid freeform fabrication technology to the production of tissue engineering scaffolds. **European Cells & Materials**. 5(29): 39-40.
- Sams, A., Zhensheng, L., Richard, F., Chao, Y. L., and Mark, P. (2009). The Application of Alginate Scaffolds for Three-Dimensional Cell Culture. **Invitrogen Corporation**. 1600 Faraday Avenue, Carlsbad, California 92008, USA.
- Scully, S., Francescone, R., Faibish, M., et al. (2012). Transdifferentiation of glioblastoma stem-like cells into mural cells drives vasculogenic mimicry in glioblastomas. **Journal of Neuroscience**. 32(37): 12950-12960.
- Shapiro, L., and Cohen, S. (1997). Novel alginate sponges for cell culture and transplantation. **Biomaterials**. 18(8): 583-590.
- Shoemaker, R. H. (2006). The NCI60 human tumour cell line anticancer drug screen. **Nature reviews cancer**. 6(10): 813-823.
- Shull, K. R. (2012). Materials science: A hard concept in soft matter. **Nature**. 489(7414): 36-37.

- Skog, J., Würdinger, T., Van Rijn, S., et al. (2008). Glioblastoma microvesicles transport RNA and proteins that promote tumour growth and provide diagnostic biomarkers. **Nature cell biology**. 10(12): 1470.
- Ulrich, C. M., Ratcliffe, S. J., R. Wallen, G., et al. (2016). Cancer clinical trial participants' assessment of risk and benefit. **AJOB empirical bioethics**. 7(1): 8-16.
- Van, K. E., Balaj, L., Skog, J., and Breakefield, X. O. (2011). Brain tumor microvesicles: insights into intercellular communication in the nervous system. **Cellular and molecular neurobiology**. 31(6): 949-959.
- Wang, Shelton, R., Cooper, P., et al. (2003). Evaluation of sodium alginate for bone marrow cell tissue engineering. **Biomaterials**. 24(20): 3475-3481.
- Wang, Yin, P., Lu, Y., et al. (2015). Cordycepin prevents oxidative stress-induced inhibition of osteogenesis. **Oncotarget**. 6(34): 35496.
- Yu, H., Mouw, J. K., and Weaver, V. M. (2011). Forcing form and function: biomechanical regulation of tumor evolution. **Trends in cell biology**. 21(1): 47-56.
- Zhang, Y., Zeng, S., Ma, J., et al. (2016). Nestin overexpression in hepatocellular carcinoma associates with epithelial-mesenchymal transition and chemoresistance. **Journal of Experimental & Clinical Cancer Research**. 35(1): 111.
- Zhou, X., Zhu, W., Nowicki, M., et al. (2016). 3D bioprinting a cell-laden bone matrix for breast cancer metastasis study. **ACS applied materials & interfaces**. 8(44).

CHAPTER V

THE TRANSCRIPTOMIC PROFILES FOR IDENTIFICATION OF DRUG RESISTANCE-RELATED MECHANISMS OF HUMAN GLIOBLASTOMA CELL ON THE 3D CULTURE CONDITION

5.1 Abstract

Among various types of brain tumors, glioblastoma is the most malignant and highly aggressive brain tumor that possesses a high resistance against anti-cancer drugs. To understand the underlined mechanisms of tumor drug resistance, the new and effective research approach is required. The 3D *in vitro* cell culture models can be a potent approach to study cancer features and biology, as well as screen for anti-cancer agents due to the close mimicry of 3D tumor environments. With my developed 3D alginate scaffolds, I used Illumina RNA-sequencing to transcriptomically compare and analyze the gene expression profiles of glioblastoma cells cultured in traditional 2D monolayer and 3D Ca-alginate scaffolds for 14 days. The results showed that 7,411 and 3,915 genes of 3D glioblastoma were upregulated and downregulated, respectively, compared with the 2D monolayer glioblastoma. Furthermore, the KEGG pathway analysis revealed the enrichment of cell cycle and DNA replication-related genes in downregulated gene group and genes involved with MAPK signaling, autophagy, drug metabolism-cytochrome P450, and ABC transporter pathway in upregulated gene group. Such alteration of gene expression, it gave us a hint to better understand the mechanisms-related to anti-cancer drug resistance of glioblastoma. Thus, the 3D glioblastoma model could potentially serve as a powerful

platform for exploring glioblastoma biology, the anti-glioblastoma drug screening, and the identification of novel molecular targets in a clinical treatment of human glioblastoma.

Keyword: Transcriptomics, 3D calcium-alginate scaffolds, Anticancer drug screening, Drug resistance, Glioblastoma

5.2 Introduction

Glioblastoma is one of the most common yet hostile malignant primary human brain tumor, originating from astrocytes or their precursors (Behin et al., 2003). Numerous efforts have been invested to develop the clinical treatment of glioblastoma including radiation therapy, neurosurgery, and chemotherapy. However, even with the good, consistent treatment, patients tended to survive for only 14 months with the recurrence of glioblastoma after 5-7 months post-treatment (Johnson and O' Neill, 2012). A unique characteristic of glioblastoma is their infiltrative ability to diffusively invade normal brain tissue (Beier et al., 2012; Clark et al., 2016) which possibly is the cause of its high recurrence and anti-cancer drug resistance (Kang and Kang, 2007). To primarily understand this glioblastoma biology and reveal the underlying mechanism of anti-cancer drug resistance, an effective *in vitro* tumor model is needed. However, the *in vitro* studies based on the traditional 2D culture cannot correctly imitate the architecture and microenvironments *in vivo* that cancer cells reside. Therefore, cells under 2D culture are different from cell growing *in vivo* in terms of proliferation, morphology, cell-cell and cell-matrix inter-connections, signal transduction, and transcriptomic profile (Abbott, 2003; Stavrinou et al., 2015). In order to develop these imitations of cell microenvironments *in vivo*, Three-dimensional (3D) culture has been alternatively used as *in vitro* tumor models, which can simulate *in vivo* cell behaviors, and provide more comparable and reliable results (Friedrich et al., 2009). Several 3D *in vitro* glioblastoma models have been established using extracellular matrix-based scaffolds elucidated the dramatically difference in terms of cell proliferation, morphology, and drug

resistance between 2D and 3D glioblastoma (Chaicharoenaudomrung et al., 2019; Kievit et al., 2010; Lv et al., 2016). My previous study reported the upregulation of stemness genes, differentiation-related genes, and VEGF angiogenesis factor in 3D glioblastoma which could play important roles in the enhancement of drug resistance (Chaicharoenaudomrung et al., 2019). Despite a numbers of 3D glioblastoma studies, the transcriptomic profile and molecular pathway need to be further explored to understand the global picture of the underlying drug resistance mechanism. In this study, the transcriptomic profiles of the glioblastoma cells under 2D and 3D conditions were elucidated and analyzed using next generation sequencing technology (Illumina HiSeq systems) to emphatically reveal anti-cancer drugs resistance related-pathway in 3D *in vitro* glioblastoma.

5.3 Materials and methods

5.3.1 Chemicals and reagents

Sodium alginate (A0682), arginine- glycine- aspartate (RGD; A8052), and calcium chloride (449709) were purchased from Sigma-Aldrich Chemical Co. (St. Louis, MO). Calcein-AM, propidium iodide (PI) and 4, 6-Diamidino-2-phenylindole (DAPI) were purchased from Life Technologies Inc. (Carlsbad, CA). The human glioblastoma (U-251) cell line was obtained from the European Collection of Authenticated Cell Cultures (ECACC; Salisbury, UK). Dulbecco's modified Eagle's medium (DMEM) and fetal bovine serum (FBS) were obtained from HyClone (HyClone, Logan, UT), while nonessential amino acids (NEAA), 0.5% trypsin-ethylenediaminetetraacetic acid (EDTA) and L-glutamax were purchased from Gibco (GIBCO, Carlsbad, CA).

5.3.2 Fabrication of porous scaffolds

3D Ca-alginate scaffolds for 3D cell culture were fabricated using freeze-drying technique as described in my previous study (Chaicharoenaudomrung et al., 2019). Briefly, 2% sodium alginate was dissolved in sterile deionized (DI) water. The sodium alginate solution was injected into 48-well culture plate with the volume of 400 μL /well. Sodium alginate solution was then frozen at -20°C for 24 h prior to the lyophilization to generate porous scaffolds. The scaffolds were cross-linked with 2% calcium chloride solution, washed several times with sterile DI water. The scaffolds were sterilized with alcohol (75%) for 24 h, and stored at room temperature until use. Before use, the scaffolds were washed several times with sterile DI water, immersed in 100 mg/L arginine-glycine-aspartate (RGD) peptide solution, and incubated overnight at 37°C in a humidified incubator supplied with 5% CO_2 and 95% air. Morphology of Ca-alginate scaffold was evaluated and shown in Figure 5.1. The porous structures Ca- alginate scaffolds were pictured using scanning electron microscope (SEM) demonstrating 100-400 μm pore size with the average 89% porosity.



Figure 5.1 (a) Morphology of Ca-alginate scaffolds. (b-c) A disk-shaped of Ca-alginate scaffolds, which 5 mm in height and 10 mm in diameter. (d) SEM images of the Ca-alginate scaffold. Scale bar: 500 μm .

5.3.3 Cell cultures

U-251 glioblastoma cell line was used as a model in this study. For 2D cell culture, 50,000 cells of U-251 in 200 mL of complete DMEM medium (supplement with 10% (v/v) FBS, 1% (v/v) penicillin-streptomycin, 1% (v/v) L-glutamine, and 1% (v/v) NEAA) was added into each well of 24-well cell culture plate. Cells were then incubated at 37°C and 5% CO₂. The fresh complete medium was replaced every 2 days. Morphology of cells were observed under an inverted microscope (Nikon Eclipse TS2; Nikon Corporation).

For 3D cell culture, Ca-alginate scaffolds were placed in 24-well cell culture plate with complete DMEM medium for overnight prior to cell seeding. 50,000 cells in 50 µL of complete DMEM medium were seeded directly onto each scaffold prior to 1 h incubation at 37°C and 5% CO₂ in a humidified incubator. Then, 1 mL of complete medium was additionally added to each well before further cultivation in the same condition. The complete DMEM medium was renewed once in every 2 days. Live/dead cell calcein AM and propidium iodide (PI) fluorescent double staining was performed to assess cell viability inside the Ca-alginate scaffolds.

5.3.4 RNA extraction

Total RNA from U-251 cells after 14 days in both 2D and 3D cell cultures was extracted with NucleoSpin RNA Kit (Macherey-Nagel, Dueren, Germany, according to the manufacturer's instructions. Each condition contained three replications. Additionally, for cells from 3D condition, 50 mM of EDTA solution was added onto Ca-alginate scaffolds for cell isolation. Then, cells were washed with PBS and collected by centrifugation at 600 rpm for 3 min. Total RNA of each sample was quantified and qualified by NanoDrop® (Thermo Fisher Scientific Inc.) at OD₂₆₀ nm/OD₂₈₀ nm and Agilent 2100 Bioanalyzer (Agilent Technologies, Palo Alto, CA, USA), respectively. The integrity of these RNA samples were checked by 1% agarose gel electrophoresis. One microgram of total RNA with RIN value above 7 was used for the following library preparation.

5.3.5 RNA sequencing library construction

RNA-seq library preparation, sequencing and analysis were carried out by Vishuo Biomedical (Thailand) Ltd. Vishuo Biomedical (Thailand) Ltd. Next generation sequencing library preparations were constructed according to the manufacturer's protocol (NEB-Next®Ultra™ RNA Library Prep Kit for Illumina®). The poly (A) mRNA isolation was performed using NEBNext Poly(A) mRNA Magnetic Isolation Module (NEB) or Ribo-Zero™ rRNA removal Kit (illumina). The mRNA fragmentation and priming was performed using NEBNext First Strand Synthesis Reaction Buffer and NEBNext Random Primers. First strand cDNA was synthesized using ProtoScript II Reverse Transcriptase and the second-strand cDNA was synthesized using Second Strand Synthesis Enzyme Mix. The purified double-stranded cDNA by AxyPrep Mag PCR Clean-up (Axygen) was then treated with End Prep Enzyme Mix to repair both ends and add a dA-tailing in one reaction, followed by a T-A ligation to add adaptors to both ends. Size selection of Adaptor-ligated DNA was then performed using AxyPrep Mag PCR Clean-up (Axygen), and fragments of ~360 bp (with the approximate insert size of 300 bp) were recovered. Each sample was then amplified by PCR for 11 cycles using P5 and P7 primers, with both primers carrying sequences which can anneal with flow cell to perform bridge PCR and P7 primer carrying a six-base index allowing for multiplexing. The PCR products were cleaned up using AxyPrep Mag PCR Clean-up (Axygen), validated using an Agilent 2100 Bioanalyzer (Agilent Technologies, Palo Alto, CA, USA), and quantified by Qubit 2.0 Fluorometer (Invitrogen, Carlsbad, CA, USA). Then, libraries with different indices were multiplexed and loaded on an Illumina HiSeq instrument according to manufacturer's instructions (Illumina, San Diego, CA, USA). Sequencing was carried out using a 2x150bp paired-end (PE) configuration; image analysis and base calling were conducted by the HiSeq Control Software (HCS)+OLB+GAPipeline-1.6 (Illumina) on the HiSeq instrument. The sequences were processed and analyzed by Genewiz specializes in R&D genomics services, Singapore.

5.3.6 Quantification of gene expression level and differential expression analysis

In order to remove technical sequences, including adapters, polymerase chain reaction (PCR) primers, or fragments thereof, and quality of bases lower than 20, pass filter data of fastq format were processed by Trimmomatic (v0.30) to be high quality clean data. Reference genome sequences and gene model annotation files of relative species were downloaded from genome website (UCSC, NCBI, ENSEMBL). Then, Hisat2 (v2.0.1) was used to index reference genome sequence. The clean data were aligned to reference genome via software Hisat2 (v2.0.1). Then, HTSeq (v0.6.1) estimated gene and isoform expression levels from the pair-end clean data (Anders and Huber, 2010). Differential expression analysis used the DESeq Bioconductor package, a model based on the negative binomial distribution. After adjusted by Benjamini and Hochberg's approach for controlling the false discovery rate, *P-value* of genes were setted <0.05 to detect differential expressed ones (Anders and Huber, 2010, 2012).

5.3.7 Bioinformatics evaluation

The genes differentially expressed of U-251 cells between 2D and 3D cultures condition were analyzed by evaluating the Gene Ontologies (GO) and using the software KEGG (Kyoto Encyclopedia of Genes and Genomes), for pathway evaluation. GO-TermFinder was used to identify Gene Ontology (GO) terms that annotated a list of enriched genes with a significant *p-value* less than 0.05. KEGG is a collection of databases dealing with genomes, biological pathways, diseases, drugs, and chemical substances (<http://en.wikipedia.org/wiki/KEGG>). I used scripts in house to enrich significant differential expression gene in KEGG pathways.

5.3.8 Quantitative real time PCR (qRT-PCR) validation

To further validate the accuracy of DESeq2 results, quantitative real-time PCR analysis were performed. RNA samples from 2D and 3D cell cultures at day14 were collected, followed by reverse transcription using ReverTra Ace® qPCR RT Master Mix with gDNA Remover (Toyobo, Osaka, Japan). The cDNA transcription was used as template for quantitative real time PCR mixed with qPCR BioSyGreen Mix Low-Rox (PCR BIOSYSTEMS, London, UK) by thermocycling using QuantStudio 5 Real-Time PCR System (Thermo Fisher Scientific), using the following program: 95°C for 3 min followed by 40 cycles of 95°C for 30 s and 60°C for 30 s and 72°C for 45 s. A melting curve analysis of the PCR products was performed by heating at 60°C for 60 s, 95°C for 15 s. Glyceraldehyde-3-phosphate dehydrogenase (*GAPDH*) was selected as the reference gene. The expression level of *ABCA1*, *ABCA2*, *ABCA3*, *ABCA5*, *ABCA6*, *ABCA8*, *ABCA9*, *ABCA10*, and *ABCA12* were examined. The primers designed for the genes of interest are shown in Table 5.1. The relative expression of such genes for 3D cell culture comparing with 2D cell culture was determined by the $2^{-\Delta\Delta C_t}$ method, and each target gene was normalized against *GAPDH* reference gene.

5.3.9 Statistical analysis

The results were expressed as mean value \pm standard deviations. Comparison between different groups was performed using a Student's t test (SPSS version 16.0, SPSS Inc., Hong Kong, China). Differences were considered significant for **p-values* ≤ 0.05 , ***p* ≤ 0.01 and ****p* ≤ 0.001 .

Table 5.1 The primer sequences used for real-time qRT-PCR.

	Forward	Reverse
<i>GAPDH</i>	5'- CTCTGCTCCTCCTGTTTCGAC-3'	5'- TTAAAAGCAGCCCTGGTGAC-3'
<i>ABCA1</i>	5'- GCACTGAGGAAGATGCTGAAA-3'	5'-AGTTCCTGGAAGGTCTTGTTCAC-3'
<i>ABCA2</i>	5'- CATCCCCCTGGTGCTGTTCCTT-3'	5'- GCTTGGGCCGTGCTATTGG-3'
<i>ABCA3</i>	5'-GCCCTCTTTACTACTCAGTTTTCA-3'	5'-GACGAGCAGTTGTCGTACCTAAT-3'
<i>ABCA5</i>	5'-TTATGGCAGTCATTGCGACAG-3'	5'-AAAGAGGTGTCAGCATTAAAGCA-3'
<i>ABCA6</i>	5'- CCGTCAAGGGGCTCAGGAA -3'	5'- GATGGCCACACGGTCACAC -3'
<i>ABCA8</i>	5'- AGTGCGCGGGCTCTTCTTTGT-3'	5'-GTTTTCTTCGCTTTTGGCTGATA-3'
<i>ABCA9</i>	5'-CCCCATGATGAAAGAGCACAGAG-3'	5'-AGGATCCCCCAAAGACAATAAGG-3'
<i>ABCA10</i>	5'-GGAGACGACAAATCTATGCAGTG-3'	5'-CCCAACAATGAGTTTCACGAGT-3'
<i>ABCA12</i>	5'-TCTCGCCGAAGTATATGGGATGTT-3'	5'-GGCTTCGGGGAGATGTGATTG-3'

GAPDH : Glyceraldehyde 3-phosphate dehydrogenase; *ABCA*: ATP binding cassette subfamily

5.4 Results

5.4.1 U-251 glioblastoma cell cultures

The morphology of the U-251 cells in the 2D and 3D culture condition at day 14 was shown as the microscopic and a fluorescence microscopic images. Obviously, cells cultured in conventional 2D condition tended to grow in the way of monolayer flat sheets; while cells cultured in 3D condition managed to expand the intercellular interactions in dimensions to form cell spheroids similarly to *in vivo* tumor. After 14 days of 3D cell culture, spheroids with the diameter of up to 50 μm could be found in the culture system (Figure 5.2).

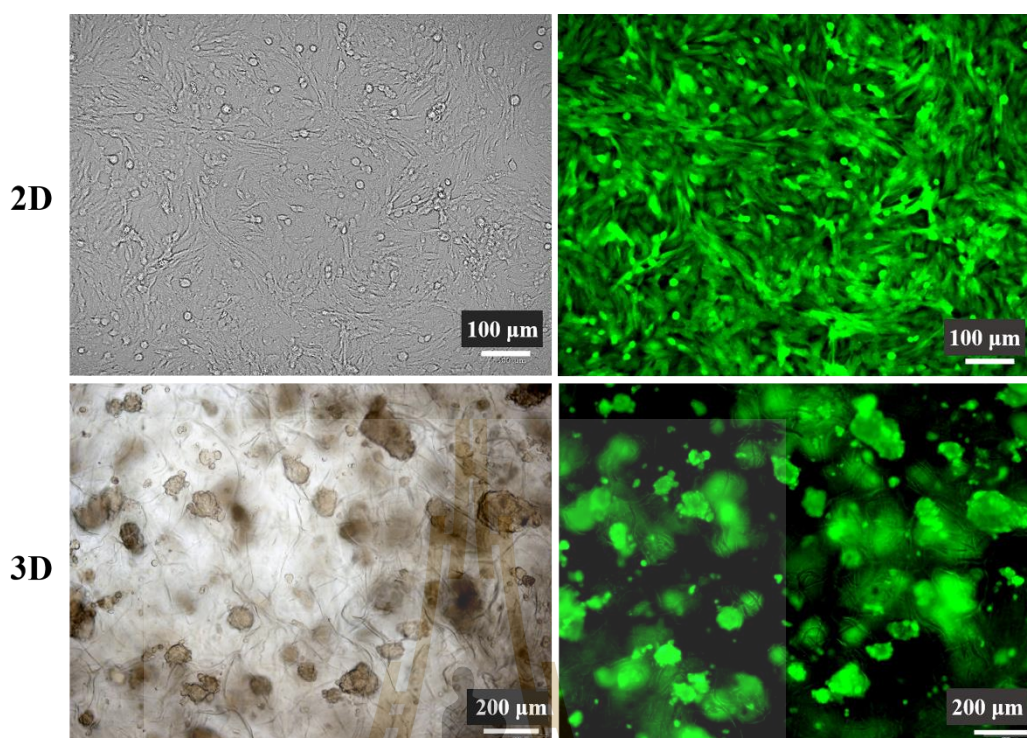


Figure 5.2 Glioblastoma cells in 2D and 3D conditions for 14 days.

5.4.2 Transcriptome sequencing and mapping to the reference genome

During sequencing, quality concerns may arise. A small number of target sequences might be read into adapter sequences, and bases toward the 3'-end might have low quality due to the lengthy sequencing cycles. To eliminate the negative effect of these technical issues, low-quality reads and contaminations were filtered out before data analysis. In addition, adapter sequences were removed. 283,439,522 raw reads were primarily generated in total; after removing low-quality reads and those containing adapter and poly-N, 281,713,096 clean reads remained (Table 5.2). The remaining clean data were used to map to the reference genome. In the 2D condition, 2D-1, 2D-2, and 2D-3 sample had 95.094%, 95.0841%, and 95.2281% of reads mapped to the reference genome respectively. In 3D condition, the percent of reads mapped to the reference genome of 3D-1, 3D-2, and 3D-3 samples were 94.1352%, 93.6812%, and 92.94%, respectively.

5.4.3 Differential gene expression between 2D and 3D culture conditions

The level of gene expression was measured by read density; the higher the read density, the higher the level of gene expression. The expected number of fragments per kilobase of target transcript length per million reads mapped (FPKM) is the most common method used to evaluate the level of gene expression (Mortazavi et al., 2008). Collaboratively, PCA (Principal Component Analysis) were used to reduce data complexity and analyze the sample relationship and the scale of the difference between the transcriptomes of 2D and 3D condition. The results of PCA revealed the significant difference between those two conditions (Figure 5.3). Plus, the differential expression DESeq2 analysis was further analyzed to specifically determine genes with significant differential gene expression profile between such groups. The significant differential gene expression was defined based on a fold change greater than 2 or less than -2 and false discovery rate (FDR) less than 0.05 to achieve both statistical and biological significance. Based on such standards, the differential gene expression of U-251 glioblastoma comparing between cells in 2D and 3D condition was recorded. As shown in Figure 5.4, 7,411 genes were upregulated and 3,915 genes were downregulated during 14 days of culture period. The heatmap and hierarchical clustering of all 6 samples, highlighting relative gene expression of the three replication of 2D and 3D cell cultures is shown in Figure 5.5, in which red represents higher expression and blue represents lower expression. According to the gene clustering heat map, 3D culture condition exhibited the highest level of variation in gene expression compared to 2D culture condition.

Table 5.2 Data quality, filtration and alignment summary for transcriptome of U-251 cells on 2D and 3D cultures condition.

Sample	Raw reads	Clean reads	Clean bases	Q20 (%)	Q30 (%)	GC (%)	Total mapped
2D-1	46709780	46436476	6877710088	96.84	91.55	50.56	44158319 (95.094%)
2D-2	48927824	48635394	7216851609	96.76	91.38	50.63	46244539 (95.0841%)
2D-3	42611526	42392708	6285675863	97.23	92.52	51.16	40369758 (95.2281%)
3D-1	54972942	54654512	8111036223	97.13	92.33	50.46	51449161 (94.1352%)
3D-2	47101130	46831888	6945874735	97.13	92.34	50.69	43872697 (93.6812%)
3D-3	43116320	42762118	6331575923	96.81	91.79	50.25	39743105 (92.94%)
Summary	283439522	281713096	41768724441				

2D-1: 2D culture condition replication 1, 2D-2: 2D culture condition replication 2,

2D-3: 2D culture condition replication 3, 3D-1: 3D culture condition replication 1,

3D-2: 3D culture condition replication 2, 3D-3: 3D culture condition replication 3

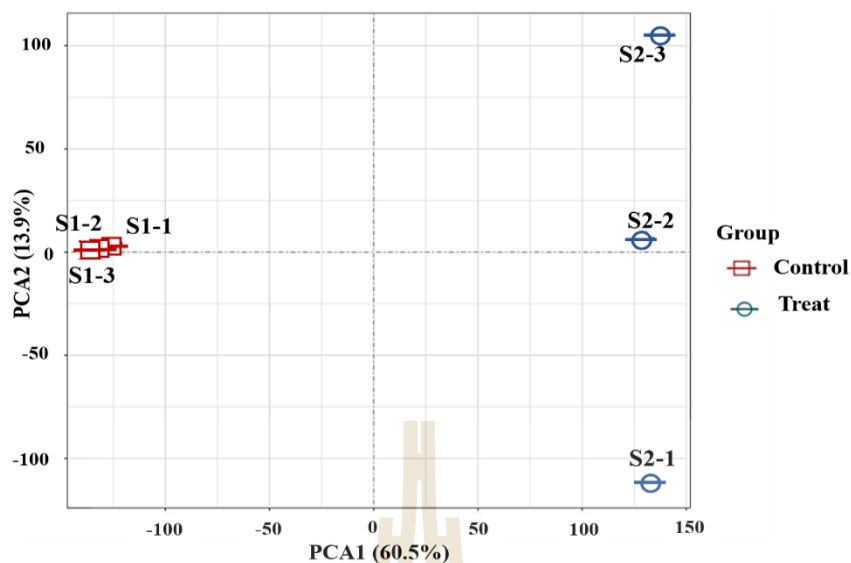


Figure 5.3 Principal Component Analysis (PCA) chart, position the sample representative of the value of each dot on each of the main components. Control; 2D condition and Treat; 3D condition.

5.4.4 Differential gene GO enrichment analysis

To explore the functions of the differentially expressed genes. Gene ontology (GO) analysis were furtherly performed as the classification system for gene function, including molecular function, cellular components, and biological processes. The differentially expressed genes, mainly enriched in the category of molecular function were the genes related to “binding”, “catalytic activity”, “transporter activity”. In the cellular components category, “cells part”, “organelle”, “organelle part”, “membrane part”, “membrane”, “macromolecular complex”, “extracellular region”, “extracellular region part”, and “cell junction” showed significant proportions of differential gene expression. Among genes categorized in the biological process category, genes related of “cellular process”, “biological regulation”, “single-organism process”, “metabolic process”, “developmental process”, “response to stimulus”, “localization”, “cellular component

organization”, “multicellular organismal process”, “immune system process” and “multi-organism process” showed the most significant differential expression (Figure 5.6).

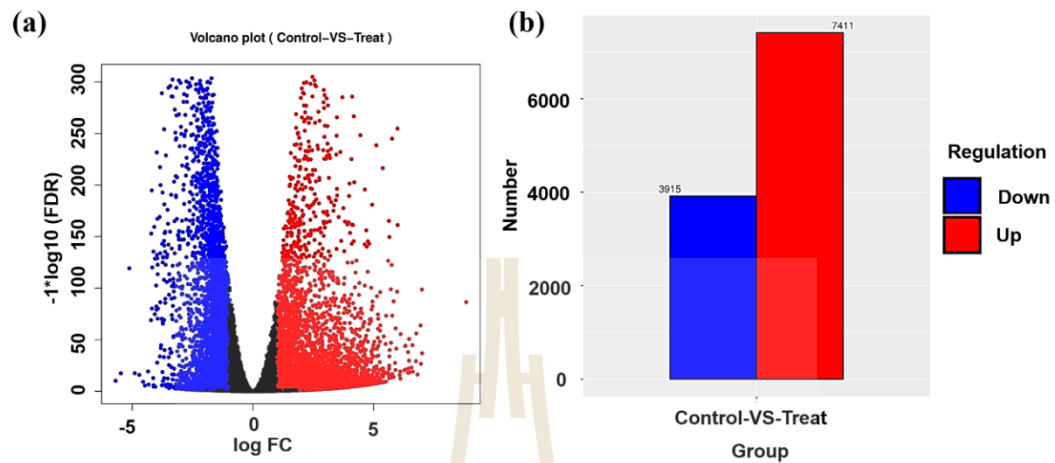


Figure 5.4 (a) Differential expression volcano plot, red dots represent genes that are significantly up-regulated and blue dots represent those that are significantly down-regulated. Abscissa represents multiple genes expressed in different samples. Ordinate represents the magnitude of gene expression changes. (b) Bar graph of genes significantly up- or down-regulation between 2D (Control) and 3D conditions (Treat).

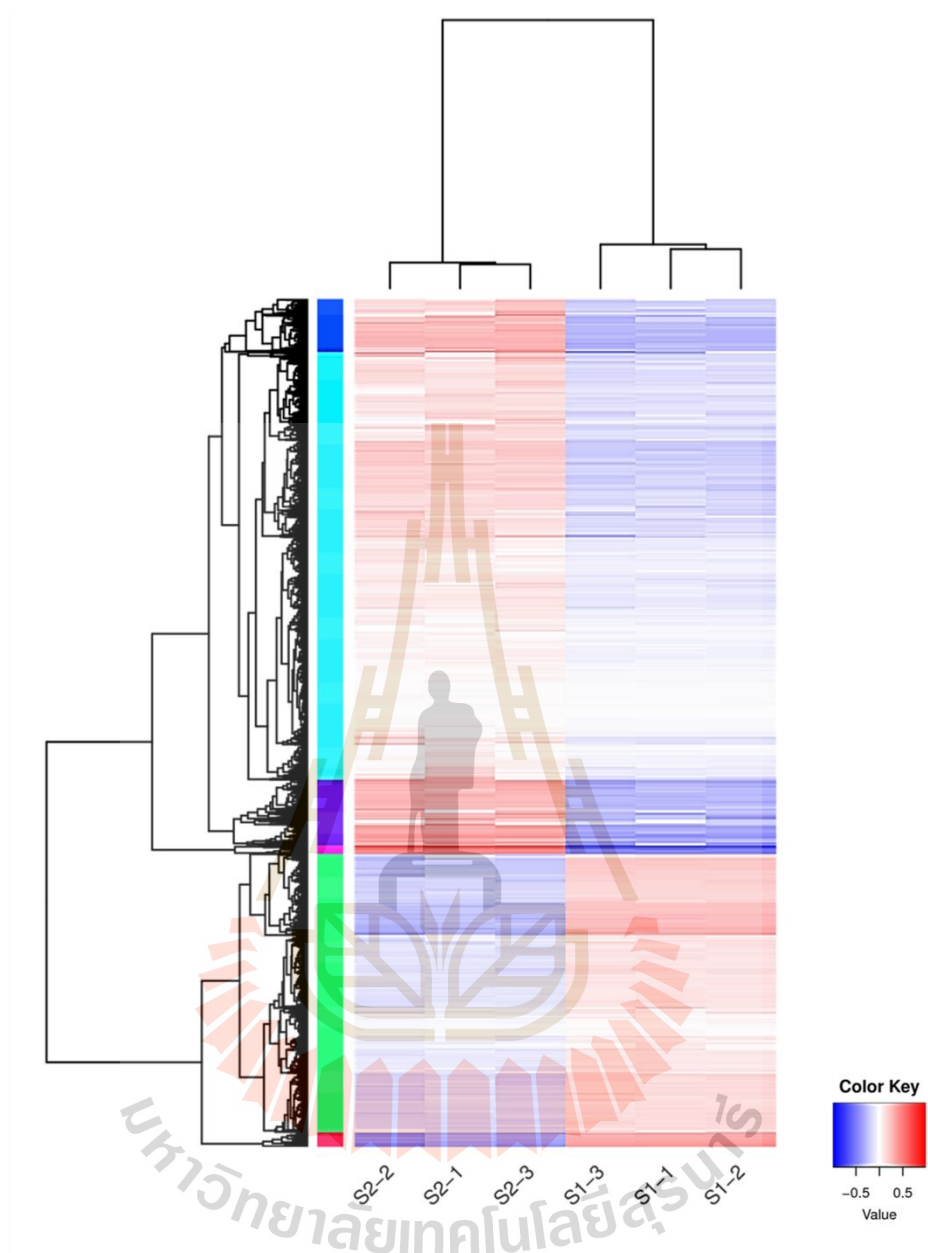


Figure 5.5 Heatmap of gene expression in 2D and 3D culture condition for 14 days. 2D-1: 2D culture condition replication 1, 2D-2: 2D culture condition replication 2, 2D-3: 2D culture condition replication 3, 3D-1: 3D culture condition replication 1, 3D-2: 3D culture condition replication 2, 3D-3: 3D culture condition replication 3.

5.4.5 KEGG pathway analysis of U-251 cells cultured under 2D and 3D conditions

Physiological activities are the cooperation between genes with various functions. Pathway functional enrichment facilitates the determination of differentially expressed genes involved in the most important biochemical metabolic pathways and signal transduction pathways. KEGG is the primary public pathway database (Kanehisa et al., 2007) used in this analysis. Pathway enrichment analysis performed in this section is based on KEGG pathway units cooperated with a hypergeometric test to point out the pathways of the differentially expressed genes that are significantly enriched against the transcriptome background. The differential gene expression was mainly enriched in mitophagy, autophagy, ECM-receptor interaction, cell cycle, fatty acid metabolism, RNA degradation, pyrimidine metabolism, DNA replication, pathways in cancer, viral carcinogenesis, steroid biosynthesis, and MAPK signaling pathway.

Here, some important pathways were focused to reveal the major differences of glioblastoma cultured in 3D and 2D conditions, as well as the pathway that caused the anti-cancer drug resistance of glioblastoma in 3D condition. As the results based on KEGG pathway analysis, the downregulated genes were mainly enriched in cell cycle and DNA replication pathway while the upregulated genes were mainly enriched in MAPK signaling, autophagy, drug metabolism-cytochrome P450, and ABC transporter pathway. Heatmaps were generated based on the differentially expressed genes of each particular pathway defined by FPKM value (Figure 5.7).

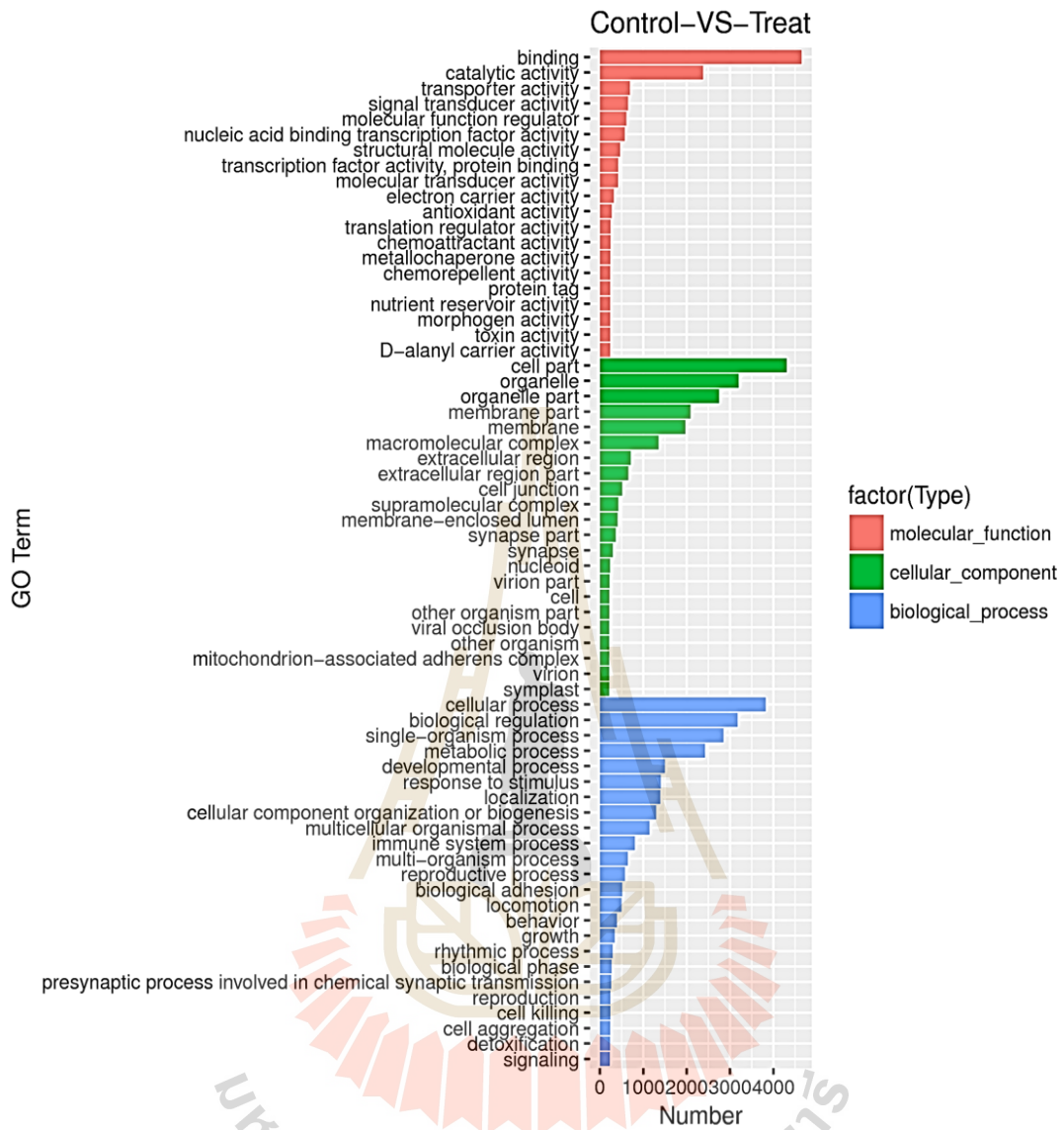


Figure 5.6 GO enrichment histogram. X axis: number of differentially expressed gene in this GO category. Color code is to distinguish the categories- biological processes, cellular components and molecular functions between 2D (Control) and 3D conditions (Treat).

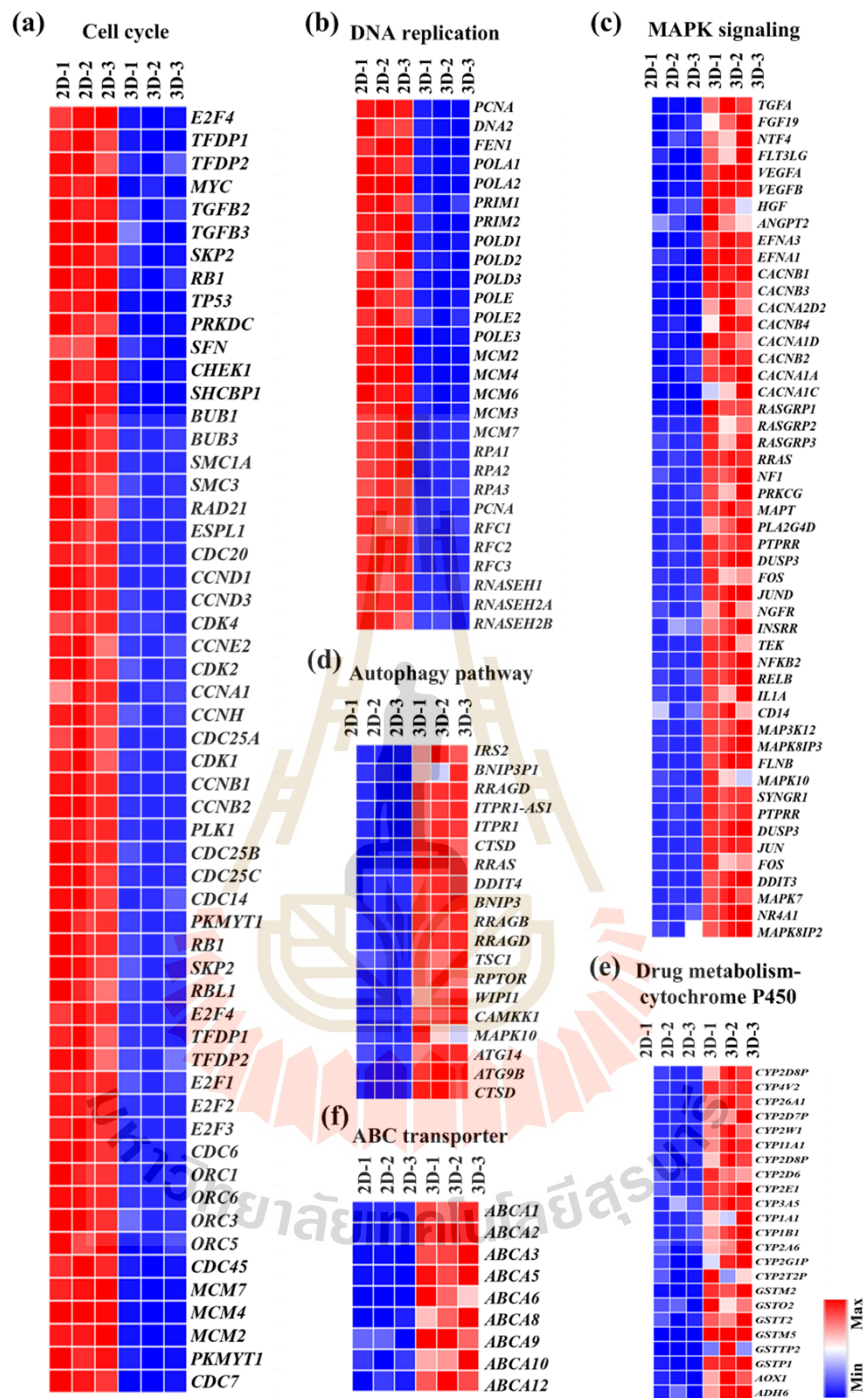


Figure 5.7 Different expressed genes within pathways under 2D and 3D cell culture condition for 14 days. (a) Cell cycle, (b) DNA replication, (c) MAPK signaling, (d) Autophagy pathway, (e) Drug metabolism-cytochrome P450, (f) ABC transporters.

5.4.6 Real-time quantitative PCR (RT-qPCR) verification

To further validate the results of Illumina RNA-Sequencing data, qRT-PCR was performed to investigate the mRNA expression of important genes that related ABC transporters including *ABCA1*, *ABCA2*, *ABCA3*, *ABCA5*, *ABCA6*, *ABCA8*, *ABCA9*, *ABCA10* and *ABCA12*. The validation qRT-PCR results were showed in Figure 5.8. The mRNA expression of these genes in 3D cell culture increased to 23.08 ± 3.63 , 13.43 ± 1.84 , 3.22 ± 1.21 , 6.16 ± 1.52 , 35.00 ± 2.43 , 28.17 ± 4.98 , 17.06 ± 1.94 , 6.11 ± 1.28 , and 3.63 ± 1.07 folds higher than that of 2D cell culture. These results indicate that all gene showed consistent expression patterns with the Illumina RNA-Sequencing data, confirming that my experimental results were valid.

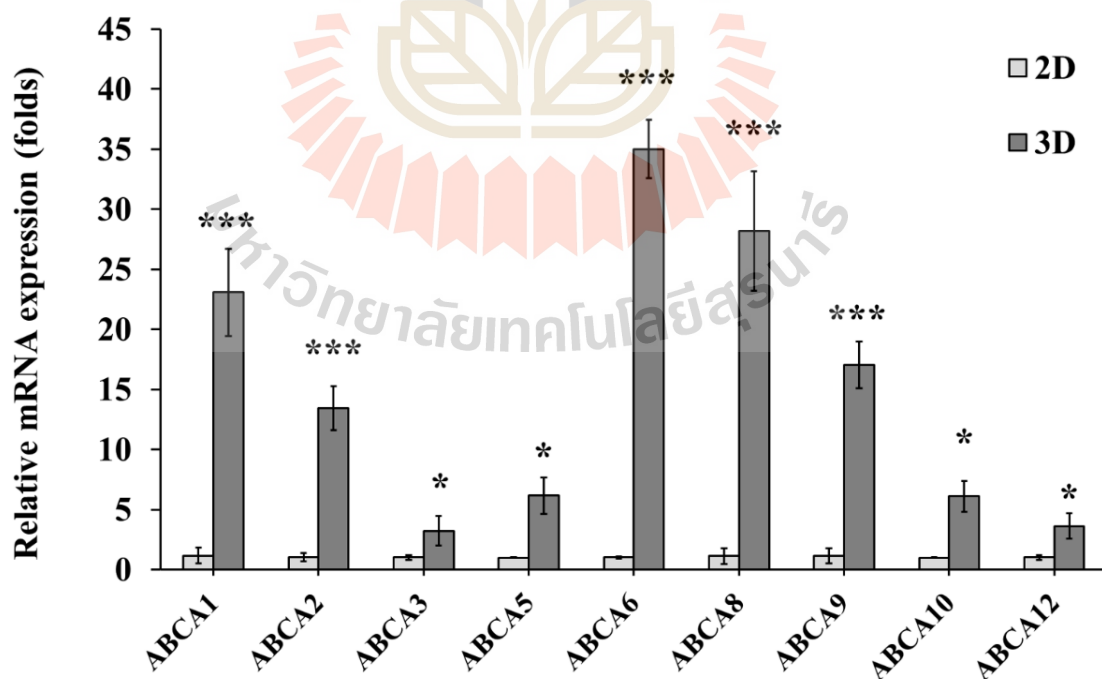


Figure 5.8 Gene expression of glioblastoma cells under 2D and 3D cell culture condition for 14 days. Asterisks indicate statistical significance, as determined by a Student's t test: * $p < 0.05$, ** $p < 0.01$, *** $p < 0.001$.

5.5 Discussion

2D cell culture has been used as *in vitro* models to drug screening for primary identification and verification of bioactive compounds that were subsequently translated into clinical cancer treatment (Shaw et al., 2011). However, there was a poor correlation in term of effectiveness of emerging anti-cancer agents tested in 2D cell culture to the actual treatment in patient which emphasized the necessary for the novel, effective and translatable *in vitro* models to be developed (Ledford, 2011). Culture conditions is known to crucially affect the regulation of cell fate and responsiveness of cells to external stimuli. 2D cultures condition are widely favored due to the easy and fast testing capability, but cells grown in such condition may lose their natural phenotypic and functional characteristics (Yamada and Cukierman, 2007). Lately, the limitations of 2D cell culture were believed to be overcome by culturing cells under more physiological 3D conditions. Thus, 3D *In vitro* tumor models would be a powerful and effective tool in cancer research and low cost anti-cancer drug screenings (Chaicharoenudomrung et al., 2019; Lv et al., 2016). With closely imitating the *in vivo* complex tumor microenvironment, it helps researchers to reveal and understand the underline molecular mechanism for tumorigenesis, development, proliferation, migration, invasion, angiogenesis, and anti-cancer drug resistance. In the present study, I utilized a 3D Ca-alginate scaffold as a model to create glioblastoma micro tumor spheroids and analyze the global gene expression

profiles of glioblastoma cells cultured under 2D and 3D culture condition by Illumina RNA-sequencing. Furthermore, I identified the putative pathways enriched with the differentially expressed genes which potentially played crucial role in the enhancement of anti-cancer drug resistance in 3D glioblastoma.

Several RNA-sequencing studies demonstrated significant, tumor-relevant molecular changes induced by 3D cell culture condition (Ma et al., 2018; Senkowski et al., 2016; Tekin et al., 2018). Glioblastoma spheroids grown in 3D cell culture condition mimicked *in vivo* tissues, organs and even patient tumors, providing resembled cellular properties including hypoxic gradients, cellular heterogeneity with both slow-dividing cells and proliferative tumor bulk (Florczyk et al., 2016; Kim, 2005) and higher drug resistance (Lv et al., 2016). My transcriptomic study provided other evidence of the global molecular alteration influenced by the different microenvironment under 2D and 3D cell culture conditions, especially for the expression of genes related to the cell cycle, DNA replication, MAPK signaling, autophagy, drug metabolism-cytochrome P450, and ABC transporter pathway.

Among all crucial cellular properties found to be differed in my 3D glioblastoma, cell proliferation governed by the cell cycle pathway seems to exhibit dramatic alteration of gene expression profile. In my experiments, there were 56 differentially expressed genes being downregulated in this pathway compared between 2D and 3D condition (Figure 5.7a). The cell cycle pathway is the series of events that inspect cell division. Regulation of the cell cycle involves to the survival of a cell, including the detection and repairing of genetic damage as well as the prevention of uncontrolled cell division. Since 3D glioblastoma spheroids are known to feature the hypoxic gradients and cellular heterogeneity which exist in *in vivo* tumors, such hypoxia could affect cell cycle.

Richards, Jenkinson, Haylock, and See (2016) demonstrated that hypoxia has the potential to induce cell cycle arrest in glioblastoma cells. 3D glioblastoma cells residing within nutrient- and oxygen-deprived regions are mostly quiescent. Transcriptional profiling data once revealed that quiescent stem cells were characterized by the downregulation of genes associated with cell-cycle progression (i.e. *CCNA2*, *CCNB1*, and *CCNE2*) (Cheung and Rando, 2013). Consistently with my study, the expression of genes related to the cell cycle, such as, *CCNA1*, *CCND3*, *CCNB1*, *CCNB2*, *CDC14*, *CDC20* and *PLK1* were downregulated in 3D culture conditions. Harmoniously, DNA replication pathway, the series of biological process to synthesize the identical replica of DNA occurring during S of cell cycle, also owned the major differential gene expression. 28 genes in the pathway of DNA replication were found to be downregulated in 3D condition compared to 2D condition (Figure 5.7b) which were possibly the consequences of cell cycle arrest.

Despite the suppression of proliferation, reflected by the downregulation of cell cycle and DNA replication pathways, the mitogen-activated protein kinase (MAPK) signaling pathway which regulates cellular response to the extracellular signals showcased the opposite manner in which 49 genes in MAPK signaling pathway were found being upregulated in 3D conditions compared to 2D conditions (Figure 5.7c). Mitogen-activated Protein Kinase (MAPK) signaling pathway, often known as the RAS-RAF-MEK-ERK signal cascade, functions to transmit upstream extracellular signals to its downstream effectors. Such pathway regulates broad-range of physiological processes such as cell growth, proliferation, differentiation, migration development, inflammatory responses and apoptosis (Dunn et al., 2005) for cell in general, and the progression, invasion, survival, and drug resistance in context of cancer. Xu et al. (2018) demonstrated that MAPK8 promoted the resistance to anti-cancer drug, accelerated cell proliferation

and inhibited the apoptosis of glioblastoma cells via activating MAPK signaling pathway. Other previous studies have reported that in tumor tissue samples derived from patient, ERK was phosphorylated, indicating that this survival pathway was active in glioma cells (Motta et al., 2015). In addition, the MAPK/c-Jun N-terminal kinase (JNK) signaling transduction pathway was also reported to induce defensive mechanisms protecting organisms against various stress situations and had been repeatedly linked to the molecular events involved in autophagy regulation (Zhou et al., 2015). Lin et al. (2012) reported that TMZ-induced autophagy was mediated by JNK activation in U87 cell lines, and the JNK inhibitor, SP600125, inhibited cell autophagy, furtherly increasing the percentage of cells undergoing apoptosis.

The involvement of MAPK signaling pathway to autophagy regulation conceivably caused the correlative upregulation manner of 19 autophagy-related genes in my study (Figure 5.7d). Autophagy is a lysosomal-based degradative pathway that processes self-cannibalization, allowing the degradation of intracellular components, including soluble proteins, aggregated proteins, organelles, macromolecular complexes, and foreign bodies to their relative biological building blocks during periods of starvation. Such self-eating and recycling provides cells with survival advantages under various stress situations (Zhou et al., 2015). Autophagy pathway can support growth of tumor at later stages, allowing tumor cells to survive with limited oxygen and nutrients, as well as under cytotoxic caused by drug treatment. Bingel et al. (2017) found that autophagy-controlling transcription factors, such as *TFEB* and *FOXO3*, were upregulated in tumors and 3D neuroblastoma cells which could be parts of underline mechanism of chemotherapy resistance. In addition, 3D glioblastoma cells could undergo metabolic reprogramming to sustain their rapid growth and proliferation. Hence, glioblastoma cells often have distinct

nutrient requirements such as higher level of glucose, a phenomena associated with Warburg effect which is characterized by high glycolytic rate (Altman et al., 2016; La et al., 2008; Liberti and Locasale, 2016). The elevated rates of glucose uptake and metabolism to sustain their rapid growth combined with nutrient deprivation in glioblastoma spheroids may cause the autophagy enhancement and the transition of cells to quiescence state (Katheder et al., 2017). Autophagy can somehow subdued cancer cell metabolism, leading to quiescence and survival, and as such constitutes a vital mechanism of drug resistance (Levy et al., 2017). Wang et al. (2018) demonstrated that upon glucose starvation, the majority of cancer cells were perished due to chemotherapeutic cytotoxicity, subsets of cancer cells can upregulate their autophagic activity, enter quiescence, and acquire survival advantage and ultimately chemoresistance.

Several mechanisms have been proposed for drug resistance of glioblastomas (Backos et al., 2012; Esteller et al., 2000). Intracellular drug inactivation may occur as a result of the increased concentrations of enzymes such as to glutathione S-transferase (GST), cytochrome p450 (CYP) and Aldehyde dehydrogenases (ALDH). These enzymes may have a role in reduced efficacy of chemotherapy against glioblastomas (Agúndez, 2004; Lo and Ali-Osman, 2007). The drug metabolism-cytochrome P450 plays a key role as a phase I drug metabolizing enzymes to catalyze the oxidative biotransformation of most drugs and other lipophilic xenobiotics (Zanger et al., 2008) by adding an oxygen atom to their substrate via monooxygenase reactions (Stavrinou et al., 2015). In this study, 23 genes in drug metabolism-cytochrome P450 were found upregulated in 3D glioblastoma (Figure 5. 7e) which emphasized the increase of malignancy of 3D glioblastoma comparing to those in 2D condition. In the context of cancer, such family of enzymes are of particular interest since they exhibited important extrahepatic function and

have been linked to various malignancies (Murray et al., 1997). Moreover, genotyping and epidemiological studies of *CYP1A1* were correlated with increased risk for brain tumor (Milne et al., 2013). *CYP1B1* is a tumor-associated protein, which has been shown to be overexpressed in various malignant tumors (McFadyen and Murray, 2005). Barnett et al. (2007) demonstrated that *CYP1B1* is expressed in gliomas and the level of expression depends on tumor type and grade. Aldehyde oxidases (AOXs), glutathione S-transferases (GSTs) along with their isoenzyme glutathione S-transferase pi 1 (GSTP1) were also upregulated in this study. Aldehyde oxidases (ALDHs) take part in the metabolism of alkylating agents mediating the resistance to anti-cancer drugs (Schäfer et al., 2012), while the phase II drug-metabolizing-enzymes, GSTs are responsible for catalyzing the formation of glutathione-S-conjugates with electrophiles inactivating and facilitating excretion of these molecules (Hayes et al., 2005). Previous studies stated that GST genes were upregulated in response to oxidative stress and inexplicably overexpressed in many tumors, causing problems during cancer chemotherapy by direct drug metabolism or by potentially reducing the ability of the drugs to interact with DNA and other cellular molecules (Ioannides, 2002). GSTP1 is the primary isoenzyme contributing to total GST activity in both normal brain and brain tumors (Lo and Ali-Osman, 2007; Strange et al., 1992). Hara et al. (1990) also examined expression of GSTP1 in 31 gliomas and 6 normal brain tissues and showed that, gliomas showed a strongly positive reaction for GSTP1 immunostaining in both *in vitro* models and glioma patients.

The other mechanism of glioblastoma can process to mediate multiple drug resistances is the active efflux anti-cancer drugs out of cells through multi-drug resistance proteins embedded in the cellular membrane (Dréan et al., 2018). Drugs can be transported across the membrane against electrochemical potentials in ATP-dependent manner via

protein transporters including the ATP-binding cassette (ABC) transporters which were found to be upregulated in this study (Figure 5.7f). The family of ABC transporters is involved in diverse physiological processes and responsible for the uptake and efflux of broad type of substances from cancer cells (Alexiou et al., 2012). Rama et al. (2014) demonstrated that ABC transporters: *ABCA1*, *MRP4*, and *MRP5* showed overexpression in the glioblastoma cells and drug resistance has been correlated with the presence of the ABC efflux transporters trying to exclude drugs for the cellular cytoplasm. Taken together, this can be a reasonable explanation for my findings, 3D glioblastoma spheroids are feature hypoxic induced cell cycle arrest and decrease DNA replication, while gene in MAPK signaling, autophagy, drug metabolism-cytochrome P450, and ABC transporter pathway were upregulated.

My work has provided transcriptomic perspective and quantitative measurements of genes differently expressed in 2D and 3D *in vitro* culture condition. Based on my findings, future research should be investigated proteomically and metabolomically in which data from proteomics and metabolomics might be adopted to understand the phenotype and identify novel therapeutic targets in glioblastoma. In addition, as previously declaring, the *in vitro* 3D glioblastoma culture models has the potential to serve as a powerful platform for tumor study and anticancer drug screening and could potentially applied to further proteomic and metabolomics studies.

5.6 Conclusion

In this study, I used Illumina RNA-Sequencing to analyze global relative gene expression of glioblastoma cells cultured in 2D monolayers and 3D Ca-alginate scaffolds

at day14 of culture period. The results showed that 7,411 and 3,915 genes were upregulated and downregulated, respectively. Moreover, KEGG pathway analysis demonstrated that the downregulated genes were mainly enriched in cell cycle and DNA replication pathway while upregulated genes were mainly enriched in MAPK signaling, autophagy, drug metabolism-cytochrome P450, and ABC transporter pathway. All of these pathways hinted the involved mechanisms related to anti-cancer drug resistance of glioblastoma and likely to prove useful for target identification of anti-cancer drug development. Thus, 3D glioblastoma model has the potential to serve as a powerful platform for glioblastoma study, anti-glioblastoma drug screening, and identification of novel molecular targets in treatment of glioblastoma.

5.7 References

- Abbott, A. (2003). Cell culture: biology's new dimension. **Nature**. 424(6951): 870-872.
- Agúndez, J. A. (2004). Cytochrome P450 gene polymorphism and cancer. **Current drug metabolism**. 5: 211-224.
- Alexiou, G. A., et al. (2012). Prognostic significance of MRP5 immunohistochemical expression in glioblastoma. **Cancer Chemotherapy and Pharmacology**.69: 1387-1391.
- Altman, B. J., Stine, Z. E., and Dang, C. V. (2016). From Krebs to clinic: glutamine metabolism to cancer therapy. **Nature reviews cancer**.16: 619.
- Anders, S., and Huber, W. (2010). Differential expression analysis for sequence count data. **Genome biology**.11: R106.

- Anders, S., and Huber, W. (2012). Differential expression of RNA-Seq data at the gene level—the DESeq package. Heidelberg, Germany: European Molecular Biology Laboratory (EMBL).
- Backos, D. S., Franklin, C. C., and Reigan, P. (2012). The role of glutathione in brain tumor drug resistance. **Biochemical pharmacology**.83: 1005-1012.
- Barnett, J. A., Urbauer, D. L., Murray, G. I., Fuller, G. N., and Heimberger, A. B. (2007). Cytochrome P450 1B1 expression in glial cell tumors: an immunotherapeutic target. **Clinical cancer research**.13: 3559-3567.
- Behin, A., Hoang-Xuan, K., Carpentier, A. F., and Delattre, J.-Y. (2003). Primary brain tumours in adults. **The Lancet**.361: 323-331.
- Beier, C. P., et al. (2012). The cancer stem cell subtype determines immune infiltration of glioblastoma. **Stem cells and development**.21: 2753-2761.
- Chaicharoenaudomrung, N., et al. (2019). Fabrication of 3D calcium-alginate scaffolds for human glioblastoma modeling and anticancer drug response evaluation. **Journal of cellular physiology**.
- Cheung, T. H., and Rando, T. A. (2013). Molecular regulation of stem cell quiescence. **Nature reviews Molecular cell biology**.14: 329.
- Clark, P. A., et al. (2016). Resveratrol targeting of AKT and p53 in glioblastoma and glioblastoma stem-like cells to suppress growth and infiltration. **Journal of neurosurgery**. 126: 1448-1460.
- Dréan, A., et al. (2018). ATP binding cassette (ABC) transporters: expression and clinical value in glioblastoma. **Journal of neuro-oncology**. 138: 479-486.

- Dunn, K. L., Espino, P. S., Drobic, B., He, S., and Davie, J. R. (2005). The Ras-MAPK signal transduction pathway, cancer and chromatin remodeling. **Biochemistry and Cell Biology**. 83: 1-14.
- Esteller, M., et al. (2000). Inactivation of the DNA-repair gene MGMT and the clinical response of gliomas to alkylating agents. **New England Journal of Medicine**.343: 1350-1354.
- Florczyk, S. J., et al. (2016). 3D porous chitosan–alginate scaffolds promote proliferation and enrichment of cancer stem-like cells. *Journal of Materials Chemistry B*.4: 6326-6334.
- Friedrich, J., Seidel, C., Ebner, R., and Kunz-Schughart, L. A. (2009). Spheroid-based drug screen: considerations and practical approach. **Nature protocols**.4: 309.
- Hara, A., et al. (1990). Immunohistochemical demonstration of the placental form of glutathione S-transferase, a detoxifying enzyme in human gliomas. **Cancer**. 66: 2563-2568.
- Hayes, J. D., Flanagan, J. U., and Jowsey, I. R. (2005). Glutathione transferases. **Annual Review of Pharmacology and Toxicology**. 45: 51-88.
- Ioannides, C. (2002). Enzyme systems that metabolise drugs and other xenobiotics. **John Wiley & Sons**. 1-32.
- Johnson, D. R., and O'Neill, B. P. (2012). Glioblastoma survival in the United States before and during the temozolomide era. **Journal of neuro-oncology**.107: 359-364.
- Kanehisa, M., et al. (2007). KEGG for linking genomes to life and the environment. **Nucleic acids research**. 36:480-484.

- Kang, M.-K., and Kang, S.-K. (2007). Tumorigenesis of chemotherapeutic drug-resistant cancer stem-like cells in brain glioma. *Stem cells and development*.16: 837-848.
- Katheder, N. S., et al. (2017). Microenvironmental autophagy promotes tumour growth. **Nature**. 541: 417.
- Kievit, F. M., et al. (2010). Chitosan–alginate 3D scaffolds as a mimic of the glioma tumor microenvironment. **Biomaterials**. 31: 5903-5910.
- Kim, J. B. (2005). Three-dimensional tissue culture models in cancer biology. **Paper presented at the Seminars in cancer biology**. 15 (5): 365-377.
- La Schiazza, R., et al. (2008). Cellular energetic metabolism of cerebral tissue: metabolic characteristics of glial tumours. Paper presented at the *Annales de biologie clinique*.
- Ledford, H. (2011). Translational research: 4 ways to fix the clinical trial. **Nature News**. 477: 526-528.
- Levy, J. M. M., Towers, C. G., and Thorburn, A. (2017). Targeting autophagy in cancer. **Nature reviews cancer**.17: 528.
- Liberti, M. V., and Locasale, J. W. (2016). The Warburg effect: how does it benefit cancer cells?. **Trends in biochemical sciences**. 41: 211-218.
- Lin, C.-J., et al. (2012). Inhibition of mitochondria-and endoplasmic reticulum stress-mediated autophagy augments temozolomide-induced apoptosis in glioma cells. **PloS one**. 7: 38706.
- Lo, H.-W., and Ali-Osman, F. (2007). Genetic polymorphism and function of glutathione S-transferases in tumor drug resistance. **Current opinion in pharmacology**.7: 367-374.

- Lv, D., et al. (2016). A three-dimensional collagen scaffold cell culture system for screening anti-glioma therapeutics. **Oncotarget**. 7: 56904.
- Ma, L., et al. (2018). The comparison genomics analysis with glioblastoma multiforme (GBM) cells under 3D and 2D cell culture conditions. **Colloids and Surfaces B: Biointerfaces**. 172: 665-673.
- McFadyen, M. C., and Murray, G. I. (2005). Cytochrome P450 1B1. **a novel anticancer therapeutic target**. 259-263.
- Milne, E., et al. (2013). Parental smoking and risk of childhood brain tumors. **International journal of cancer**. 133: 253-259.
- Mortazavi, A., Williams, B. A., McCue, K., Schaeffer, L., and Wold, B. (2008). Mapping and quantifying mammalian transcriptomes by RNA-Seq. **Nature methods**. 5: 621.
- Motta, C., et al. (2015). PJ-34 inhibits PARP-1 expression and ERK phosphorylation in glioma-conditioned brain microvascular endothelial cells. **European journal of pharmacology**. 761: 55-64.
- Murray, G. I., et al. (1997). Tumor-specific expression of cytochrome P450 CYP1B1. **Cancer research**. 57: 3026-3031.
- Rama, A. R., Alvarez, P. J., Madeddu, R., and Aranega, A. (2014). ABC transporters as differentiation markers in glioblastoma cells. **Molecular biology reports**. 41: 4847-4851.
- Schäfer, A., et al. (2012). Aldehyde dehydrogenase 1A1—a new mediator of resistance to temozolomide in glioblastoma. **Neuro-oncology**. 14: 1452-1464.

- Senkowski, W., et al. (2016). Large-scale gene expression profiling platform for identification of context-dependent drug responses in multicellular tumor spheroids. **Cell chemical biology**. 23: 1428-1438.
- Shaw, A. T., Yasothan, U., and Kirkpatrick, P. (2011). Crizotinib: Nature Publishing Group. 897.
- Stavrinou, P., et al. (2015). Expression profile of genes related to drug metabolism in human brain tumors. **PloS one**. 10: 0143285.
- Strange, R. C., et al. (1992). The human glutathione S-transferases: comparison of isoenzyme expression in normal and astrocytoma brain. **Biochimica et Biophysica Acta (BBA)-Molecular Basis of Disease**. 1139: 222-228.
- Tekin, H., et al. (2018). Effects of 3D culturing conditions on the transcriptomic profile of stem-cell-derived neurons. **Nature Biomedical Engineering**. 2: 540.
- Wang, L., et al. (2018). Autophagy mediates glucose starvation-induced glioblastoma cell quiescence and chemoresistance through coordinating cell metabolism, cell cycle, and survival. **Cell death & disease**. 9: 213.
- Xu, P., Zhang, G., Hou, S., and Sha, L. G. (2018). MAPK8 mediates resistance to temozolomide and apoptosis of glioblastoma cells through MAPK signaling pathway. **Biomedicine & Pharmacotherapy**. 106: 1419-1427.
- Yamada, K. M., and Cukierman, E. (2007). Modeling tissue morphogenesis and cancer in 3D. **Cell**. 130: 601-610.
- Zanger, U. M., Turpeinen, M., Klein, K., and Schwab, M. (2008). Functional pharmacogenetics/genomics of human cytochromes P450 involved in drug biotransformation. **Analytical and bioanalytical chemistry**. 392: 1093-1108.

Zhou, Y.-Y., Li, Y., Jiang, W.-Q., and Zhou, L.-F. (2015). MAPK/JNK signalling: a potential autophagy regulation pathway. **Bioscience reports**. 35: 00199.

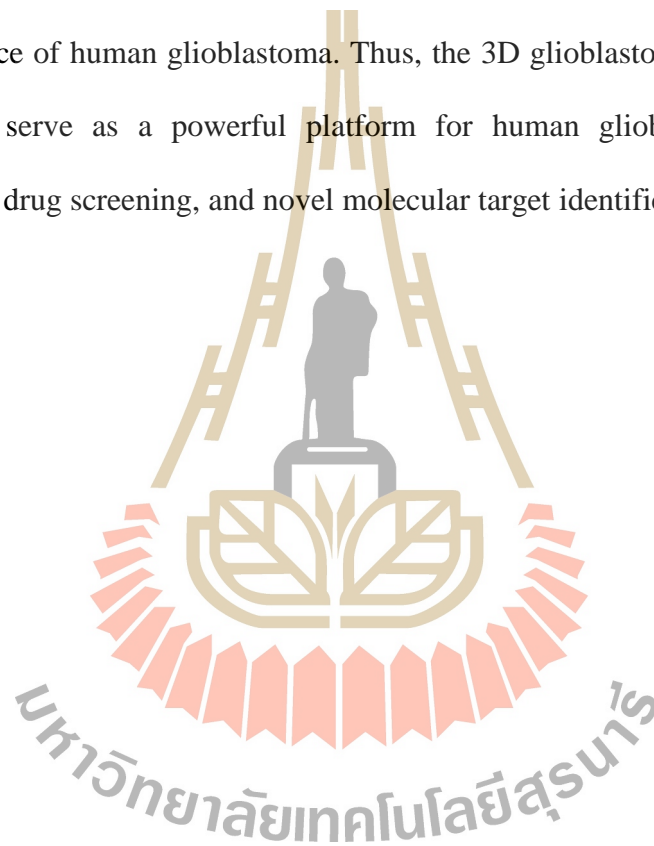


CHAPTER V

SUMMARY

Cordycepin could effectively inhibit the proliferation and induce apoptotic cell death of human nerve cancer cells through the generation of reactive oxygen species and modulation of autophagy under the 2D *in vitro* cell culture model. The control of autophagy activity within cells by small molecules might be an alternative approach for a better treatment of human nerve cancers. Importantly, this finding revealed the mechanism of action of cordycepin, which is a foundation to study other relevant mechanistic insights of cordycepin. In addition, the development of the *in vitro* 3D glioblastoma cell culture system by using Ca-alginate scaffolds could mimic human nerve tissue cancer microenvironment, with high cell viability and proliferation. In the 3D Ca-alginate scaffolds, human glioblastoma U-251 cells line can proliferate, retain characteristics of cancer stem cells, as well as exhibit differentiation potential. Moreover, the 3D glioblastoma cell culture system showed a high resistance to the anticancer agents, temozolomide, doxorubicin and cordycepin, compared with the 2D culture system. My findings suggested that the 3D Ca-alginate scaffolds are promising *in vitro* research platforms for the screening of anti-glioblastoma therapeutic agents. Then, Next Generation Sequencing Illumina RNA-Sequencing was used to analyze the gene expression profiles of glioblastoma cells in 2D monolayers and 3D Ca-alginate scaffolds with the culture period of 14 days. The results showed that 7,411 and 3,915 genes were upregulated and downregulated, respectively. Moreover, the

KEGG pathway analysis presented that the downregulated genes were mainly enriched in clustering of cell cycle and DNA replication, while the upregulated genes were mainly enriched in MAPK signaling, autophagy, drug metabolism-cytochrome P450, and ABC transporter pathways. All of these pathways showed related-mechanisms to anti-cancer drug resistance of human glioblastoma. Moreover, I believe that the provided NGS dataset is useful for a better understand of anti-cancer drug resistance of human glioblastoma. Thus, the 3D glioblastoma model contain the potential to serve as a powerful platform for human glioblastoma study, anti-glioblastoma drug screening, and novel molecular target identification.



BIOGRAPHY

Ms. Nipha Chaicharoenaudomrung was born in August 27, 1988 in Suphanburi Province, Thailand. She received Bachelor's Degree in B.Sc. (Food Technology) from Institute of Agricultural Technology, Suranaree University of Technology, Thailand in 2010. In 2011-2015, she received the degree of Master of Food Technology from Suranaree University of Technology, Thailand. In 2015, she received a scholarship from Suranaree University of Technology (SUT) Research and Development Fund, One Research One Grant (OROG) Scholarship to study for the degree of Doctor of Philosophy in Biotechnology at Suranaree University of Technology. She also published her research work under the title of "Cordycepin induces apoptotic cell death of human brain cancer through the modulation of autophagy" and "Fabrication of 3D calcium-alginate scaffolds for human glioblastoma modeling and anticancer drug response evaluation".

มหาวิทยาลัยเทคโนโลยีสุรนารี